Distribution Agreement

In presenting this thesis or dissertation as a partial fulfillment of the requirements for an advanced degree from Emory University, I hereby grant to Emory University and its agents the non-exclusive license to archive, make accessible, and display my thesis or dissertation in whole or in part in all forms of media, now or hereafter known, including display on the world wide web. I understand that I may select some access restrictions as part of the online submission of this thesis or dissertation. I retain all ownership rights to the copyright of the thesis or dissertation. I also retain the right to use in future works (such as articles or books) all or part of this thesis or dissertation.

Signature:

_____ _____

Nathan W. Schultheiss Date

Intrinsic and Synaptic Determinants of Spike Timing Revealed by Phase Response Analyses of a Morphological Globus Pallidus Neuron Model

By

Nathan W. Schultheiss
Doctor of Philosophy

Graduate Division of Biological and Biomedical Sciences
Neuroscience

_____

Dr. Dieter Jaeger
Advisor

_____

Dr. Robert Butera
Committee Member

_____

Dr. Ronald Calabrese
Committee Member

_____

Dr. Astrid Prinz
Committee Member

_____

Dr. Yoland Smith
Committee Member

Accepted:

_____

Lisa A. Tedesco, Ph.D.
Dean of the James T. Laney School of Graduate Studies

_____

Date

Intrinsic and Synaptic Determinants of Spike Timing Revealed by Phase Response Analyses of a Morphological Globus Pallidus Neuron Model

By

Nathan W. Schultheiss
B.S.

Advisor: Dieter Jaeger, Ph.D.

An abstract of
A dissertation submitted to the Faculty of the
James T. Laney School of Graduate Studies of Emory University
in partial fulfillment of the requirements for the degree of
Doctor of Philosophy
in the Graduate Division of Biological and Biomedical Sciences
Neuroscience
2010

Abstract

Intrinsic and Synaptic Determinants of Spike Timing Revealed by Phase Response Analyses of a Morphological Globus Pallidus Neuron Model

By Nathan W. Schultheiss

In neuronal systems the phase response curve (PRC) describes how synaptic inputs to a neuron at different times during the spike cycle affect the timing of subsequent spikes. The shapes of neuronal PRCs have been related extensively to entrainment of spiking to correlated or periodic input and to the emergence of synchronous modes in synaptically-coupled networks of neurons. Using a full morphological model of a globus pallidus (GP) neuron, the studies presented here explore differences in PRC shape that result 1) when stimuli are targeted to different regions of the neuronal morphology; 2) when the densities of active conductances in the neuronal membrane are varied; and 3) when intrinsic spiking is driven to different frequencies either by tonic somatic current injection or by ongoing synaptic background activity. We demonstrate that during intrinsic spiking, somatic PRCs for our GP neuron model are type I, indicating that excitatory inputs at all phases of the spike cycle advance the spontaneous spiking rhythm. In contrast, we show that distal dendritic PRCs are type II, i.e. excitatory inputs at early phases of the spike cycle can *delay* subsequent spiking as a consequence of dendritic activation of the small conductance calcium-activated potassium current, SK. Further analyses presented in this dissertation demonstrate the robustness of somatic and dendritic PRC shapes against stochastic barrages of excitatory and inhibitory synaptic inputs. We also analyze on a trial-by-trial basis how PRC stimuli interact with fluctuations in the synaptic background activity resulting in added or skipped spike events, and we derive phase response-variance curves (PRVCs) illustrating a major source of spike time variability that can be expected across populations of GP neurons *in vivo*. Lastly, we develop a tool, the cumulative PRC, for differentiating the contributions of intrinsic mechanisms and synaptic backgrounds to the responses of the model across multiple spike cycles. Taken together our results highlight the need to consider different effects of somatic and dendritic synapses in the control of network activity, and we identify a potential role for dendritic SK conductance in the orchestration of normal pallidal activity as well as the pathological β-frequency synchronization accompanying Parkinson's disease.

Intrinsic and Synaptic Determinants of Spike Timing Revealed by Phase Response Analyses of a Morphological Globus Pallidus Neuron Model

By

Nathan W. Schultheiss
B.S.

Advisor: Dieter Jaeger, Ph.D.

A dissertation submitted to the Faculty of the
James T. Laney School of Graduate Studies of Emory University
in partial fulfillment of the requirements for the degree of
Doctor of Philosophy
in the Graduate Division of Biological and Biomedical Sciences
Neuroscience
2010

Acknowledgements

The Neuroscience Program at Emory University has been an ideal nursery for my development as a scientist and is a model collegial scientific community. I thank the program's staff, administrators, and faculty for creating this environment that has been invaluable in allowing me to pursue my educational and research goals. In particular, I wish to express my gratitude to Ron Calabrese, Astrid Prinz, Rob Butera, and Yoland Smith who have graciously served as my thesis committee for the past few years. They have guided the development and refinement of the projects described in this dissertation as well as nurturing my own growth, and I am happy to have developed friendships with each that I will continue to value in the years to come.

My excellent mentor, Dieter Jaeger, has been a patient and knowledgeable teacher, a fair critic, and an insightful leader. His commitment to exacting science in general and to my own training in particular have provided not only an excellent model for success that I will emulate in the future, but also innumerable lessons for negotiating the challenges that lay ahead.

I would also like to thank Risa, my brother Thomas, and my friends, Ryan, Cengiz, Tomasz, and Jeremy, who have been my companions throughout much of my graduate school career at Emory, helping me to maintain some semblance of sanity more often than not.

I also thank my parents for their commitment to my education and for their many and various forms of support and encouragement for all of my endeavors, of which graduate study has been only the most recent.

I dedicate this work, for what it's worth, to my mother, Susan, without whose love and steadfastness I would be lost.

You have my deepest affection and sincerest thanks.

Table of Contents

Table of Figures

Chapter 1

General Introduction

The neuron is widely considered to be the fundamental unit of computation in the brain, however coordinated dynamics of neuronal networks can embody aspects of the neural code that are not captured by any single neuron. Computational models of neuronal and network activity are numerous, and ideally each targets the functional properties of a system while preserving the essential dynamics of its components (Segev, 1992; De Schutter et al., 2005; Herz et al., 2006). For instance single neuron models used to study spiking behavior or integration of synaptic inputs commonly implement the Hodgkin Huxley formalism describing the activation properties of voltage-gated ion channels (Hodgkin and Huxley, 1952d, c, a, b; Hodgkin et al., 1952). At the network level, the complexity of individual neurons is often reduced in order to allow more direct investigation of the interactions between different types of neurons or the functional consequences of different patterns of synaptic connectivity within a network. Of course, these levels of complexity are nested, and the dynamical properties of individual neurons influence their participation in coordinated network behaviors such as synchrony and oscillations (LeMasson et al., 1995; Marder and Thirumalai, 2002). Phase response analysis is a powerful technique derived from dynamical systems theory that targets the interface between computation at the single neuron and network levels. The phase response curve (PRC) describes how inputs to a neuron at different times during the spike cycle affect the timing of subsequent spikes, and the shape of PRCs has been related extensively to the emergence of synchronous modes in networks (Hansel et al., 1995;

Ermentrout, 1996; Goel and Ermentrout, 2002; Galan et al., 2005a; Abouzeid and Ermentrout, 2009; Bogaard et al., 2009) and to entrainment of spiking to oscillatory input (Rinzel and Ermentrout, 1998).

Oscillations in neural systems take place at both the single neuron and network levels and on many timescales. Rhythmic spiking of individual neurons is driven intrinsically by the dynamic interaction of membrane voltage and voltage-gated membrane conductances. Network oscillations result from the complex interactions of intrinsic neuronal properties with the architecture of neuronal networks (Buzsaki and Draguhn, 2004), and in normal brains oscillations are thought to underlie important aspects of memory, attention, and the binding of sensory streams into multidimensional conscious percepts (Roskies, 1999; Ward, 2003). Oscillatory activity between or within neuronal networks implies phase-locking of neuronal assemblies, and synchronized oscillations are an efficient and often stable mode of network dynamics (Winfree, 2001; Buzsaki and Draguhn, 2004). This stability can pose a problem in some systems, however, where synchronized oscillations supplant normal patterns of activity contributing to dysfunctional network states (Schnitzler and Gross, 2005).

Pathological synchronization and oscillations within and between nuclei of the basal ganglia (BG) are key features of the pathophysiology of Parkinson's disease (PD) (Wichmann and DeLong, 2006; DeLong and Wichmann, 2007). In particular, phase-locked bursting and oscillations in low frequency bands between the globus pallidus (GP) and subthalamic nucleus (STN) are prominent (Bevan et al., 2002). The emergence of parkinsonian β-frequency oscillatory activity in GP may reflect increased susceptibility under conditions of dopamine depletion to entrainment with cortical oscillations or could

also be a consequence of enhanced reciprocal GP-STN coupling (Magill et al., 2000; Brown et al., 2001; Magill et al., 2001; Williams et al., 2002; Sharott et al., 2005). Several lines of evidence including anatomical (Smith et al., 1998; Plenz and Kitai, 1999; Parent et al., 2000), physiological (Magill et al., 2000, 2001; Loucif et al., 2005), and network simulation studies (Terman et al., 2002) suggest that the GP-STN microcircuit embodies an oscillatory pattern generator within the BG (Bevan et al., 2002). Furthermore, GP neurons make perisomatic GABAergic synapses throughout the BG (Smith et al., 1998) contributing to the patterning of BG outputs (Kita et al., 2005; Obeso et al., 2006), and recent evidence from Mallet et al. (2008) suggests that GP may play an important role in the β-frequency synchronization of BG oscillatory activity (Wilson et al., 2004) that accompanies loss of dopamine. It is unknown how the cellular properties of GP neurons may be related to pathological synchronization and oscillations accompanying PD.

Computation by Neurons and Networks

Neuronal Excitability and Active Membrane Conductances. On a fundamental level, neuronal excitability is a consequence of voltage-sensitive membrane channel proteins that, when open, allow ions to cross the membrane feeding back onto the membrane voltage. Working with squid giant axons, Alan Hodgkin identified two important classes of neuronal excitability representative of dynamical mechanisms by which neurons typically fire action potentials (Hodgkin, 1948). When driven to spike by increasing the amplitude of injected current, some neurons, e.g. layer 5 pyramidal neurons from rat primary visual cortex (Izhikevich, 2006), begin spiking at an arbitrarily low frequency which increases with stronger current. In response to increasing injected

current, other neurons, e.g. brainstem mesencephalic V neurons (Izhikevich, 2006), begin spiking with a relatively fixed, non-zero frequency and are relatively insensitive to the strength of injected current. These types of excitability, which Hodgkin termed classes I and II, have importantly different implications for computation as the former lends itself to encoding of input strength (either experimental stimulation or synaptic input *in vivo*) in terms of spike frequency, while the latter serves to threshold the cumulative strength of inputs. Class I and II excitability were later identified by dynamical systems theorists to result from a saddle-node on invariant circle (SNIC) bifurcation and either a saddle-node (off invariant circle) or Hopf bifurcation, respectively (Brown et al., 2004; Izhikevich, 2006).

The Hodgkin Huxley (HH) model of action potential generation was developed a few years subsequent to Alan Hodgkin's characterization of neuronal excitability and consists of a system of ordinary differential equations describing the relationship between membrane voltage and activation of sodium, potassium, and leak conductances (Hodgkin and Huxley, 1952d, c, a, b; Hodgkin et al., 1952). Using the HH formalism, a multitude of conductance-based models have revealed the complexity and diversity of dynamics in various neuronal systems. The Connor-Stevens model is one such conductance-based model, similar to the HH model, which contains an A-type potassium current in addition to fast sodium and delayed-rectifier potassium currents (Connor and Stevens, 1971; Connor et al., 1977). The intact Connor-Stevens model demonstrates type I excitability, but with the A-type conductance effectively turned off, the Connor-Stevens model demonstrates class II excitability. Thus, a neuron's contingent of membrane

conductances determines its class of excitability, and manipulation of conductances can cause a switch between them by altering the mechanism of spike initiation.

While the simplest instantiations of class I and II excitability can be accomplished with relatively few variables, neurons are actually high dimensional dynamical systems whose electrical activity is influenced by a large contingent of membrane conductances. Detailed studies of the interactions between membrane conductances and the electrophysiological properties of neurons have revealed that each conductance affects multiple aspects of the spiking behavior of individual neurons, and most electrophysiological properties of a neuron are influenced by multiple conductances (Prinz et al., 2003b; Gunay et al., 2008; Taylor et al., 2009). Neuronal recordings can be matched by non-unique combinations of channel densities, possibly reflecting how neuronal activity patterns can be similar across neurons despite conductance density variability observed across neurons (Turrigiano et al., 1995; Desai et al., 1999; MacLean et al., 2005; Marder and Bucher, 2007). By independently varying conductance density parameters for 8 conductances in a single compartment model of a lobster stomatogastric neuron, Prinz and colleagues demonstrated that silence, spiking, busting, and irregular spike patterns were all achievable by several, markedly different contingents of membrane conductances (Prinz et al., 2003b). Furthermore, close matches to normal bursting patterns observed experimentally for these neurons also resulted from very different combinations of conductances, suggesting that neurons and are not limited to a specific balance between conductances to achieve functional spiking. It is significant to note that physiological properties typically vary smoothly over large regions of conductance parameter space (Foster et al., 1993; Olypher and Calabrese, 2007), and

multidimensional ‘solution spaces’ connect singular parameter sets that give good matches to data. Using a similar brute-force approach as Prinz et al., Gunay and colleagues demonstrated that distributions within a database of spiking measures from multi-compartmental globus pallidus (GP) neuron models, e.g. spike width, depth of after-hyperpolarizations (AHPs), and the frequency-injected current relationship (FI curve), reproduce the variability observed between measurements made from these neurons *in vitro* (Gunay et al., 2008). Thus, the complex electrical behavior of individual neurons and variability between neurons of a given type can be explained in large part by the membrane conductances which they express.

Experimental manipulation of neurons, particularly using electrophysiological techniques in combination with pharmacological blockers of membrane conductances, has generated a multitude of data revealing the complex interplay between chemical and electrical behaviors of neurons. It is important to keep in mind however, that experimental control of a neuron’s membrane voltage using voltage clamp or dynamic clamp techniques is limited to the region of membrane local to the experimental electrode, a limitation termed ‘space clamp error.’ In nearly all cases the electrode is targeted to the soma, affecting the dendritic membrane to a lesser degree depending on the morphology and passive and active properties of the dendrite. Thus, current injections or application of conductance waveforms to the soma are useful for studying neuronal dynamics and synaptic integration to precisely the extent that the soma is representative of the synaptic input processing of the neuron as a whole.

Dendritic integration. The architecture of the dendritic tree is a critical feature of the computational machinery employed by neurons with diverse functional objectives

(Mainen and Sejnowski, 1996; Vetter et al., 2001; Krichmar et al., 2002; Stiefel and Sejnowski, 2007; Chen et al., 2009; Komendantov and Ascoli, 2009). In electrotonically compact neurons or in models that lack a spatially extended dendrite, synaptic inputs impinge relatively directly on the intrinsic machinery of spike generation. In such cases, space clamp error is of minimal consequence. Early studies viewed the passive properties of dendrites as a challenge to the efficacy of distal synaptic inputs to affect somatic spiking (Rinzel and Rall, 1974). However, subsequent experimental (Amitai et al., 1993; Cauller and Connors, 1994; Lipowsky et al., 1996) and modeling investigations of distal dendritic inputs (Spruston et al., 1993; Mainen and Sejnowski, 1996) demonstrated that dendritic sodium currents can compensate for passive attenuation in the dendrite. Hanson and colleagues observed that sodium channels can be clustered near excitatory synaptic inputs on the dendrites of GP neurons suggesting local amplification of excitatory postsynaptic potentials (EPSPs) (Hanson et al., 2004). The diversity of dendritic conductances and their patterns of distribution throughout the dendritic tree continue to be a topic of significant interest. Dendritic conductances can not only amplify synaptic currents but can lead to a complex profile of total membrane conductance activated by synaptic activation thereby reshaping the ‘effective input’ of the synapse (Acker et al., 2003). Co-localization of ion channels into membrane micro-domains can create highly specialized functional units of dendritic integration often, but not exclusively, organized on or around dendritic spines (Ngo-Anh et al., 2005). In particular, calcium activated potassium currents are often co-localized with the membrane conductances that serve as their sources for calcium (Marrion and Tavalin, 1998; Bowden et al., 2001; Loane et al., 2007).

Phase Response Curve Analysis

Phase reduction. Neurons and neuron models with class I or II excitability spontaneously fire action potentials rhythmically, or can be driven to do so by tonic injection of a small amount of current. When the rhythm is stable and unperturbed, i.e. a stable limit cycle, the membrane voltage follows a repeating trajectory through the spike waveform, AHPs, and leading again to threshold and the next spike. Likewise, the activation states of all conductance gates, e.g. m, h, and n gates for sodium and potassium conductances, follow a repeating trajectory during the intrinsic spiking rhythm. Thus, during spontaneous spiking, these systems (neurons) are well described as oscillators such that all of the dynamic variables (voltage and gates) can be reduced to a single variable, the phase of the oscillation. Phase can be expressed as the time since the most recent spike (t) divided by the intrinsic period (T), t/T, and essentially represents the states of all dynamic variables at a single time-point within the spiking rhythm.

PRC derivation. Small current or conductance inputs delivered at different phases of the intrinsic spiking rhythm perturb the membrane voltage. These perturbations correspond to shifts in the effective phase of the oscillation, since after the stimulus the spiking rhythm returns to its rhythmic spiking pattern but is advanced or delayed in time relative to the unperturbed spiking rhythm. Most importantly, the difference between the new effective phase and the unperturbed phase, i.e. the phase shift, depends on when the perturbation was delivered during the spiking rhythm. The phase response curve (PRC) is obtained by plotting the advancement or delay of the spiking rhythm against the input phase for perturbations sampling the entire intrinsic period (Glass and Mackey, 1988; Izhikevich, 2006). All PRCs in this text are plotted such that positive values correspond

to advancements of the spiking rhythm in response to depolarizing perturbations, and negative values reflect that the next spike was delayed.

Two general classes of PRC with distinct functional consequences for network dynamics are defined more or less precisely by their shape. Type I PRCs are characterized by being composed purely of positive values, indicating that depolarizing input delivered at any point within the intrinsic spiking rhythm advances the phase of the oscillation. However, a small negative region very early in the PRC (corresponding to stimulus delivery during the down-stroke of an action potential) may not disqualify a PRC as type I (Rinzel and Ermentrout, 1998; Oprisan and Canavier, 2002). Type II PRCs, by contrast, contain a significant negative region in addition to one or more positive regions, indicating that excitatory inputs can paradoxically delay the next spike event when delivered at some phases of the intrinsic spike cycle.

Weak coupling and the infinitesimal PRC. When the inputs used to derive a PRC are sufficiently small, there is little effect on the activation states of the intrinsic conductances, and the perturbation is equivalent to a transient jump of fixed magnitude in the membrane voltage. Within this range of stimulus amplitudes, termed the 'weak coupling domain', the PRC scales linearly with input strength such that, for example, a 2 pA current pulse will evoke exactly twice the phase shift of a 1 pA input. Thus, within the weak coupling domain the shape of the PRC is an invariant neuronal property called the infinitesimal PRC (iPRC).

To make PRC analysis analytically tractable, it is most commonly implemented *in silico* using brief, weak perturbations that adhere to the weak coupling assumption. These inputs are typically applied to simple neuron models that lack a recognizable

morphology and a full contingent of membrane conductances. Under such idealized circumstances the form of a neuron's phase response curve (Hansel et al., 1995) reflects the intrinsic mechanism of spontaneous spiking (Rinzel and Ermentrout, 1998) and maps onto Hodgkin's classes of neuronal excitability (Hodgkin, 1948) such that type I PRCs result from neurons with class I excitability. However, in neuron models with spatially extended dendrites, passive processing of dendritic inputs can significantly affect the shape of the PRC without affecting the axo-somatic spiking mechanism (Goldberg et al., 2007).

Averaging. In complex neuronal networks, each neuron is likely to receive many inputs from the other neurons during each spike cycle. This presents a host of potential nonlinear effects of multiple stimuli on the spiking pattern of a given postsynaptic neuron. For example, the activation states of intrinsic conductances in the membrane of the postsynaptic neuron will be perturbed, and as a consequence, multiple inputs may sum supra-linearly if sodium conductance in the postsynaptic membrane is brought near the steep part of its activation curve. Conversely, multiple conductance inputs may sum sub-linearly if the local membrane voltage is pushed near to the excitatory reversal potential reducing the synaptic driving force. In many cases, therefore, it is useful to reduce the complexity of such systems by making simplifying assumptions, e.g. that neurons of the network are identical and connectivity between them is weak. If the inputs to a postsynaptic neuron from the other members of a network are sufficiently small, it can be assumed that their effect on that neuron's spike timing will be the linear sum of the individual perturbations. Therefore, the effective perturbations caused by synaptic inputs to each neuron in a connected network can be described by the convolution of the

iPRC with the synaptic current waveform (Ermentrout and Kopell, 1991). In the weak coupling domain, these can be averaged across the spike cycle allowing the derivation of phase distributions and prediction of stable phase-locked modes for networks with well defined connectivity architectures (Ermentrout and Kopell, 1991; Nakao et al., 2007).

In some systems, synaptic inputs do seem to adhere to the weak coupling assumption (Butera and Preyer, 2006), but there is no reason *a priori* to expect this convenience. Acker and colleagues determined that physiological inputs to layer II stellate cells of medial entorhinal cortex violate the weak coupling assumption (Acker et al., 2003). By generating spike time difference maps describing the evolution of synchronous states from asynchrony in 2-neuron networks, Acker et al. also evaluated the effects of varying conductance densities of a slow potassium current and the hyperpolarization activated mixed-cation current (h-current). When these 'slow' conductances were strong, the strength of inputs to the model was effectively increased, yielding nonlinear increases in the phase shifts evoked by stimuli. Similarly, when input strength is outside the domain of weak coupling, the resultant voltage deflection is sufficient to evoke membrane conductances in nonlinear fashion causing deviations in the shape of derived PRCs from the shape of the iPRC. Thus, there is a bidirectional relationship between input strength and active membrane conductances such that strong inputs activate conductances more strongly, and high densities of active conductances can make inputs effectively stronger. However, Netoff and colleagues demonstrated that predictions made based on weak coupling can be valid even when nonlinear effects of stimuli are evident (Netoff et al., 2005a).

Active Conductances and PRC Modulation. The contributions of active conductances to neuronal phase response curves has been typically investigated by evaluating the additional contribution of a single active conductance to the dynamics of a well-analyzed canonical model of type I or type II excitability. For example, Ermentrout et al (2001) and Gutkin et al (2005) evaluated the contribution of a spike frequency adaptation (SFA) potassium current to skewness of PRCs and the consequent emergence of network synchronization using a theta model of type I excitability. Recently, Stiefel et al. (2008a) demonstrated that in principle cholinergic modulation of cortical pyramidal neurons could switch the PRC from type II to type I as a consequence of SFA current (I_M) down regulation. Stiefel and colleagues (2008b) also provide *in vitro* evidence that such switching can occur with modulation.

Modulation of the Globus Pallidus. Recent work has focused on the presence of neuromodulatory projections to GP and on the effects of neuromodulators on spiking patterns and physiology of GP neurons in normal animals and PD models. Bouali-Benazzouz et al. observed that injection of 6-hydroxydopamine (6-OHDA) into GP of urethane-anaesthetized rats reduced spike rates without changing the proportions of recorded GP neurons exhibiting regular, irregular, or bursting firing patterns (Bouali-Benazzouz et al., 2009). The injection of 6-OHDA in GP, however, caused not only degeneration of dopaminergic projections to GP from the substantia nigra pars compacta (SNpc) but also killed approximately 50% of neurons in SNpc reducing the dopaminergic innervation of striatum as well. In normal animals GP also receives serotonergic modulation from the dorsal raphe nucleus, and this innervation also degenerates with PD (Jellinger, 1991). Several studies have identified both pre- and postsynaptic effects of

serotonin modulation on inhibitory and excitatory synapses within the pallidum as well as serotonergic modulation of the hyperpolarization-activated cation current (h-current) in GP neurons through activation of multiple serotonin receptor subtypes (Querejeta et al., 2005; Di Giovanni et al., 2006; Kita et al., 2007; Chen et al., 2008; Hashimoto and Kita, 2008; Rav-Acha et al., 2008). Removal of dopaminergic and serotonergic modulation of GP neurons occurring with PD may affect their physiology and the shape of corresponding PRCs through alteration of membrane conductances, but these effects have not been investigated directly.

Entrainment and Stochastic Synchronization. In response to noisy current injection, neurons fire spikes stochastically, however, the pattern of spikes is remarkably reliable across trials with the same noisy input (Mainen and Sejnowski, 1995). By extension, when a population of neurons receives common synaptic inputs from one or a set of presynaptic neurons, the spike patterns exhibited by the postsynaptic population can be very similar to one another. Thus, although each neuron may fire stochastically, there is synchrony across the population of postsynaptic neurons in the timing of spikes, a phenomenon termed stochastic synchronization (Galan et al., 2006). The degree of stochastic synchronization that occurs depends on the strength of the correlation between inputs to different postsynaptic neurons and the similarity of postsynaptic neurons to each other. Recent evidence has demonstrated that neuron models with type II phase response curves spike more reliably (Galan et al., 2007b) and synchronize more readily than models with type I PRCs in response to correlated noisy inputs at all levels of input correlation (Galan et al., 2007b; Marella and Ermentrout, 2008; Abouzeid and Ermentrout, 2009).

High conductance states of neurons in vivo. PRC analysis typically focuses on the responses of neurons during spontaneous pacemaking. These methods have been extended fruitfully to describe the relationship between PRCs and stochastic synchronization of uncoupled populations of neurons receiving correlated noisy inputs as an experimental stimulus. Neurons under *in vivo* conditions are subject to high rates of synaptic inputs putting each neuron in a state of high conductance. Such high conductance states affect neuronal dynamics, integration, and spiking behavior in several ways (Destexhe and Pare, 1999; Rudolph and Destexhe, 2001; Destexhe et al., 2003; Rudolph and Destexhe, 2003b, a). The neuronal response function during high conductances states is altered such that: 1) A neuron's responsiveness to small amplitude inputs is augmented through a process similar to stochastic resonance; and 2) the elevated membrane conductance resulting from ongoing backgrounds of synaptic inputs attenuates responsiveness to high amplitude inputs. Whereas inputs to a quiescent neuron yield output spiking only when they cross a relatively sharp threshold, these effects of high conductance states yield a smoother neuronal response function allowing graded response probability to inputs of increasing amplitude (Destexhe et al., 2003).

High conductance states also affect the intrinsic excitability of neurons *in vivo*. Because neurons maintain a depolarized membrane potential during high conductance states, the activation levels of membrane conductances are elevated relative to quiescence. This can switch a neuron's class of excitability by recruiting additional voltage-gated conductances in the near-threshold voltage range that are not strongly activated during pacemaking (Prescott et al., 2006, 2008). Thus, high conductance states represent a distinct mode of neuronal dynamics *in vivo*, and although it is likely that they

will significantly affect mechanisms of synaptic integration and the effects of individual inputs on spike timing, the consequences of high conductance states for neuronal PRCs have not been analyzed.

Phase Response Analysis of a Morphological GP Neuron Model

Spatially Distributed Inputs to GP. The normal firing patterns of GP neurons *in vivo* are notably asynchronous (Bar-Gad et al., 2003), perhaps as a consequence of local inhibitory collaterals which terminate perisomatically in basket-like structures and yield approximately 10-20% of the GABA synapses onto GP neurons (Millhouse, 1986; Kita, 1994; Kita and Kitai, 1994a; Sato et al., 2000; Sadek et al., 2007; Sims et al., 2008). It is therefore particularly significant that, with PD, GP neurons become synchronous at fast single spike time-scales and fire synchronous bursts of action potentials that are phase-locked to oscillations in other basal ganglia nuclei. GP neurons are oriented perpendicular to inhibitory

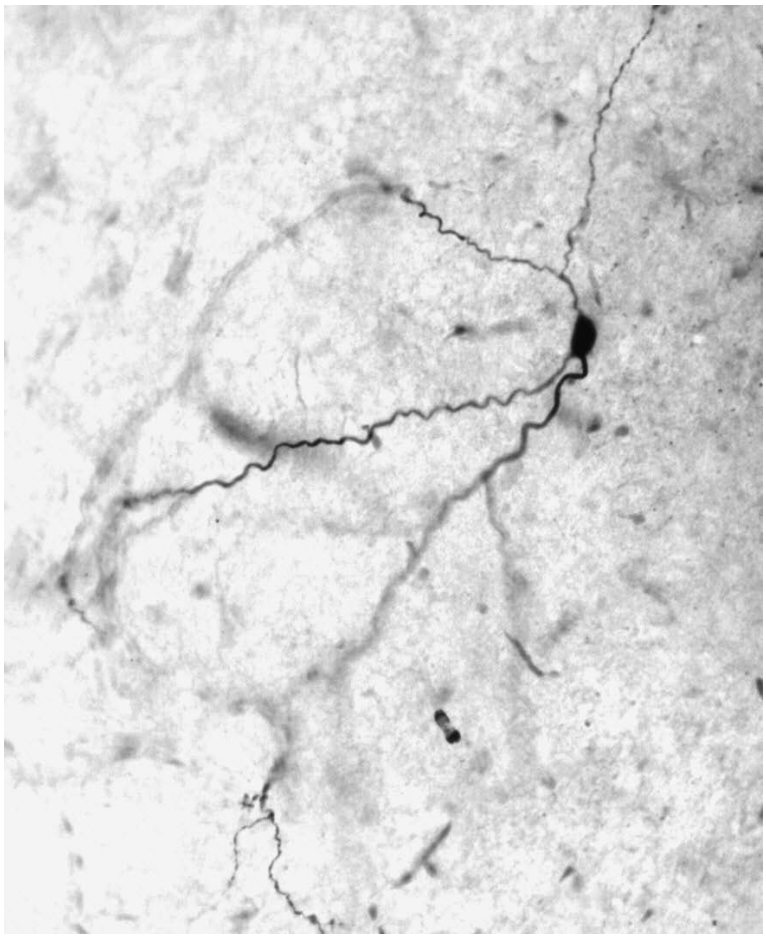

Figure 1. Photograph of the biocytin-filled GP neuron that was reconstructed to give the morphology of our GENESIS model.

inputs from striatum such that different regions of dendrite are likely to sample inputs from different populations of striatal neurons. This arrangement suggests the possibility of a topographic pattern of synaptic connectivity that separates perisomatic from distal dendritic inputs to any given GP neuron. The graded distribution of Ca_{HVA} channels along the length of GP dendrites (Hanson and Smith, 2002) further suggests a division of labor between perisomatic and distal dendritic membrane for calcium-dependent input processing. It is unclear whether excitatory subthalamic inputs to GP are spatially organized, but if so, distal dendritic inputs from STN could selectively activate spatially distinct conductance-based mechanisms of synaptic integration. Therefore, the morphology of GP neurons seems to be a key element in the functional architecture of pallidal and basal ganglia networks.

Morphological GP neuron model. The reduction of complex neuronal dynamics to a minimal set of dynamic variables is not likely to adequately represent the functional machinery of neurons *in vivo*. Furthermore, the spatial distribution of active conductances throughout the dendritic morphology and specialized mechanisms of synaptic integration make it unlikely that point neuron models are capable of the computational compartmentalization exhibited by real neurons. These factors constrain the utility of networks of simple phase models for capturing the potential repertoire of complex network dynamics.

Such high dimensional systems as neurons can be challenging to model without sacrificing potentially essential dynamics in favor of computational efficiency. Using a morphologically reconstructed model of a biocytin-filled GP neuron (Figure 1) and a database strategy, we have previously investigated the influence of conductance densities

on the electrophysiological behaviors of GP neurons (Gunay et al., 2008). These efforts provided considerable insight into the multidimensional solution space that gives realistic GP physiology. Next, we used a semi-automated iterative process to fine-tune parameters yielding a base model, GP_{base}, defined by a parameter set situated within a large continuous parameter space across which physiological measures varied smoothly. Importantly, the sparse, sprawling dendrite possesses spatially-distributed conductances important for the physiology of GP neurons (Hanson and Smith, 2002; Hanson et al., 2004) and allowing synaptic integration that is not dominated by the conductances contributing to spike generation.

Morphological modeling approach to PRC analysis of GP. PRC analysis is a powerful technique bridging the single neuron and network levels of computational complexity. The approach taken in the studies described in this thesis focuses on the interactions of the intrinsic properties of GP neuron models with the synaptic inputs they receive. We apply phase response curve analysis to our GP_{base} model in order to characterize mechanisms of synaptic integration at the soma and throughout the dendrite during intrinsic pacemaking and in the presence of *in vivo*-like backgrounds of stochastic synaptic input. So doing, this thesis targets computation in GP neurons in order to elucidate synchronization of pallidal networks and entrainment to cortical oscillations. In chapter 2 we identify and characterize intrinsic mechanisms underlying the shape of somatic and dendritic PRCs and evaluate the effect of spike frequency on PRC shape. We also vary widely conductance parameters of the GP_{base} model to evaluate the robustness of our results to potential variability across GP neurons and the effects of potential targets of modulation. These manipulations also serve to demonstrate that our

results are not particular to the specific parameter choices incorporated in our base model. In chapter 3 we extend these investigations to address high conductance states of GP neurons *in vivo*. We first evaluate the consequences of elevated membrane conductance on the somatic and dendritic PRCs and compare these results to those obtained during spontaneous pacemaking. Next we analyze on a trial-by-trial basis the ways in which phasic synaptic inputs interact with coincident fluctuations in the applied synaptic background activity. Finally, we develop a method for describing the phase response properties of GP neurons during *in vivo*-like high conductance states that illustrates the distinct contributions of intrinsic and synaptic effects on spike timing elicited by phasic inputs delivered against stochastic synaptic backgrounds. Taken together these investigations extend conventional phase response methods to highlight the importance of the neuronal morphology, spatially-distributed membrane conductances, and the *in vivo* conditions that control neuronal spike timing.

Chapter 2

Phase response curve analysis of a full morphological globus pallidus neuron model reveals distinct perisomatic and dendritic modes of synaptic integration

*Published (Schultheiss et al., 2010)

Abstract

Synchronization of globus pallidus (GP) neurons and cortically-entrained oscillations between GP and other basal ganglia nuclei are key features of the pathophysiology of Parkinson's disease. Phase response curves (PRCs), which tabulate the effects of phasic inputs within a neuron's spike cycle on output spike timing, are efficient tools for predicting the emergence of synchronization in neuronal networks and entrainment to periodic input. In this study we apply physiologically realistic synaptic conductance inputs to a full morphological GP neuron model to determine the phase response properties of the soma and different regions of the dendritic tree. We find that perisomatic excitatory inputs delivered throughout the inter-spike interval advance the phase of the spontaneous spike cycle yielding a type I PRC. In contrast, we demonstrate that distal dendritic excitatory inputs can either delay or advance the next spike depending on whether they occur early or late in the spike cycle. We find this latter pattern of responses, summarized by a biphasic (type II) PRC, was a consequence of dendritic activation of the small conductance calcium-activated potassium current, SK. We also evaluate the spike-frequency dependence of somatic and dendritic PRC shapes, and we demonstrate the robustness of our results to variations of conductance densities,

distributions, and kinetic parameters. We conclude that the distal dendrite of GP neurons embodies a distinct dynamical subsystem that could promote synchronization of pallidal networks to excitatory inputs. These results highlight the need to consider different effects of perisomatic and dendritic inputs in the control of network behavior.

Introduction

The emergence of synchronous activity in neuronal networks can result from changes in the synaptic response function of component neurons described by the phase response curve (PRC). The PRC is constructed by plotting spike time shifts caused by inputs at different times within the spike cycle. Type I PRCs for excitatory (inhibitory) stimuli are composed predominantly of positive (negative) values indicating that inputs throughout the spike cycle advance (delay) the next spike. In contrast, type II PRCs contain both positive and negative regions indicating that excitatory inputs can either advance or, paradoxically, delay the next spike depending on input phase. Type II PRCs have been related extensively *in vitro* and *in silico* to synchronization of connected neuronal networks with particular architectures (Hansel et al., 1995; Ermentrout, 1996; Crook et al., 1998b, a; Ermentrout et al., 2001; Netoff et al., 2005a; Netoff et al., 2005b; Goldberg et al., 2007; Achuthan and Canavier, 2009; Bogaard et al., 2009) and of uncoupled neurons receiving correlated inputs (Galan et al., 2007b; Marella and Ermentrout, 2008; Abouzeid and Ermentrout, 2009).

Recent experimental and theoretical studies have demonstrated that passive dendritic filtering of inputs and the contributions of active membrane currents are critically involved in shaping the PRC and therefore network dynamics (Crook et al., 1998b, a; Gutkin et al., 2005; Goldberg et al., 2007; Stiefel et al., 2008; Stiefel et al., 2009). Sensitivity of the PRC to neuromodulation may underlie switching between different network functional states (Stiefel et al., 2008; Stiefel et al., 2009), and chronic alterations of functional network connectivity or removal of modulation are related by their effects on phase response properties to pathological network synchronization

characteristic of epilepsy (Netoff et al., 2004; White and Netoff, 2008), which may similarly apply to Parkinson's disease (PD).

Synchronized oscillations and bursting in basal ganglia (BG) structures are key features of the pathophysiology of PD, and several physiological studies (Plenz and Kitai, 1999; Magill et al., 2000, 2001; Loucif et al., 2005) and network simulations (Terman et al., 2002) suggest that the GP-Subthalamic Nucleus (STN) feedback loop within the BG can promote oscillatory pattern generation (Bevan et al., 2002). Furthermore, recent evidence indicates an orchestrating role for GP in the β-frequency synchronization of BG activity in PD (Mallet et al., 2008). To elucidate how cellular properties of GP neurons may be involved in the emergence of synchronous states, it is important to examine what conditions can support biphasic PRCs. We used a well-characterized, full morphological GP neuron model (Gunay et al., 2008) to determine how PRCs of these neurons may depend on input characteristics and intrinsic cellular mechanisms. Using a model analysis allowed us to fully trace the parameter dependence of PRC shape and circumvented the experimental problems underlying accurate PRC estimation due to intrinsic spike cycle variability, which is prominent in GP (Deister and Wilson, 2008). We found that perisomatic PRCs in GP model neurons were type I, whereas distal dendritic excitatory inputs yielded type II PRCs due to local activation of the small conductance calcium-activated potassium current (SK) at the site of stimulation. The influence of this dendritic SK mechanism on spike timing is likely to promote GP synchronization and entrainment to oscillatory STN inputs that are prominent in PD.

Methods

Simulations were run on Emory University High Performance Compute Clusters (Sun Microsystems) using the GENESIS simulation platform (www.genesis-sim.org/GENESIS). Approximately 1.5 min of processor time was required to simulate one second of data with 20 μs time steps using the full 585-compartment GP neuron model. Custom routines were written using Matlab (The MathWorks, Natick, MA) for the analysis of voltage, current, conductance, and spike time data.

GP Neuron Model

Morphology and Passive Electrical Properties. The morphology and passive electrical properties of our baseline GP neuron model (GP_{base}) were determined as previously described (Hanson et al., 2004; Gunay et al., 2008). Briefly, the Neurolucida (MicroBrightField, Inc.) reconstruction of a GP neuron that showed electrophysiological properties (spike width, spike height, input resistance, spike adaptation) typical of GP neurons in our recorded population of GP neurons (Gunay et al., 2008) was converted to a GENESIS morphology file using CVAPP software (www.compneuro.org). The resultant somato-dendritic morphology contained a spherical soma and 511 dendritic compartments (Fig. 2.1A), each no more than 0.02 lambdas in electrotonic length. Matching of the model to experimental voltage responses was achieved by setting passive biophysical parameters as follows: specific membrane capacitance (C_M=0.024 F/m^2), specific membrane resistivity (R_M=1.47 Ωm^2), & specific axial resistivity (R_A=1.74 Ωm). To allow axonal spike initiation and realistic axonal current sources and sinks, a standard axon consisting of a highly excitable axon initial segment and nodes of Ranvier separated

by myelinated inter-node segments, was adapted from Shen et al. (1999) and attached to the soma.

Active Conductances. Based on experimental evidence of their presence in GP neurons, one calcium-activated conductance and eight voltage-gated membrane conductances were added to the soma and dendrite of the passive model. Because distinct electrophysiological cell types are not apparent in GP when examined with rigorous statistical tests (Gunay et al., 2008), we made a single active model resembling the mean behavior of recorded GP neurons. The voltage-gated conductances were modeled using standard Hodgkin-Huxley equations and included the following channel types: fast-transient and persistent sodium currents, NaF & NaP (Magistretti and Alonso, 1999; Magistretti et al., 1999; Raman and Bean, 2001; Magistretti and Alonso, 2002; Khaliq et al., 2003; Hanson et al., 2004; Mercer et al., 2007); fast and slow delayed-rectifier (K_{dr}) potassium currents, K_V3 & K_V2 (Baranauskas et al., 1999; Baranauskas et al., 2003); A-type potassium current, which we modeled as two channel populations in order to accurately match fast and slow components of the inactivation kinetics, K_V4F & K_V4S (Tkatch et al., 2000); M-type potassium current, KCNQ (Gamper et al., 2003; Prole and Marrion, 2004); hyperpolarization-activated mixed cation current, or h-current, which we also modeled as two channel populations, HCN1 & HCN2 (Wang et al., 2002; Chan et al., 2004); and a high-voltage-activated calcium current (Ca_{HVA}) representing a mixture of L-, N-, and P/Q-type currents. The calcium dependence of the small-conductance calcium-activated potassium current (SK) (Hirschberg et al., 1998a; Xia et al., 1998; Hirschberg et al., 1999; Keen et al., 1999) was modeled using the Hill equation. Table 1 in the online supplemental materials lists the activation and inactivation

parameters for the conductances implemented in GP_{base}, and Supp. Fig. 2.1 illustrates the steady-state voltage or calcium dependencies of activation and inactivation gates for each channel type.

Conductance Distributions and Density Tuning. Each conductance was distributed uniformly throughout the dendrite with the exception of Ca_{HVA} whose density was greater in thinner dendritic compartments (Hanson and Smith, 2002). Since dendritic diameter tapered further from the soma, the highest densities of Ca_{HVA} occurred at distal regions of dendritic branches.

During the original tuning process, somatic and dendritic conductance densities were determined using a semi-automated process comparing model behaviors with physiological recordings, and a thorough exploration of parameter space was performed (Gunay et al., 2008). For this study, we updated the model to incorporate recent data describing ion channel kinetics in GP (Mercer et al., 2007) and used conductance densities within the previously explored parameter space that provided a good match with physiological current clamp data (see supplemental tables 1 and 2 for final parameters). The resultant base model, GP_{base}, exhibited a spontaneous spike waveform closely matching the average spike from 50 recorded GP neurons (Fig. 2.1B) and fell well within the limits of physiological variability for spontaneous spike frequency (Supp. Fig. 2.3A), the somatic FI curve (Fig. 2.1D), spike frequency adaptation (SFA) and spike height attenuation (SHA) during positive current steps, voltage 'sag' (a consequence of h-current activation) during negative current steps, and latency to the first spike following the offset of negative current steps (Supp. Fig. 2.2). The K_V2 and K_V3 conductances, in the model as in GP neurons, were the primary contributors to the delayed rectifier current

(Baranauskas et al., 1999), and the peak amplitudes of the respective currents were similar (Fig. 2.1C). The conductance density and somato-dendritic distribution of the small-conductance calcium-activated potassium current, SK, were the primary determinants of the depth of the mAHP, and together with NaP and KCNQ, contributed significantly to the spontaneous spike frequency (Supp. Fig. 2.3A). Interestingly, the slope of the somatic FI curve was also influenced by the density and distribution of SK conductance (Supp. Fig. 2.3B). To determine the robustness of our PRC findings with this model, we varied key conductance parameters through a large range deviating from the base model (see Results). These manipulations also serve as explorations of potential heterogeneity among pallidal networks and of possible effects of altered modulation of GP neurons. The full GENESIS model used in this study is available for download from ModelDB (http://senselab.med.yale.edu/ModelDB/).

Simulation Protocols

PRC Stimulation Protocol. In 72 separate simulations, inputs were delivered at each of 72 evenly-distributed time points within the first inter-spike interval (ISI) of the control spike train. The onset of the earliest input was timed to be coincident with the somatic spike delineating the start of the spike cycle. Spike times were recorded using the GENESIS spikehistory element which provided precision of 1e-6 s, and input-evoked shifts in spike timing were calculated relative to the spike terminating the first control spike cycle. PRCs were plotted as spike advances (in units normalized to the period of the control ISI) as a function of input phase, such that positive values reflected advancements of the spike cycle. Separate PRCs were constructed for somatic stimulation and for stimulation of 7 dendritic sites each composed of 25 contiguous

compartments. The dendritic sites of stimulation were distributed across the three major branches of the dendrite (Fig. 2.1A) such that the first and second dendritic branches each had proximal and distal stimulation sites ($D1_{P\&D}$ and $D2_{P\&D}$), while the longer third branch had proximal, mid, and distal stimulation sites ($D3_{P,M,\&D}$). In order to conduct PRC analyses during steady state behavior, we let the spontaneous activity of the model settle for a 10 s period and used the first spontaneous spike cycle after this period to apply PRC stimulation. To avoid repeating the simulation of 10 s settling time many times, we saved all state variables in a 'snapshot' file after conducting this simulation once, and used it for all subsequent simulations.

Inputs to the model. Stimuli were either 3 ms square-wave current injections or dual exponential conductance injections representing excitatory AMPAergic (1 ms rise time, 3 ms decay time, $E_{AMPA} = 0$ mV) or inhibitory $GABA_A$ (1 ms rise time, 12 ms decay time, $E_{GABA} = -80$ mV) synaptic inputs. Input strength was manipulated by varying current injection amplitude or the synaptic peak conductance. Current injections or synaptic conductance inputs to dendritic regions were divided evenly amongst the 25 component compartments such that each received 4% of the total reported current or conductance.

Faster Spiking and Higher-Order PRCs. Since GP neurons *in vivo* spike at approximately 30 Hz, we drove the GP model faster than the spontaneous spike frequency by applying tonic inward current to the soma. To test how increasing spike frequency affects the PRC, we derived somatic and dendritic PRCs using 2 nS AMPA inputs while the model spiked at specific rates between 10 and 60 Hz. Applied current

strengths necessary to achieve the desired spike frequencies (± 0.5 Hz) were determined by precise interpolation from the FI curve.

Synaptic inputs to the model, particularly the dendrite, evoked membrane currents that contributed to shifts in spike timing. In many cases the time courses of these evoked currents were not limited to the ongoing ISI, however, so it was necessary to consider multiple spike cycles to capture to full effect of an input. Effects of inputs on the timing of the second, third, and fourth subsequent spikes were calculated to give the F2, F3, and F4 PRCs, respectively. By convention (Preyer and Butera, 2005), these higher-order PRCs were plotted to the left of the primary PRC (F1). The 'permanent' PRC reflects the ultimate advancement or delay of spiking measured after several spike cycles (Prinz et al., 2003a). The permanent PRCs depicted in this report were calculated by summing single-cycle PRCs F1 through F5.

Categorization of PRCs as type I or type II. The distinction between type I and type II PRCs can be somewhat ambiguous. Type I PRCs are characterized by being composed predominantly of positive values for excitatory inputs. However, there may be a small negative region early in phase corresponding to stimulus delivery during the down-stroke of an action potential, without disqualifying the corresponding PRC as type I (Rinzel and Ermentrout, 1998; Oprisan and Canavier, 2002). Using a morphological model compounds this ambiguity, because back-propagating action potentials in the dendrite are wider than somatic spikes, and dendritic stimuli lead to a correspondingly wide negative region in the PRC. To distinguish these effects from dendritic mechanisms responsible for significant delays of spike timing, we limited categorization of PRCs as type II to cases where delays of spike timing were not the consequence of direct

interactions between PRC stimuli and somatic or back-propagating dendritic spikes. This was accomplished by categorizing PRCs using a variant of the r-value convention of Tateno and Robinson (Tateno and Robinson, 2007) as follows: The r-value of a PRC, a measure of how biphasic the PRC is, was defined for this study as the ratio of the negative area of the PRC (absolute value) to the positive area of the PRC (or the inverse of that ratio, whichever was smaller). PRCs were deemed type I when the r-value was less than 0.175, and PRCs were deemed type II when the r-value exceeded 0.175.

Membrane potential and channel current analysis. To characterize the size and spatial decay of voltage transients in response to inputs we recorded membrane voltage at the soma, axon, and dendritic sites in each simulation. Dendritic voltages were recorded from the middle and edge compartments of each of the 7 sites of dendritic stimulation (Fig. 2.1A). In addition we recorded current traces for each type of membrane conductance at the soma, axon, and the 7 dendritic sites used for stimulation. Current traces described in this report as 'somatic' reflect the sum of currents from the soma and hillock, and recordings of currents from any of the 7 dendritic sites reflect sums taken across the compartments composing that site.

To evaluate the contributions of membrane currents to input-evoked shifts in spike timing, we calculated 'difference' or 'evoked' currents by subtracting current traces from control simulations (without stimulus) from the corresponding stimulated traces. This subtraction isolated the *evoked* component of membrane current flows.

Results

Responses to Weak Phasic Inputs

Much of conventional PRC theory relies on the assumption that inputs to a neuron are weak such that multiple inputs within a spike cycle result in the linear sum of the corresponding individual phase perturbations. Within the 'domain of weak coupling', the PRC scales linearly in amplitude as a function of input strength, because two inputs arriving simultaneously have exactly twice the effect on spike timing as one input of the same strength. Thus, for sufficiently weak inputs the normalized PRC has a static shape called the 'infinitesimal' PRC (iPRC). However, realistic synaptic conductances can violate the assumption of weak coupling causing the measured phase response curve to deviate from the iPRC (Acker et al., 2003; Netoff et al., 2005a). To evaluate the range of weak input strengths for which the somatic PRC scales linearly in our GP model, we applied 3 ms square-wave somatic current steps of varying amplitude at different phases of the spontaneous spike cycle and measured the resultant shifts in spike timing. Depolarizing current pulses elicited advances of the spontaneous spike rhythm that persisted indefinitely (Fig. 2.2A&B). For these inputs (<=100 pA) there were no higher order effects of somatic stimuli on phase, i.e. all ISIs after the stimulated spike cycle were equal in duration to the spontaneous period (Fig. 2.2A). The magnitude of phase advancement varied smoothly with input phase (the PRC), showing greater sensitivity to inputs in the last quarter of the spike cycle and relative insensitivity to inputs arriving during the first half of the spike cycle (Fig. 2.2C). The somatic PRC was type I, because it was composed purely of positive values reflecting that depolarizing inputs at any phase of the spike cycle advanced the next spike. The positive peaks of normalized somatic

PRCs obtained with stronger inputs occurred earlier in the spike cycle (Fig. 2.2C), indicating a deviation from linearity and thus the mathematical domain of weak coupling already at input amplitudes below 100 pA. Another non-linearity was evident when 3 ms negative current injection pulses were applied: Within the domain of weak coupling, the iPRC obtained using positive current pulses should be an exact mirror image of that obtained with negative pulses. We observed that only for very small stimuli was the spike delay caused at different input phases equal and opposite to the spike advance caused by positive current pulses of the same amplitude. Hyperpolarizing stimuli of increasing amplitude yielded PRCs that scaled much more linearly than those obtained with depolarizing inputs of the same amplitudes, suggesting that even small amounts of depolarization caused the activation of non-linear response properties. This leads to a fundamental difference in phase response properties between inhibitory and excitatory stimuli not predicted by PRC theory.

To delimit the domain of weak coupling for somatic inputs in our GP model we examined the features of the PRC that were most sensitive to input strength and used them as a means to evaluate the convergence of PRC shape to the iPRC. The peak of the somatic PRC occurred later in the spike cycle for weaker depolarizing inputs (Fig. 2.2C) and converged to a phase of ~0.903 for inputs of 7.5 pA or less (Fig. 2.2G, solid black line). At this amplitude, PRCs also became symmetrical for depolarizing and hyperpolarizing stimuli (Fig. 2.2H), again indicating that 7.5 pA stimulus amplitude was the upper limit for linear phase response behavior in a strict sense.

Next, we compared the effects of phasic somatic inputs on output spike timing with inputs delivered to a distal dendritic site ($D3_D$, Fig. 2.1). Because the local input

resistance of small dendrites is much higher than that of the soma, the voltage response to current injection of equal amplitude is greater. For example a 10 pA 3 ms stimulus at 0.5 phase resulted in a 0.4 mV peak voltage deflection in the soma, whereas the amplitude of the local voltage deflection in the distal dendrite ($D3_D$ site) was 9.0 mV in response to the same stimulus. Therefore, the domain of weak coupling for dendritic stimuli was even smaller than for the soma, and divergence for our 2 measures of linearity (peak shift, Fig. 2.2G and peak symmetry Fig. 2.2H) was seen for stimuli exceeding just 1 pA amplitude. The resultant distal dendritic iPRC was type I (r-value = 0.066) (Fig. 2.2D&F and Supp. Fig. 2.4), but surprisingly, inputs delivered within a brief time-window just after a spontaneous spike resulted in slight delays of the subsequent action potential. These delays and the corresponding negative region early in the PRC (Fig. 2.2D, inset) were increased with higher input strengths (Supp. Fig. 2.4) and are analyzed in detail below.

Infinitesimal PRCs (1 pA stimuli) for the soma and 7 dendritic stimulation sites are shown in Figure 2.2I. More distal inputs yielded attenuated PRCs with peaks occurring earlier in phase as a partial consequence of passive filtering of inputs by the dendrite (Goldberg et al., 2007). Nonetheless, iPRCs for all regions of the GP model were type I, and they differed smoothly from one another as a function of distance of the stimulation sites from the soma.

Responses to Larger Somatic Current Injections and Realistic Synaptic Inputs

The peak conductance of a single AMPAergic synaptic event is on the order of 250 pS to 1 nS producing a peak synaptic current of approximately 15-60 pA (Hernandez et al., 2006). Thus, in our GP model currents due to the activation of even a single

synapse lie outside the domain of weak coupling that provides a basis for analytical mathematical treatment of PRCs. To address the question of how the input phase of physiologically realistic synaptic input affects spike timing, we delivered stronger current injections or dual exponential AMPA-type or $GABA_A$ conductance inputs to somatic and dendritic sites of the model. Like the weaker inputs discussed above, somatic current pulses of up to 300 pA yielded type I PRCs, and the peak of the somatic PRC occurred earlier in the spike cycle for stronger depolarizing inputs (Fig. 2.3A). This pattern reflects: 1) that maximal sensitivity to weak somatic inputs occurs just before a spike, and 2) the theoretical limit of spike advancement for strong inputs (Fig. 2.3A, long-dashed black line) is reached when a spike is initiated immediately with delivery of the stimulus. Stronger somatic inputs caused the PRC to approach the limit of spike advancement over a larger range of phase. Thus, the peak of the PRC occurred earlier within the spike cycle and the region of the PRC just before the peak became increasingly steep (Fig. 2.3A).

The phase shifts elicited by hyperpolarizing or inhibitory inputs are not bounded by a theoretical limit, since arbitrarily strong inhibitory inputs can theoretically delay subsequent spiking indefinitely. As a result, negative current injection delivered just prior to spike initiation resulted in maximal phase delays (Fig. 2.3D). PRCs resulting from negative current injection scaled nearly linearly with input strength and maintained the same qualitative shape (Fig. 2.3D).

AMPAergic synaptic inputs to the soma elicited a similar pattern of spike advances as did depolarizing current injections (Fig. 2.3A), and the spike delaying effects of somatic GABAergic inputs were similar to those of hyperpolarizing current injections to the soma (Fig. 2.3D). The only notable difference between peak-amplitude-matched

somatic PRCs obtained using synaptic inputs and those obtained using current injections was that the peaks of synaptic PRCs occurred slightly earlier in the spike cycle, both for excitation and inhibition. This effect is likely due to the gradual onset and delayed peak of synaptic inputs compared to the sharp onset of square-pulse current steps, thus giving rise to responses resembling those elicited by current steps occurring slightly later in phase. GABAergic inputs of 0.7 nS to 2.9 nS yielded somatic PRCs that matched in amplitude the somatic PRCs obtained using current injections of -50 pA to -300 pA, whereas AMPAergic inputs of 0.5 nS to 4.2 nS were necessary to match the peaks of somatic PRCs for +50 pA to +300 pA current injections (Fig. 2.3A,D; Supp. Fig. 2.5A,B). Overall, we found good agreement between stimuli using current step inputs or conductance waveform inputs, indicating that probing PRCs with brief current steps does not limit the validity of PRC analysis.

Type II PRCs from Stronger, More Distal Dendritic Inputs

Globus pallidus neurons have long, thin dendrites that create a flat disc-like field up to 1 mm wide and oriented perpendicular to striatal inputs (Park et al., 1982; Yelnik et al., 1984; Kita and Kitai, 1994b). Non-uniform dendritic distributions of membrane conductances (Hanson and Smith, 2002; Hanson et al., 2004) and higher local input resistance at thinner, more distal dendritic segments make it unlikely that inputs to different sites along the length of GP dendrites will evoke equivalent voltage transients. To test how the strength and timing of physiologically realistic inputs to different sites of the dendritic tree affect output spike timing, we constructed PRCs for seven dendritic sites using synaptic inputs of a range of peak conductance amplitudes. In each case PRCs for proximal dendritic inputs were qualitatively similar to somatic PRCs (data not

shown). Surprisingly, larger AMPAergic inputs to the distal sites of the first and second dendrites and to the middle of the longest dendrite ($D1_D$, $D2_D$, & $D3_M$) yielded PRCs with increasing type II character. (PRCs for $D2_D$ are shown in Figure 2.3B, and r-values quantifying the increase in type II character for stronger synaptic inputs are plotted in Supplemental Figure 2.6A.) Whereas $D2_D$ PRCs for excitatory inputs of 0.5 nS and 1 nS were type I (r-values of 0.0183 and 0.0449, respectively), inputs stronger than 1 nS significantly delayed the next spike when delivered any time during the first half of the spike cycle. For AMPAergic inputs of 1.5 nS to 3 nS to $D2_D$, the negative regions of the corresponding type II PRCs (r-values of 0.24 to 0.71) were progressively deeper. Thus, paradoxically, strengthening 'excitatory' synaptic input to $D2_D$ changed the net effect of the input from phase-advancing to phase-delaying for a significant portion of the spike cycle. Increasing AMPA input strength also increased the proportion of the spike cycle for which inputs delayed the subsequent spike. The positive peaks of those PRCs were also increased for stronger excitatory inputs (Fig. 2.3B) resulting in biphasic, type II PRCs of increasing amplitude.

Excitatory synaptic inputs to the distal-most site of the longest dendrite ($D3_D$) yielded type II PRCs for all input strengths tested (r-values >= 4.75 for inputs >= 0.5 nS) (Fig. 2.3C and Supp. Fig. 2.6B), but as was the case for $D2_D$, stronger AMPA inputs to $D3_D$ increased the depth of the negative region in the PRC (Fig. 2.3C). (Note that in Fig. 2.2D, current injections of as little as 10 pA notably increased the type II character of the $D3_D$ PRC.) A prominent step in the depth of the negative region of the $D3_D$ PRC occurred between AMPA input strengths of 0.5 nS (Fig. 2.3C, red line) and 1 nS (Fig. 2.3C, magenta line), but strengthening AMPAergic synaptic inputs beyond 1 nS

increased the amplitude of the $D3_D$ PRC without qualitatively affecting its shape (Fig. 2.3C and Supp. Fig. 2.6B). In general, inputs that were applied at distal dendritic sites shifted spike timing by smaller amounts than stimuli at more proximal sites. Comparing the $D2_D$ and $D3_D$ stimulation sites, the maximal spike advance for stimuli occurring late in phase was reduced approximately 10-fold, however, the spike delays reflected in the negative region of the PRC were of similar magnitude. This indicates that excitatory inputs even at very distal sites can contribute significantly to spike delays resulting from early-phase excitatory inputs.

GABAergic inputs to distal sites of the three major dendritic branches, $D1_D$, $D2_D$, & $D3_D$, yielded monophasically negative, type I PRCs for all input strengths tested (Fig. 2.3E&F). Thus, inhibitory inputs to the distal dendrite delivered at any time within the spike cycle delayed the next spike, and there was no dependence of the qualitative shape of the PRC on the strength of those inputs. Since increasing the strength of inhibitory inputs did not qualitatively affect PRC shape, we hypothesized that intrinsic membrane currents activated more strongly by stronger depolarizing inputs were responsible for the increasing type II character of excitatory distal dendritic PRCs.

Strong AMPA Inputs to D2D Evoked Outward SK Current in Excess of Combined Inward Synaptic and Membrane Currents.

Increasing the strength of excitatory inputs to $D2_D$ transitioned the PRC from type I to type II in a graded fashion (Fig. 2.3B). To evaluate which membrane currents contributed to this transition we compared the local voltage trajectories and patterns of locally-evoked currents for weak and strong inputs to $D2_D$ (Fig. 2.4). Each panel in Figure 2.4 shows voltage or current transients evoked by inputs at three different times

within the spike cycle. Note that the control voltage traces from $D2_D$ (Fig. 2.4A&B, solid black lines) contain attenuated back-propagated spikes of ~5 mV amplitude which delineate the spike cycle, and red and blue dashed traces illustrate advancements or delays of the next spike, respectively.

The gross shape of the PRC for inputs to $D2_D$ can be inferred from inspection of the local voltage trajectories relative to the control. Following the depolarizing transients evoked by 0.5 nS AMPA input to $D2_D$, the local voltage trajectories for stimulated trials converged back towards the control trajectory, but remained slightly depolarized relative to the control until the next spike event (Fig. 2.4A). Thus, 0.5 nS AMPA input at all phases of the spike cycle resulted in spike advances (Fig. 2.4A, red traces). In contrast, following the larger depolarization transients evoked by 2 nS AMPA inputs to $D2_D$, the local voltage trajectories hyperpolarized below the control until the time of the next spike (Fig. 2.4B). For the 'late-phase' stimulus, the next spike occurred almost immediately after the depolarization transient (Fig. 2.4B, red trace) corresponding to an advancement of the spike cycle. However, inputs to $D2_D$ delivered earlier in the spike cycle resulted in delays of the subsequent spike (Fig. 2.4B, blue traces) as the local membrane remained hyperpolarized below control traces.

Figure 2.4 (C&D) depicts the five intrinsic membrane currents evoked most strongly by distal dendritic synaptic inputs in the stimulated compartments. Local voltage transients in response to 0.5 nS and 2 nS inputs to $D2_D$ were approximately 5 mV and 25 mV, respectively (Fig. 2.4A&B). This supralinear relationship between input and response amplitudes was primarily due to stronger activation of inward NaF current by the stronger stimulus (Fig. 2.4C&D, red lines). The most pronounced effect, however, of

strengthening synaptic input to the distal dendrite was the increased local activation of the small conductance calcium-activated potassium current, SK (Fig. 2.4C&D, green lines). The peak of the SK current evoked by the 2 nS input was fifteen-fold that of the 0.5 nS input. Though the peak amplitude of the evoked SK current was smaller than the peak evoked NaF current, the duration of SK activation was much longer lasting, resulting in local hyperpolarization and a net current sink in response to early-phase AMPA stimulation and explaining how excitatory inputs can yield phase delays.

Comparison of voltage-gated and synaptic currents explains somatic type I and dendritic type II PRCs

Whereas $D2_D$ PRCs transitioned from type I to type II for stronger synaptic inputs, somatic PRCs were type I and $D3_D$ PRCs were type II over the entire physiological range of stimulus strengths tested. Figure 2.5 (A-D) shows the local responses to 1 nS AMPA inputs to the soma and $D3_D$ allowing the comparison of voltage and current transients between morphological sites for which identical inputs yielded type I and type II PRCs, respectively. The voltage trajectories elicited by somatic inputs remained depolarized relative to the control until the next spike event (Fig. 2.5A). In contrast, inputs to $D3_D$ evoked larger transients of depolarization (~40mV) followed by deep hyperpolarizations of the local membrane (Fig. 2.5B), similar to the effect of strong AMPA inputs to $D2_D$.

During the spontaneous spike cycle the somatic voltage traversed a much larger sub-threshold range (~10 mV) than did the distal dendritic voltage (<5 mV). Consequently, the contingent of currents evoked locally by somatic AMPA inputs depended more strongly on the phase of the input (Fig. 2.5C) than did the pattern of

currents evoked by inputs to $D3_D$. However, the somatic membrane currents evoked by 1 nS AMPA inputs were insignificant relative to the synaptic current (Fig. 2.5E), because the voltage deflection caused by the stimulus was small. Therefore, somatic inputs resulted in type I PRCs, because for stimuli at all phases of the spike cycle the inward synaptic current overshadowed the net-outward contribution of evoked membrane currents (Fig. 2.5E).

Because action potentials did not back-propagate efficiently into the distal dendrite in our GP_{base} model, the control voltage trajectory at $D3_D$ was relatively flat throughout the spike cycle (Fig. 2.5B). Consequently, the pattern of intrinsic currents evoked by $D3_D$ inputs was relatively independent of input phase. AMPA inputs of 1 nS to $D3_D$ evoked intrinsic membrane currents with a fast inward component and a slower outward component (Fig. 2.5D&F), as follows: Strong, 'fast' NaF current (~30 pA) amplified the immediate depolarization evoked by an input. In turn, higher calcium influx through the high-voltage-activated calcium channel (Ca_{HVA}, the calcium source for SK in the model) elicited greater activation of the long-lasting, 'slow' SK current (peak>20 pA). (Fig. 2.5D). As depicted in Figure 2.5F, the net outward charge transfer by local intrinsic membrane currents at $D3_D$ was sufficiently large to exceed the depolarizing charge carried by the inward synaptic current (Fig. 2.5F).

The Type II Character of Distal Dendritic PRCs Directly Reflects Local SK Conductance

The analysis of membrane currents elicited locally by strong synaptic stimulation of distal dendritic sites indicated that activation of the SK conductance by calcium influx played a predominant role in sculpting type II dendritic PRCs. To test this hypothesis

directly we manipulated the conductance densities of Ca_{HVA} and SK in the distal dendrite. Importantly, the intrinsic spiking rhythm of the model was not disturbed, because this manipulation was limited to the 25 distal dendritic compartments composing the stimulated site ($D2_D$ or $D3_D$). Local up- or down-regulation of Ca_{HVA} and SK in tandem directly scaled the magnitude of SK current evoked at the distal dendrite (Fig. 2.6A&C) and resulted in type II distal dendritic PRCs with deeper or shallower negative regions, respectively (Fig. 2.6B&D). Removal of *either* Ca_{HVA} *or* SK from $D2_D$ eliminated the type II character of the corresponding PRCs almost completely resulting in visually identical type I PRCs (r-values of 0.0351 and 0.0357, respectively) (Fig. 2.6B and Supp. Fig. 2.6C). However, despite the local removal of the Ca_{HVA} or SK conductance, these PRCs still contained shallow negative regions (Fig. 2.6B, asterisks) as a consequence of SK activation in compartments adjacent to the stimulated site. Activation of SK in compartments neighboring the $D3_D$ stimulation site was particularly strong, and $D3_D$ PRCs met our criterion for type II categorization even when Ca_{HVA} or SK was removed from the site (r-values of 0.78 and 0.80, respectively) (Fig. 2.6D and Supp. Fig. 2.6D). Models with different distributions of SK conductance between the soma and dendrite (Supp. Fig. 2.3) also exhibited type II distal dendritic PRCs for which the negative region scaled in depth with the dendritic density of SK irrespective of the somatic SK density (Supp. Fig. 2.7).

Spike Frequency Dependence of Somatic and Dendritic PRCs

Whereas GP neurons in slice typically spike spontaneously at frequencies below 15 Hz, GP neurons *in vivo* spike with a mean frequency of approximately 30 Hz in rodents (Ruskin et al., 1999; Urbain et al., 2000). A change in PRC shape with

increasing firing frequency has been previously described for a simple θ-neuron model and may shift synaptic integration from coincidence detection at low rates to acting as an integrator at high rates (Gutkin et al., 2005). To evaluate the dependence of PRC shape on spike frequency in our full morphological GP neuron model, we drove the model to 10-60 Hz firing frequency with 15-371 pA tonic somatic current injection.

During 7.9 Hz spontaneous spiking, only the ongoing ISI was affected by 2 nS AMPA input to the soma. At this spike frequency, the PRC for the 2nd interval (F2) was therefore flat (Fig. 2.7A3, Fig. 2.8A1) indicating the absence of higher-order effects of synaptic excitation.

During 30 Hz spiking, however, the soma was depolarized by 5 mV on average compared to 10 Hz spiking (Fig. 2.7A1), and 2 nS AMPA inputs were capable of eliciting immediate spike initiation at earlier phases of the spike cycle than during 10 Hz spiking (Fig. 2.7A3&A4). This led to a left shift in the peak of the corresponding F1 PRCs (Fig. 2.8A1) for higher spike frequencies that was gradual between 10 and 60 Hz. During 30 Hz spiking, the activation profile of somatic currents was substantially changed. Notably, when spiking was driven from 10 Hz to 30 Hz, the baseline somatic SK current was elevated from ~50 pA to ~125 pA (Fig. 2.7A2) and stimulus elicited SK transients were additionally enhanced (Fig 2.7A2, asterisk). As a consequence, during faster spiking the somatic SK current activation accompanying spikes triggered by AMPA inputs was greater than the SK current activation accompanying control spikes. Therefore, the mAHP following an AMPA-evoked spike was slightly deeper than the mAHP during control spiking, and the subsequent spike cycle was longer than the control ISI (Fig. 2.7A4). While spike initiation immediately after AMPA stimulation

corresponded to a large phase advance (F1, Fig. 2.8A1), a part of this advance was lost in the 2nd spike cycle following stimulation (F2, Fig. 2.8A1), because this 2nd ISI was longer than the baseline ISIs (Fig. 2.7A4). Therefore, at *in vivo* spike frequencies, an important effect of somatic SK conductance is to resist lasting advancements of the spiking rhythm. By lengthening the spike cycle following an AMPA-evoked spike, somatic SK makes the effect of the input more transient and significantly restores the original pattern of spiking. This effect of somatic SK conductance appears in the single-cycle somatic PRCs as a positive peak in the F1 that is nearly symmetrically opposed by a negative peak in the F2 (Fig. 2.8A1).

The so called 'permanent' PRC (Prinz et al., 2003a) consists of the sum of PRCs for the stimulated spike cycle and all subsequent spike cycles that show changed ISIs compared to baseline. Therefore, the permanent PRC reflects the lasting shift of the spike train (measured after several spike cycles) compared to the control oscillation. For somatic AMPA stimulation the permanent PRC remained type I for all spike frequencies from 10-60 Hz (Fig. 2.8A2), indicating that the spike delay during the F2 period never exceeded the original spike advance in the stimulated spike cycle.

Distal dendritic voltage and current transients elicited by AMPA stimuli were generally unaffected by faster somatic spike rates (Fig. 2.7B1-B3), e.g. the SK transient elicited by input to $D3_D$ was identical at 10 Hz and 30 Hz firing frequencies (Fig. 2.7B3). Nevertheless, the PRC for $D3_D$ stimulation showed a dramatic shift at faster somatic spike rates, because the elicited dendritic SK current had a fixed time course that now showed a different phase relationship with respect to the somatic spike cycle. The PRC of the stimulated spike cycle showed a positive peak shifted to the left, which resulted in

a type I primary PRC for spike frequencies above 30 Hz (Fig. 2.8B1). Because the waveform of AMPA-evoked SK lasted more than 50 ms (Fig. 2.7B3), at spike frequencies above 15 Hz the effect of SK current evoked by late-phase AMPA inputs to the distal dendrite impinged primarily on the 2nd spike cycle (F2) following the stimulus. Consequently, the 2nd ISI was prolonged, and the F2 PRC contained a significant negative peak for late-phase inputs (Fig. 2.8B1). In the case of $D3_D$ stimulation, the delayed spikes in F2 and F3 intervals more than compensated any spike advance occurring in the stimulated spike cycle. The corresponding permanent PRC became entirely negative at spike frequencies above 10 Hz, i.e. a strong AMPA stimulus at any phase of the spike cycle ultimately resulted in a delay of the spike oscillation. Therefore, our model predicts that at *in vivo* spike rates strong AMPA input to the distal dendrites of GP neurons will advance the first subsequent spike but ultimately reduce spike frequency.

Stimulus locations at intermediate electrotonic distance from the soma showed a combination of the effects seen at the soma and the distal dendrite. The voltage at these locations was somewhat more depolarized during faster spiking (as at the soma), but local SK transients evoked by AMPA inputs were still relatively invariant across spike frequencies (as at the more-distal dendrite). Like the $D3_D$ case, AMPA stimuli applied late in the spike cycle led to a negative region in the PRC that moved from the F1 to the F2 ISI for increasing spike rates (Fig. 2.8B1&C1, blue arrowheads). The lasting effects of AMPA inputs on spike timing were similar for $D2_D$ and $D3_D$, such that the peak of the permanent PRC was shifted leftward and became flatter at higher spike frequencies

(Fig. 2.8B2&C2). However, for mid-distal AMPA stimuli the PRC retained a positive region for all spike frequencies, and thus remained type II.

It will be of significant interest to evaluate how well the permanent PRC explains the emergence of synchronous states of network activity, or whether the development of network synchrony from asynchronous modes is better explained by the single-cycle primary and higher-order PRCs. It is important to note that the time-period during which the SK current evoked by excitatory dendritic stimulation is strongest lasts approximately 40 ms (~25 Hz), suggesting the possibility that dendritic SK current could cause GP neurons to resonate with β-frequency oscillatory excitation from STN.

Dendritic Conductance Densities Modulate Dendritic PRCs

The preponderance of synaptic inputs on GP neurons is located on dendrites, which are quite long, but thin and sparsely branching (Falls et al., 1983; Shink and Smith, 1995). To understand how dendritic inputs remote from the soma could influence spiking one needs to consider the local processing of inputs by active conductances in the dendrite. However, dendritic currents have not been recorded experimentally because the dendritic diameter is generally too thin for whole cell recording. Therefore dendritic conductance properties are not well constrained for GP neurons and the assumptions of our model with respect to dendritic conductance densities are tentative, and predominantly derived from matching somatic current clamp data. To examine the robustness of our findings with respect to parameter variations of dendritic conductance densities, we varied dendritic conductance densities over a large range and determined the consequences for PRCs. Specifically, we either adjusted the fast spike conductances

(NaF, NaP, K_V3, and K_V2) together between 0 and 150% of their baseline values, or we separately adjusted the major slow dendritic inward (NaP) or outward (SK) currents.

We focus our analysis of how manipulating dendritic parameters affects PRCs on 2.5 nS AMPA stimulation of the $D2_D$ stimulation site, because this location showed a combination of local dendritic and somato-dendritic coupling effects in our preceding analyses (Fig. 2.8). To eliminate spike rate effects on PRC shape, we drove all models to 30 Hz spiking with somatic current injection to match *in vivo* rates (103-202 pA current depending on dendritic parameters). Varying the density of NaP alone or of the 4 spike conductances together had relatively slight effects on PRC shape that were similar between the two manipulations. Notably, for the largest values of NaP or the spike currents both the maximal spike advances in the stimulated spike cycle (F1) and the maximal spike delays in the subsequent spike cycle (F2) were increased (Fig. 2.9A1&B1). The combination of these effects led to permanent PRCs that showed an increased spike advance for AMPA stimulation at mid spike-cycle and increased spike delay for AMPA stimulation at the beginning or end of the spike cycle (Fig. 2.9A2&B2). These effects can be understood by examining the differences in dendritic membrane currents between models with different dendritic conductance densities (Supp. Fig. 2.8). Higher dendritic densities of NaP or of the spike conductances increased the positive peaks of the corresponding F1 PRCs by supporting larger inward current transients, and increased the negative regions of the corresponding F2 PRCs by amplifying outward evoked SK currents. Consequently the permanent PRCs showed increased positive and negative peaks while the basic shape was retained (Fig. 2.9A2). Overall, these manipulations show that the PRC results we have described are quite robust even for

large changes in the density of persistent inward and spike currents. The dependencies of PRC shape on dendritic conductance densities also provide insight into important potential sources of heterogeneity in pallidal networks, and they illustrate potential mechanisms of modulatory influence on neuronal and network dynamics. Note that we kept the increase in spike currents below the threshold for full blown propagating dendritic action potentials. When spike conductance densities were sufficient to support dendritic spike initiation in response to AMPA input, the type II character of dendritic PRCs disappeared and spike advances were much more pronounced (Supp. Fig. 2.9). Thus, neurons or neuron models with spiking dendrites should be seen as integrating dendritic inputs in a completely different fashion resulting in type I PRCs.

Dendritic SK conductance. As described above, we found that dendritic SK can powerfully alter PRC shape by converting the inward synaptic current of an AMPA input into a net outward membrane charge flow and resulting in spike delays for early-phase inputs. Not surprisingly, decreasing or increasing the dendritic SK density had important effects on dendritic PRCs (Fig. 2.9C). When SK conductance was removed from the dendrite, the permanent PRC became entirely positive (Fig. 2.9C2, red trace). In this case, activation of somatic SK still resulted in F2 spike delays, because the advancement of the first (F1) spike led to a larger somatic SK current that impacted the second (F2) spike cycle (Fig. 2.9C1, blue arrowhead). Increasing the density of dendritic SK smoothly affected the corresponding PRCs. Models with greater dendritic SK showed a diminished positive peak in the F1 PRC and a larger negative peak in the F2 PRC (Fig. 2.9C1, red arrowhead). The mechanism underlying this result is straightforward, as increased dendritic SK conductance led to increased outward current and greater spike

delays in response to dendritic AMPA inputs (Supp. Fig. 2.8). Other effects of increasing dendritic SK were mild, mainly resulting in slight hyperpolarization of the dendrite during the control spike cycle and a concomitant decrease of other depolarization-activated currents. These results indicate that dendritic SK can be varied over a large range while maintaining a smoothly changing type II dendritic PRC, whereas a complete absence of dendritic SK would lead to type I phase response dynamics.

Type II Dendritic PRCs are robust within a large range of SK activation parameters

There is uncertainty in our model about kinetic parameter settings governing SK activation, because the precise calcium dynamics governing SK activation as well as SK activation time constants in GP neurons are not experimentally well constrained. Therefore, we performed a final set of simulation experiments to determine the dependence of our results on variables central to the mechanism of SK activation that could importantly affect phase response dynamics in response to dendritic excitation. SK was activated by inward calcium pulses carried by the Ca_{HVA} conductance. The transient spike in intracellular calcium elicited by an AMPA input to the dendrite lasted less than 10 ms in our simulations (Supp. Fig. 2.10), approximating the dynamics of the interaction of calcium channels with SK channels in membrane micro-domains. However, SK deactivated relatively slowly as a consequence of the default SK deactivation time constant of 76 ms in our simulations. This slow deactivation of SK in the model prolonged SK current transients that shaped the spontaneous mAHP to match experimental data (Gunay et al., 2008). Direct measurements of SK deactivation in oocyte expression systems indicate time constants between 22 and 38 ms (Xia et al., 1998), consistent with a relatively slow calcium dependent deactivation.

To determine the effects of key kinetic parameters affecting SK activation on PRC behavior we varied 1) the rate of intracellular calcium clearance between 0.25 and 2 ms, 2) the steady-state calcium dependence of SK activation between 0.175 and 1 μM, and 3) the time constant of calcium-dependent SK activation between 25 and 100 ms (Supp. Fig. 2.11). Each of these manipulations affected the spontaneous spike frequency, so each model was again driven to 30 Hz by somatic applied current for PRC analysis. Permanent $D2_D$ PRCs were type II for all levels of each manipulation, although the amplitude and skewness were modulated by varying the activation and kinetic parameters for SK. Therefore, the dendritic mechanism that yields type II dynamics in our model was not a consequence of specific parameter choices and is likely to encompass the regime of dendritic processing of strong AMPA inputs *in vivo*.

Discussion

The primary result of our analysis of phase response curves of GP model neurons was that perisomatic and dendritic excitatory inputs yielded distinctly different PRCs. Perisomatic excitation at all times in the spike cycle led to spike advances and thus a type I PRC, whereas dendritic excitation led to spike delays for inputs early in the spike cycle thus yielding a biphasic type II PRC. We found that the type II character of dendritic PRCs was the consequence of stimulus-elicited calcium transients and subsequent SK activation that occurred even for stimuli simulating a single small distal synaptic input. Type II PRCs can enhance the ability of neurons to synchronize in connected networks (Hansel et al., 1995; Goel and Ermentrout, 2002; Galan et al., 2007a; Tsubo et al., 2007; Bogaard et al., 2009) and populations of neurons with type II PRCs synchronize more readily to correlated inputs (Galan et al., 2007b; Marella and Ermentrout, 2008; Abouzeid

and Ermentrout, 2009). Because most excitatory input to GP neurons is on dendritic sites (Shink and Smith, 1995) our results suggests a novel cellular mechanism important in the integration of excitatory input in GP network activity in normal conditions and to the pathological synchronization of GP neurons in Parkinson's disease.

Phase Response Curve Analysis of a Morphological GP Neuron Model

We turned to computer modeling to examine detailed PRC behavior in GP neurons, as spike firing even in brain slices is not sufficiently regular or precise (Deister et al., 2009) to reliably quantify small spike shifts caused by individual synaptic inputs. In addition application of dendritic inputs of controlled amplitude and location is not currently experimentally feasible. These factors put severe limits on the experimental measurement of PRCs.

GP model construction. For this study we adapted a GP neuron model that we have previously used to investigate the influence of conductance densities on spiking properties (Gunay et al., 2008). We observed that most electrophysiological properties of the models were affected by multiple conductances, and each conductance affected multiple electrophysiological measures (Gunay et al., 2008), which is consistent with modeling studies of other types of neurons (Prinz et al., 2003b; Achard and De Schutter, 2006; Taylor et al., 2009). Adaptations to the model were primarily made to include new experimental findings on sodium channel properties in GP neurons (Mercer et al., 2007). The new base model was located in a broad basin of models with similar spiking properties when channel densities were varied, as described in our earlier publication (Gunay et al., 2008). Hence, it is important to note that the model used here does not

represent a unique solution to GP spiking properties, but that all findings are robust against considerable parameter variations.

Dendritic properties. The architecture of dendritic trees and the complement of active dendritic conductances are critical features of the computational machinery employed by neurons with diverse functional objectives (Mainen and Sejnowski, 1996; Vetter et al., 2001; Krichmar et al., 2002; Stiefel and Sejnowski, 2007; Chen et al., 2009; Komendantov and Ascoli, 2009). We used full morphological reconstructions from biocytin filled neurons to obtain a correct representation of the thin, long and sparsely branched structure of GP dendrites (Falls et al., 1983). No dendritic recordings of GP dendrites exist, leading to considerable uncertainty about dendritic current densities in GP. Channel antibody staining has revealed the presence of voltage-gated sodium channels (Hanson et al., 2004) and calcium channels (Hanson and Smith, 2002) in GP dendrites, however. Somatic conductances in GP have been characterized in multiple studies (Baranauskas et al., 1999; Tkatch et al., 2000; Baranauskas et al., 2003; Chan et al., 2004; Mercer et al., 2007) and were matched to these results in our model (Gunay et al., 2008). The SK conductance has been found to govern the mAHP waveform in GP neurons (Deister et al., 2009) and in other cell types has been shown to be activated by calcium inflow through L-type (Marrion and Tavalin, 1998) or N-type (Hallworth et al., 2003; Goldberg and Wilson, 2005) HVA calcium channels. Immunocytochemistry showed an increased density of L- and N- type HVA calcium channels in GP dendrites (Hanson and Smith, 2002), which would support a high level of dendritic SK activation. Dendritic SK has not been examined in GP, but has been found to be present in other

types of neurons with SK conductance (Sailer et al., 2002; Cai et al., 2004; Maher and Westbrook, 2005).

Dependence of PRC shape on physiological properties. Traditional PRC analysis relies on linear scaling of PRCs for positive and negative stimuli of varying amplitudes. We found that excitatory dendritic inputs in particular may not have a regime of weak coupling in GP, because the local input resistance is so high that any stimulus of physiological amplitude results in local depolarization that triggers changes in active conductances and hence response non-linearities. Dendritic depolarization following AMPA inputs leads to a transformation of a type I infinitesimal PRC for very small (<1 pA) stimuli to a type II PRC for physiologically sized stimuli due to SK activation. The property of symmetry for positive and negative stimuli was also lost, as GABA inputs were associated with type I PRCs at all amplitudes. These results were robust for a large range of Ca_{HVA} and SK conductance densities and different parameters for SK activation kinetics, though the precise shape of biphasic PRCs smoothly changed when parameters were varied. Another important observation was that when spike frequency was driven to frequencies typically observed *in vivo*, the negative region of biphasic PRCs was pushed into the F2 spike interval, because the time course of SK activation with AMPA stimulation exceeded the inter-spike interval at fast firing frequencies.

Implications of PRC Behavior for GP Network Interactions

To make PRC analysis analytically tractable, it is most commonly implemented *in silico* using brief, weak perturbations applied to simple point neuron models that lack a full contingent of membrane conductances. In such cases explicit predictions of phase-locked modes can be made for networks with well defined connectivity architectures, and

type II PRCs have been associated with synchronization in networks coupled through excitation (Hansel et al., 1995; Goel and Ermentrout, 2002; Galan et al., 2007a; Tsubo et al., 2007). Further work recognized the importance of active conductances in shaping PRC behavior. Ermentrout et al (2001) and Gutkin et al (2005) evaluated the contribution of a spike frequency adaptation (SFA) potassium current to skewness of PRCs and the consequent emergence of network synchronization. Recently, Stiefel and colleagues (2008, 2009) demonstrated that in principle cholinergic modulation of cortical pyramidal neurons could switch the PRC from type II to type I as a consequence of SFA current (I_M) down regulation.

Dendrites can change PRC shape through an attenuation and delay of an input's effect on somatic spiking and hence a left-shift of the dendritic PRC in the domain of weak coupling (Goldberg et al., 2007). It has also been shown that the electrotonic length of dendritic cables can determine the mode of synchronization in a reciprocal network of two distally coupled ball-and-stick neuron models (Crook et al., 1998b). These studies demonstrate that active dendritic conductances can sculpt effective input waveforms and compensate for the passive filtering properties of dendrites. Our own results indicate that active dendritic conductances can have far reaching consequences for dendritic PRCs, and that SK conductance in particular can lead to dendritic type II PRC behavior in neurons showing somatic type I PRCs. Thus, dendritic conductances can bestow phase response characteristics that are not predicted by somatic excitability, causing the dendrite to act as a distinct dynamical subsystem. This mechanism also gives excitatory input a special relevance for network synchronization, as type II phase response properties were not observed with inhibition.

Given that phenomena of network synchronization are highly sensitive to PRC shapes, our finding of type II dendritic PRCs in GP likely has important consequences for considering network activity in globus pallidus. GP neurons shift from an asynchronous firing mode to synchronous bursting in Parkinson's disease (PD) that is phase-locked to oscillations in other basal ganglia nuclei (Bergman et al., 1994; Nini et al., 1995; Raz et al., 2000). An important mechanism underlying synchronization in basal ganglia networks is believed to be given by STN-GP feedback activity (Plenz and Kitai, 1999; Bevan et al., 2002; Terman et al., 2002). For cortical slow wave oscillations elicited under anesthesia, STN fires bursts in synchrony with cortical oscillations in normal or dopamine depleted animals, whereas GP only shows robust synchronized bursting following dopamine depletion (Magill et al., 2001). This result suggests that modulation in the Parkinsonian state may induce a change in the propensity of GP neurons to engage in network synchronization. Synchronization of pallidal networks would in turn increase the effectiveness of GP inhibition to cause correlated pauses and rebound bursting in STN (Terman et al., 2002), and entrainment of GP neurons to β-frequency STN oscillations would promote resonance between these coupled nuclei. Previous work suggested that HCN channels play a major role in GP neurons in controlling firing regularity and bursting in PD (Chan et al., 2004). Our PRC analysis suggests that in addition dendritic SK may be a key determinant in controlling synchronization through changing the phase dependence of synaptic effects on spike timing. Dopamine modulates SK conductance through $Ca_V2.2$ down-regulation in STN neurons (Ramanathan et al., 2008). If this mechanism holds for GP neurons as well, a $Ca_V2.2$ upregulation and hence

increased SK activation and an increase in type II phase response dynamics might be expected in PD based on our results.

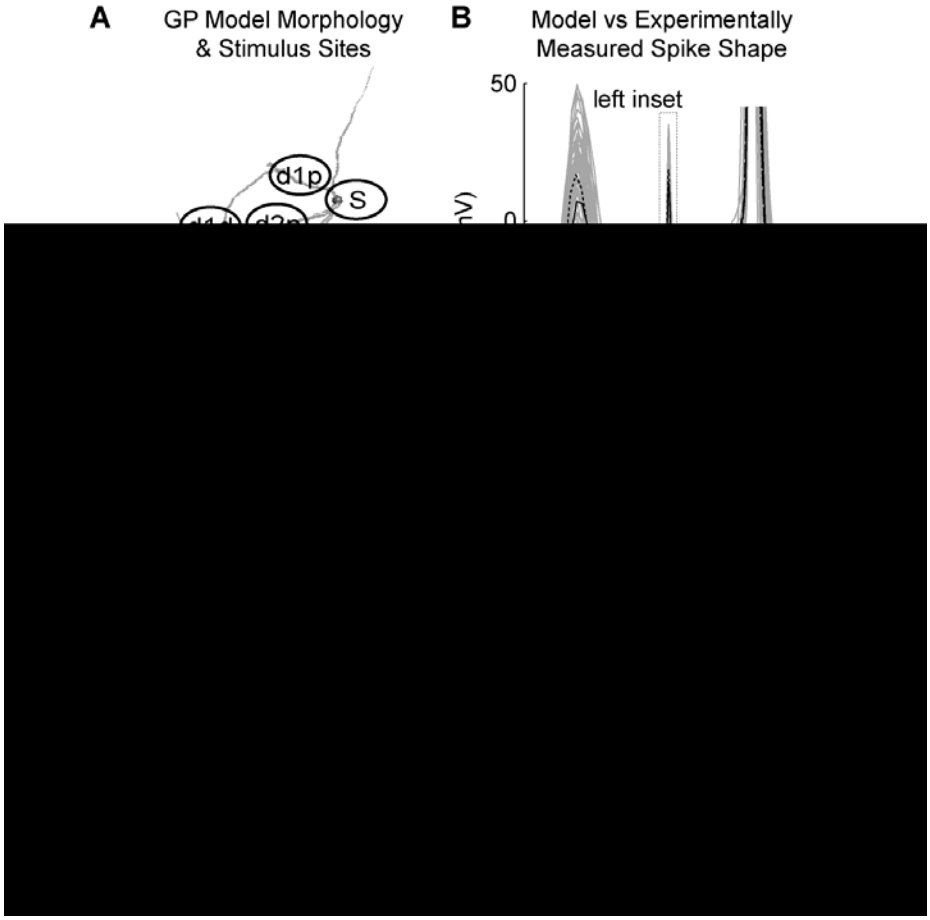

Figure 2.1. GP model morphology, conductances, and electrophysiological properties reproduce those of recorded GP neurons. **A.** Neurolucida (MicroBrightField, Inc) reconstruction of the GP neuron morphology used for all versions of the GP model. Somatic (S) and proximal, mid and distal dendritic stimulus locations for PRC analysis are indicated by oval labels. **B.** Matching of model spike shapes to physiological recordings. The model spike trace (solid line) matched the average recorded spontaneous spike trace (dashed line) well within the biological variability (grey lines) of spike onset, spike height, and spike width, and AHPs. Average spikes from 50 recorded neurons (grey lines) are anchored to the population mean voltage 5 ms prior to spike peaks (black arrowhead) in order to illustrate the variability of AHPs

across neurons. **C.** Somatic voltage- and calcium-gated currents during a spontaneous action potential of GP_{base}. Note that the NaF current peak is curtailed by the x-axis to better distinguish the other current traces. H-current is not shown because it had minimal activation. **D.** Frequency-current (FI) curves for the base model compared to the average experimentally measured FI curve.

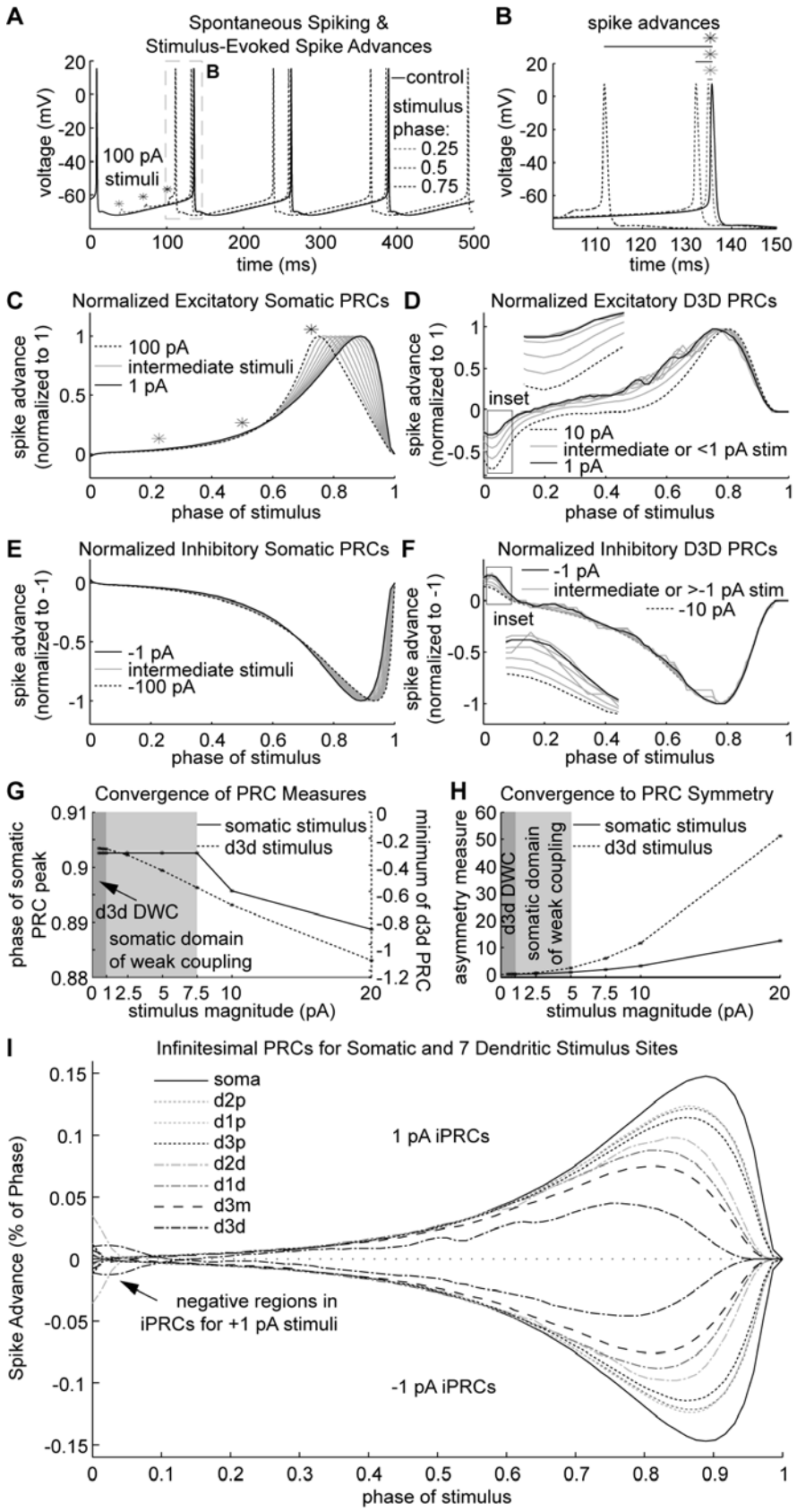
A
Spontaneous Spiking &
Stimulus-Evoked Spike Advances
B
control
stimulus phase:
0.25
0.5
0.75
100 pA stimuli
voltage (mV)
time (ms)
B
spike advances
voltage (mV)
time (ms)
C
Normalized Excitatory Somatic PRCs
100 pA
intermediate stimuli
1 pA
spike advance (normalized to 1)
phase of stimulus
D
Normalized Excitatory D3D PRCs
inset
10 pA
intermediate or <1 pA stim
1 pA
spike advance (normalized to 1)
phase of stimulus
E
Normalized Inhibitory Somatic PRCs
-1 pA
intermediate stimuli
-100 pA
spike advance (normalized to -1)
phase of stimulus
F
Normalized Inhibitory D3D PRCs
-1 pA
intermediate or >-1 pA stim
-10 pA
inset
spike advance (normalized to -1)
phase of stimulus
G
Convergence of PRC Measures
somatic stimulus
d3d stimulus
d3d DWC
somatic domain
of weak coupling
phase of somatic PRC peak
minimum of d3d PRC
stimulus magnitude (pA)
H
Convergence to PRC Symmetry
somatic stimulus
d3d stimulus
d3d DWC
somatic domain
of weak coupling
asymmetry measure
stimulus magnitude (pA)
I
Infinitesimal PRCs for Somatic and 7 Dendritic Stimulus Sites
soma
d2p
d1p
d3p
d2d
d1d
d3m
d3d
1 pA iPRCs
negative regions in
iPRCs for +1 pA stimuli
-1 pA iPRCs
Spike Advance (% of Phase)
phase of stimulus

Figure 2.2. Physiologically realistic inputs to GP are outside somatic and dendritic domains of weak coupling. A. Voltage traces illustrating spontaneous 7.9 Hz spiking of the model and voltage deflections and spike advances elicited by 100 pA somatic stimuli delivered at one of three points in phase (indicated by asterisks). Note, spike advances persist indefinitely (3 spike cycles shown). **B.** Expansion of **A** highlighting spike advances resulting from stimuli delivered at different phases. The earliest stimulus (indicated in **A, B,** & **C** by the lightest grey asterisk) yields the smallest spike advance, and the latest (black asterisk) yields the largest. **C.** Normalized PRCs for somatic current injections between 1 pA (solid black line) and 100 pA (dotted black line). Larger somatic stimuli yield PRCs with peaks occurring earlier in phase. The shape of normalized somatic PRCs converges for stimuli weaker than 7.5 pA. **D.** Normalized PRCs derived by stimulating the distal region of dendrite 3 ($D3_D$) with current pulses between 0.5 pA and 10 pA (dotted black line). The shape of normalized $D3_D$ PRCs converges for stimuli $\leq$ 1 pA (solid black line) with an r-value of 0.0675 indicating that the iPRC for $D3_D$ is type I. This can be seen most readily by examining the negative peaks of these PRCs occurring at a phase of approximately 0.025 (box and inset). **E.** Normalized PRCs for negative somatic current injections between −1 pA (solid black line) and −100 pA (dotted black line). Larger negative stimuli yield PRCs with more right-shifted peaks. Note by comparison to **C**, 1 pA and −1 pA somatic PRCs are symmetrical across zero. **F.** Normalized PRCs for $D3_D$ current injections between −0.5 pA and −10 pA (dotted black line). The shapes of these normalized $D3_D$ PRCs converge for stimuli of or greater than −1 pA (solid black line). This can be seen most readily by noting the positive peaks of PRCs at a phase of approximately 0.025 (box and inset). **G.** Domains of somatic and

$D3_D$ weak coupling illustrated by plotting the relationships between features of the PRCs and stimulus strength. For somatic current injections of 7.5 pA or less, the phase at which the peak of PRCs occurs (left y-axis) has converged. For $D3_D$ current injections of 1 pA or less, the negative peak of PRCs (right y-axis) has converged. **H.** Domains of somatic and $D3_D$ weak coupling illustrated by plotting a measure of PRC asymmetry (obtained by summing together PRCs for positive and negative current injections of equal magnitude at all points in phase) against stimulus strength. Excitatory somatic PRCs for stimulus strengths greater than 5 pA are increasingly asymmetric with inhibitory somatic PRCs of equal strengths. Excitatory $D3_D$ PRCs for stimulus strengths greater than 1 pA are increasingly asymmetric with inhibitory $D3_D$ PRCs of equal strengths. **I.** Infinitesimal PRCs (1 pA and -1 pA) for all stimulus locations are Type I.

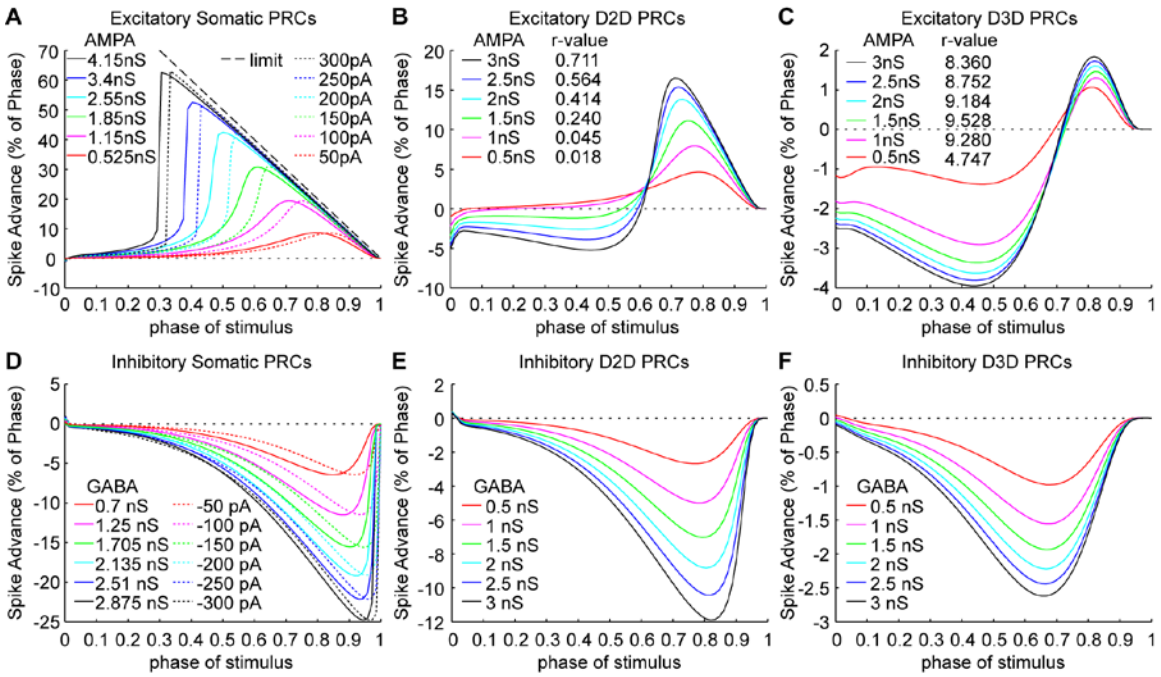

Figure 2.3. PRC shape depends both on stimulus location and strength. A. Somatic PRCs are always Type I for square-pulse positive current injections and for simulated excitatory synaptic AMPA conductances. Somatic PRCs have peaks that scale approximately linearly with stimulus magnitude, and larger stimuli cause more of the late-phase PRC to approach the limit of spike advancement. **B.** Small excitatory synaptic inputs to the end of a shorter dendrite ($D2_D$) yield type I PRCs, however, larger inputs to $D2_D$ yield PRCs of increasing Type II character. Both positive and negative peaks of $D2_D$ PRCs increase in size with stimulus strength. **C.** Excitatory synaptic inputs to the end of the longest dendrite ($D3_D$) yielded type II PRCs for all input strengths tested in this set of experiments. **D.** Somatic PRCs are always Type I for square-pulse negative current injections and for simulated inhibitory $GABA_A$ synaptic conductances. **E&F.** Distal dendritic PRCs for inhibitory synaptic input (to $D2_D$ in **E**; to $D3_D$ in **F**) are Type I.

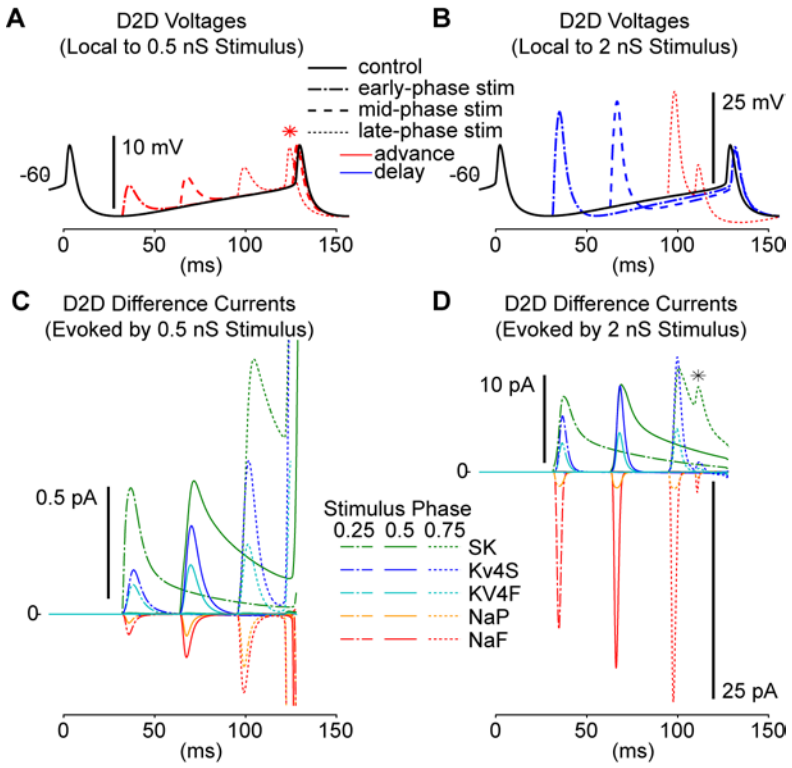

Figure 2.4. Different input strengths evoke different contingents of membrane currents at the distal dendrite. Shown are stimulus-evoked voltage and current transients for 0.5 nS and 2 nS excitatory inputs to $D2_D$. **A.** Voltage deflections elicited by 0.5 nS excitatory synaptic input to $D2_D$ at phases of 0.25, 0.5, or 0.75 (red dashed lines, indicating phase advances). Importantly, these stimuli yield a type I $D2_D$ PRC. The un-stimulated voltage trajectory at $D2_D$ (black trace) illustrates the back-attenuated voltage oscillation driven by spontaneous axo-somatic spiking. Small spike advancements are evident in the stimulated $D2_D$ voltage traces relative to the control trace (red *), particularly for the late-phase stimulus. **B.** Voltage deflections elicited by 2 nS excitatory synaptic input to $D2_D$ at phases of 0.25, 0.5, or 0.75 (dashed blue or red lines, indicating phase delays or advances, respectively). Importantly, these stimuli yield a type II $D2_D$ PRC. **C.** Difference currents (I_{Diff}) local to 0.5 nS $D2_D$ stimuli were calculated by the

subtraction of control current traces from stimulated current traces. The five largest difference currents are shown, and of these, $I_{Diff\text{-}SK}$ (green traces) is both the largest and longest lasting. Only slight differences are evident in the currents evoked by stimuli at difference phases (here, and in **D**), because the control voltage trajectory at $D2_D$ is relatively flat. Note that for visual clarity, I_{Diff} traces in **C** are curtailed at the time of the next spike. **D.** Difference currents local to 2 nS $D2_D$ stimuli. A four-fold increase in input strength (compared to **C**) yields a much larger transient increase in $I_{Diff\text{-}NaF}$ which amplifies the voltage deflection (red traces) and a twenty-fold increase in peak $I_{Diff\text{-}SK}$ (green traces). Note that the spike advancement caused by the late-phase stimulus results in a second peak in $I_{Diff\text{-}SK}$ (*).

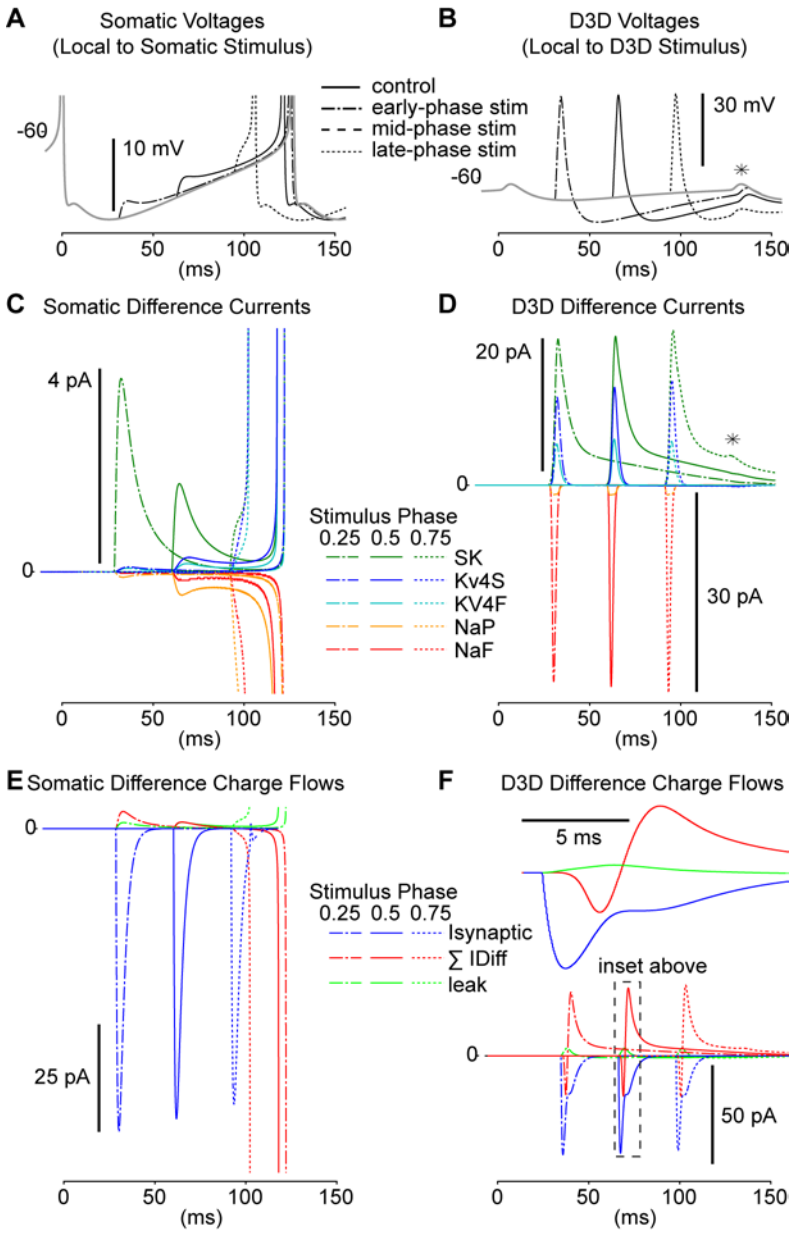

Figure 2.5. Targeting identical stimuli to different regions of the model evokes different contingents of membrane currents. Shown are stimulus-evoked voltage and current transients for 1 nS excitatory inputs to the soma *vs.* the most-distal region of dendrite, $D3_D$. **A.** Voltage deflections elicited by 1 nS excitatory synaptic input delivered to the soma at phases of 0.25, 0.5, or 0.75 (dashed or solid black lines, as indicated).

Importantly, these stimuli yielded a type I somatic PRC. The un-stimulated somatic voltage trajectory (grey line) covers approximately a 10 mV range between the depth of the AHP and spike threshold. As in Figure 2.4, spike advancements relative to control are evident, particularly for the late-phase stimulus. **B.** Voltage deflections elicited by 1 nS excitatory synaptic input to $D3_D$ at phases of 0.25, 0.5, or 0.75 (dashed or solid black lines, as indicated) are more than ten-fold larger than those elicited by equivalent somatic inputs, because $D3_D$ input resistance is much higher. Importantly, these stimuli yield a type II $D3_D$ PRC. Slight spike delays and advancements relative to control are again evident (∗). **C.** Difference currents local to 1 nS somatic stimuli. The pattern of evoked currents differs depending on input phase, because the control somatic voltage trajectory is not flat. As in Figure 2.4, I_{Diff} traces are curtailed at the time of the next spike. **D.** Difference currents local to 1 nS $D3_D$ stimuli. $D3_D$ stimuli yielded a peak $I_{Diff\text{-}SK}$ (green traces) that is five times greater than that elicited by identical somatic stimuli. Minimal differences are evident in the pattern of currents evoked by stimuli at difference phases, because the control voltage trajectory at $D3_D$ is flat. **E.** The synaptic current of the stimulus overwhelms membrane currents evoked at the soma. The sum of all somatic difference currents and difference leak are negligible relative to the synaptic current of a 1 nS AMPA input which is approximately 70 pA. **F.** A 1 nS AMPA input to $D3_D$ yields a smaller synaptic current than the equivalent conductance input applied to the soma, because the $D3_D$ voltage deflection is much larger, reducing the synaptic driving force. The sum of all $D3_D$ difference currents, of which NaF and SK are the major contributors (**D**), is sufficiently large (and long-lasting) to rival the synaptic current.

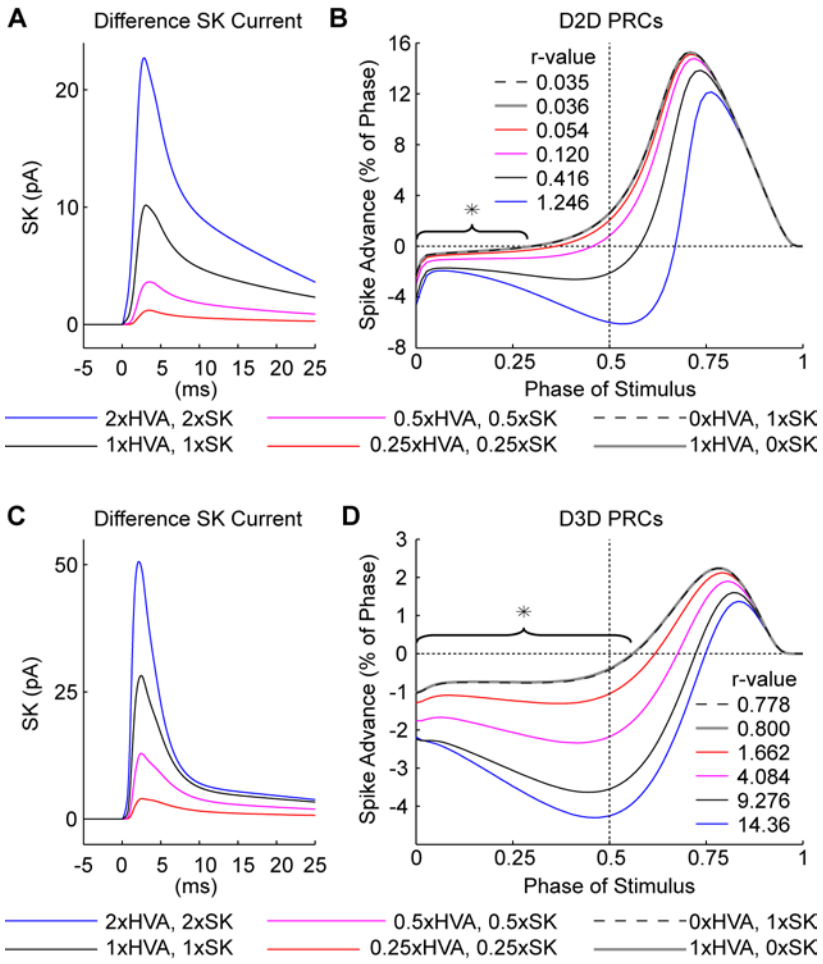

Figure 2.6. Tandem local up- and down-regulation of CaHVA and SK modulates the depth of the negative peak of distal dendritic PRCs. A. SK difference currents evoked by 2 nS excitatory synaptic input to $D2_D$ in models where the densities of Ca_{HVA} and SK have been dialed up or down in the compartments composing the $D2_D$ stimulus site. (Note that since the manipulation of conductance densities was limited to the 25 compartments of the $D2_D$ site, the spontaneous spiking behavior of the model was unaffected.) Traces are aligned such that stimulus onsets are at zero. **B.** $D2_D$ PRCs transition from type I to type II as Ca_{HVA} and SK are up-regulated local to stimulus delivery. Visually identical type I PRCs result when *either* Ca_{HVA} *or* SK are eliminated

from $D2_D$ (grey and dashed black lines). The negative region of $D2_D$ PRCs (asterisk) that remains when the Ca_{HVA} /SK mechanism had been locally disabled (by eliminating *either* Ca_{HVA} *or* SK) stems from compartments neighboring $D2_D$ where the mechanism was left intact and that also experience significant voltage deflection evoked by the stimulus. **C.** Ca_{HVA} difference currents evoked by 2 nS excitatory synaptic input to $D3_D$ in models where the densities of Ca_{HVA} and SK have been dialed up or down in the compartments composing the $D3_D$ stimulus site. Traces are aligned such that stimulus onsets are at zero. **D.** The negative region of $D3_D$ PRCs is deeper for models where Ca_{HVA} and SK has been up-regulated local to stimulus delivery. Elimination of *either* Ca_{HVA} *or* SK from $D3_D$ yields visually identical type II PRCs, and like the $D2_D$ case, the remaining negative regions of these PRCs (asterisk) stem from compartments adjacent to the stimulated region where the Ca_{HVA} /SK mechanism remains intact.

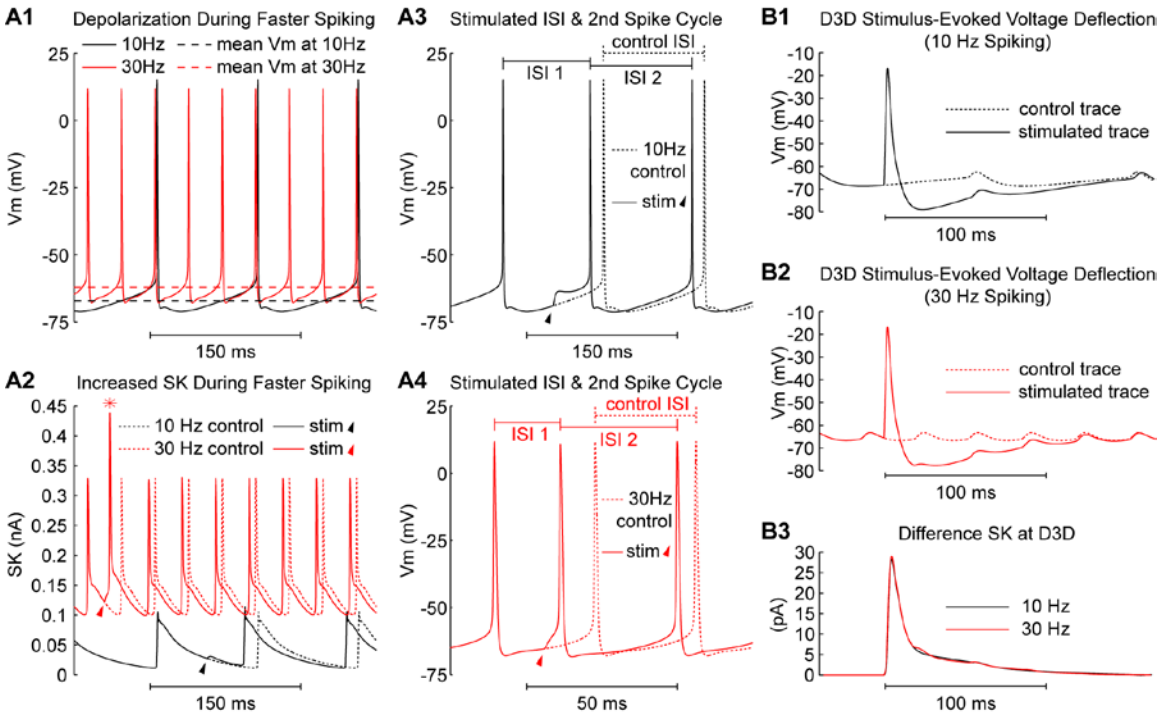

Figure 2.7. Spike frequency affects somatic but not distal dendritic SK activation. **A.** Faster spiking elevates baseline levels and augments stimulus-evoked transients of somatic SK current. **A1.** When spiking was driven from 10 Hz (black trace) to 30 Hz (red trace) by increasing somatic applied current, the mean voltage at the soma (dashed black and red lines) was elevated ~5 mV. **A2.** Driving faster spiking with somatic applied current elevated the baseline level of somatic SK current. Note that a 2 nS AMPA stimulus (red and black arrowheads) elicited immediate initiation of a spike when applied to the soma during 30 Hz spiking but not when applied during 10 Hz spiking. The stimulus applied during 30 Hz spiking evoked a larger peak in SK current (red asterisk) than is evoked by spontaneous spikes (red dashed traces). **A3.** During 10 Hz spiking, the somatic stimulus (black arrowhead) shortened the ISI during which it was delivered, but did not affect the subsequent ISI. **A4.** During 30 Hz spiking the somatic

stimulus (red arrowhead) shortened the ISI during which it was delivered. However, the subsequent ISI was longer in duration, reflecting the larger SK current evoked by the stimulus during faster spiking. **B.** The time-course of distal dendritic SK current flow is unaffected by spike frequency, spanning additional spike cycles during faster spiking. **B1.** During 10 Hz spiking, the local depolarization transient elicited by a 2 nS AMPA input to $D3_D$ (solid black line) was approximately 55 mV relative to the control voltage trace (dashed black line). (Note that the ripples in the control voltage trace which demarcate the 100 ms spike cycles reflect attenuated spikes reaching the distal dendrite.) **B2.** During 30 Hz spiking, the local depolarization transient elicited by a 2 nS AMPA input to $D3_D$ (solid red line) was also approximately 55mV relative to the control voltage trace (dashed red line). **B3.** The peak and time-course of the SK difference current (~30pA) evoked locally by AMPA inputs to D3D was not dependent on spike frequency. Difference current traces for 10 Hz (black) and 30 Hz (red) spiking overlay one-another nearly perfectly.

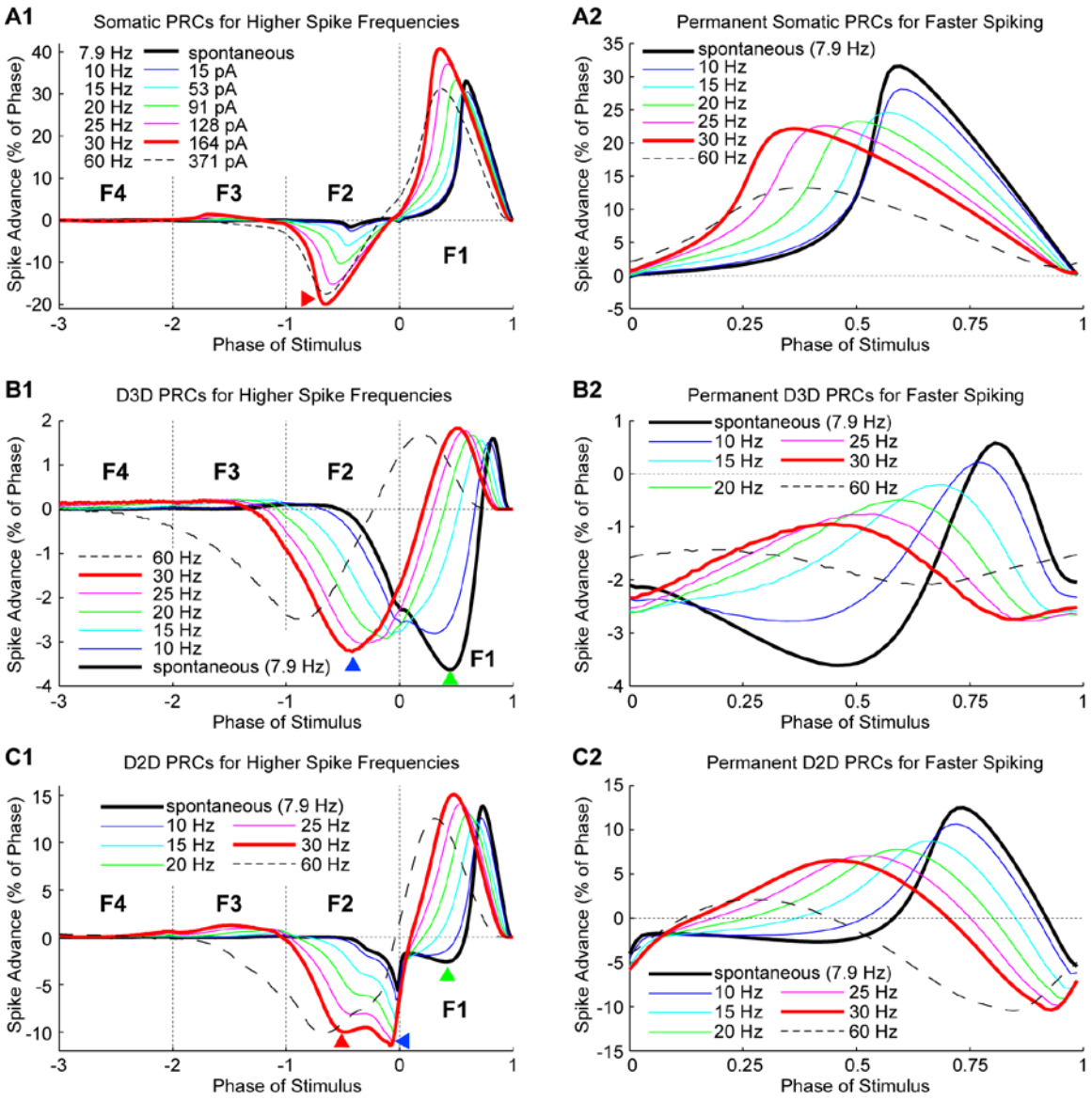

Figure 2.8. Faster axo-somatic spiking changes the shapes of somatic and dendritic PRCs, and it is necessary to consider stimulus effects that outlast a single spike cycle. A1. When the model is driven faster (from 10 Hz to 30 Hz) by increasing applied current to the soma, excitatory synaptic inputs of 2 nS yield somatic PRCs with larger, earlier peaks and less skewness. **A2.** Permanent PRCs are calculated by summing single cycle PRCs F1 through F5. At higher spike frequencies the peak of the permanent

somatic PRC is reduced, occurs earlier in phase, and is less skewed. **B1.** Like the somatic case, during faster spiking the positive peak of distal dendritic ($D3_D$) PRCs, occurs earlier in phase. The negative region present in F1 PRCs for $D3_D$ inputs delivered during slower spiking (green arrowhead) is pushed into F2 when spiking is driven faster (blue arrowhead). **B2.** Permanent PRCs for $D3_D$ inputs have only a slight positive peak for the slowest spike frequencies, and at 15 Hz or faster, the entire permanent PRC is negative. **C1.** Single cycle PRCs for inputs to $D2_D$ show an amalgam of the effects of somatic or $D3_D$ stimulation. The red and blue arrowheads correspond to the red arrowhead in A1 and the blue arrowhead in B1. **C2.** The permanent PRCs for $D2_D$ inputs are type II for all spike frequencies up to 60 Hz, and they vary smoothly as a function of spike frequency. For high spike frequencies a negative region develops for stimuli late in phase.

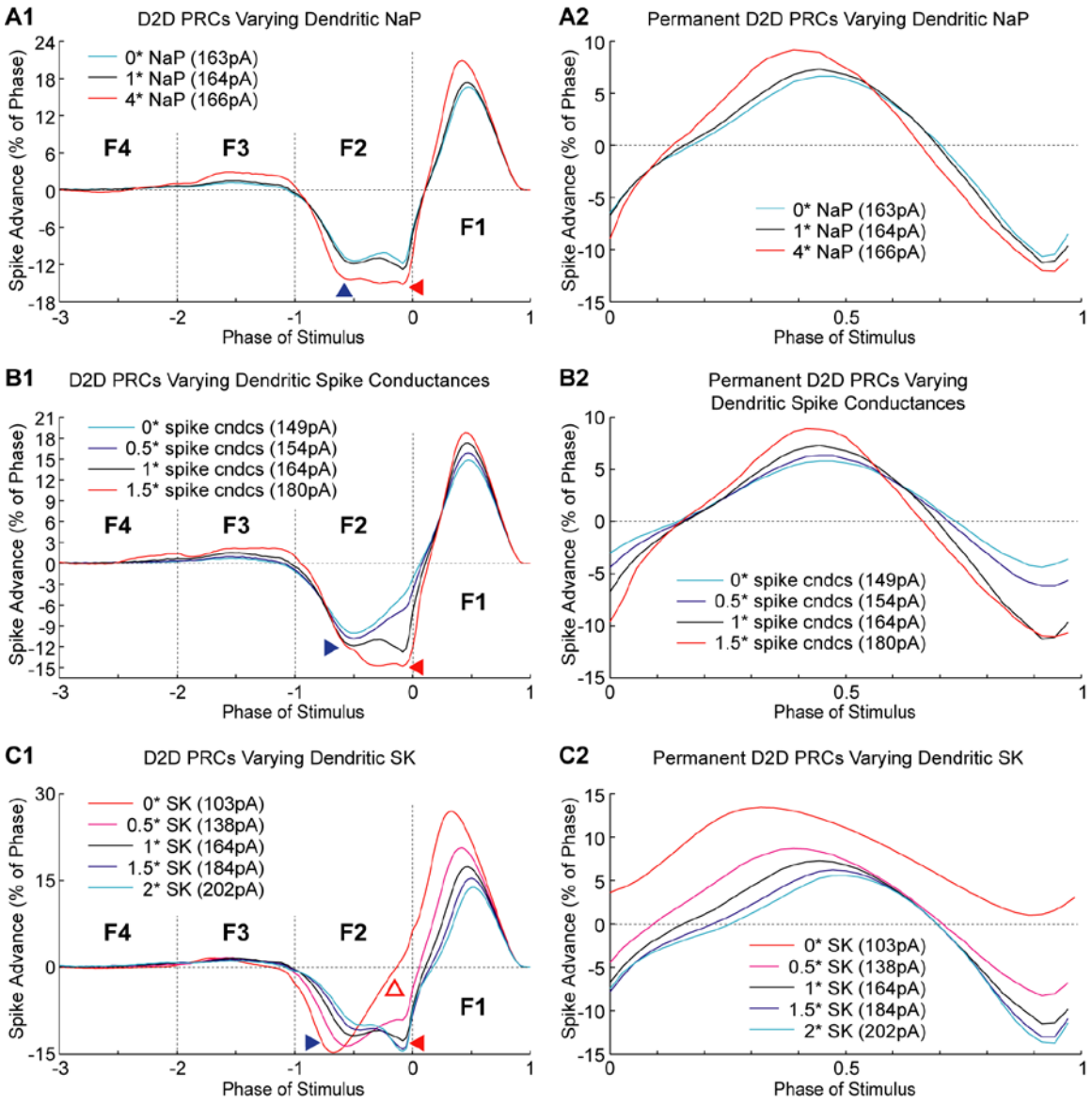

Figure 2.9. Distal dendritic PRCs are robustly type II against significant variation of dendritic conductance densities. A. Single-cycle PRCs (**A1**: F1 through F4) and the permanent PRC (**A2**) for models with 0, 1, and 4 times the base dendritic density of NaP. For models with greater dendritic densities of NaP the positive peak in the F1 PRC and both of the negative peaks in the F2 PRC were increased. **B.** Single cycle PRCs (**B1**: F1 through F4) and the permanent PRC (**B2**) for models with 0.5, 1, and 1.5 times the

default dendritic density of the 4 spike conductances (NaF, NaP, KV3, & KV2). For models with greater dendritic densities of the spike conductances the positive peak in the F1 PRC and both of the negative peaks in the F2 PRC were increased. **C.** Single-cycle PRCs (**C1**: F1 through F4) and the permanent PRC (**C2**) for models with 0.5, 1, 1.5, and 2 times the base dendritic density of SK. For models with greater dendritic densities of SK the positive peak in the F1 $D2_D$ PRC and the early-phase negative peak (blue arrowhead) are reduced, whereas the late-phase negative peak in the F2 $D2_D$ PRC (solid red arrowhead) is increased. Complete removal of SK conductance from the dendrite (red traces in **C1**&**C2**) eliminates the late-phase negative peak in the F2 $D2_D$ PRC (red box arrowhead) and the corresponding permanent PRC is purely positive.

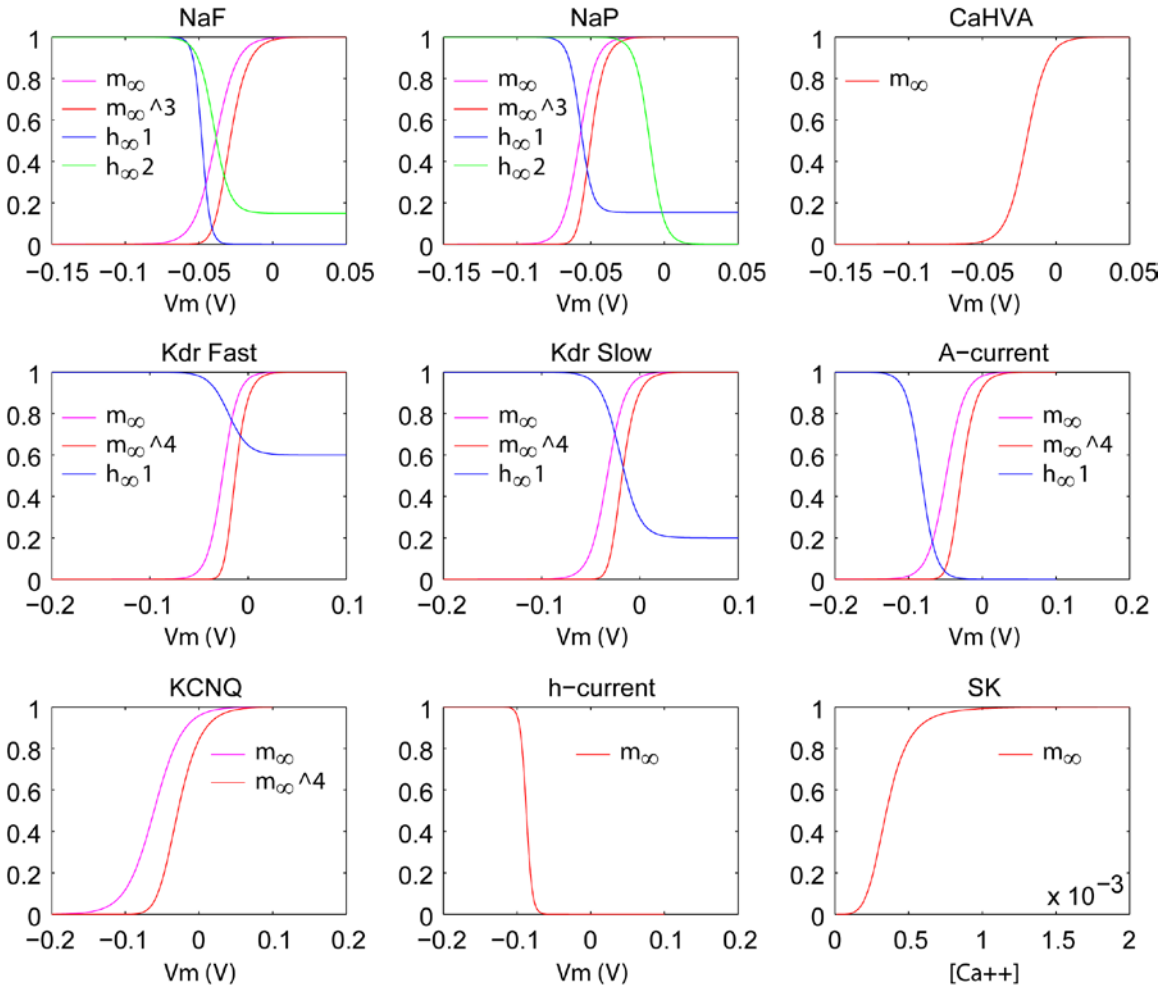

Supplemental Figure 2.1. Steady-state voltage and calcium dependencies of activation and inactivation for the membrane conductances in GP_{base}.

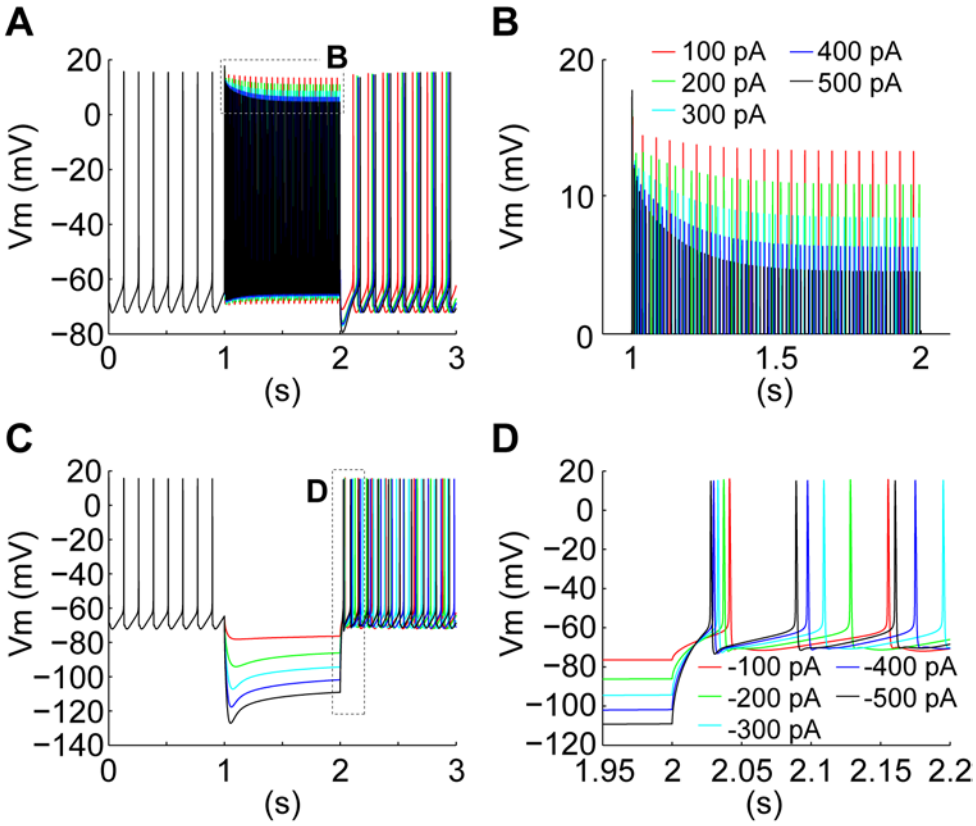

Supplemental Figure 2.2. Voltage responses of the model to injected current steps. **A.** Somatic voltage traces from 3 second simulations where positive current was injected during the middle second. **B.** Enlargement of spike peaks in **A** showing spike height attenuation during positive current injections. **C.** Somatic voltage traces from 3 second simulations where negative current was injected during the middle second. Sag is increasingly evident for larger hyperpolarizing steps. **D.** Enlargement of the region of time following the offset of hyperpolarizing steps in **C** showing that the latency to the first spike is least following the strongest hyperpolarization.

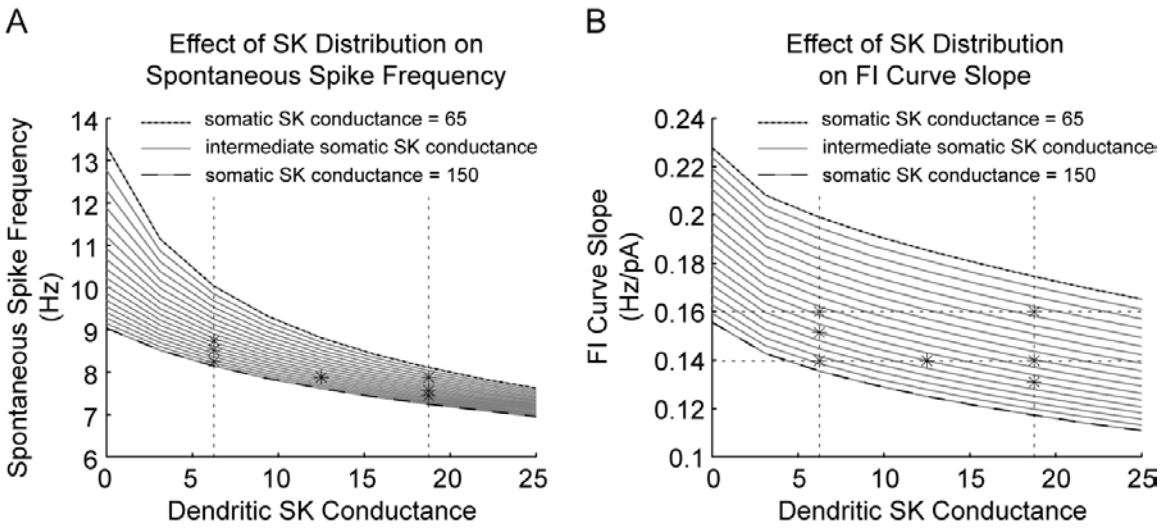

Supplemental Figure 2.3. Effects of the distribution of SK conductance between the soma and dendrite on spontaneous spike frequency and the slope of the FI curve. A. Models with greater SK conductance in either the soma or dendrite spike spontaneously at a slower pace. Models with more dendritic SK have a narrower range of possible spontaneous spiking frequencies even for a wide range of somatic SK densities. Asterisks indicate the location in SK distribution – spike frequency space of models for which PRCs analysis was performed. (See Supp. Fig. 2.5.) **B.** The slope of the FI curve is steeper in models with less somatic or dendritic SK. Asterisks indicate the location in SK distribution – FI slope space of models for which PRCs analysis was performed. (See Supp. Fig. 2.5.)

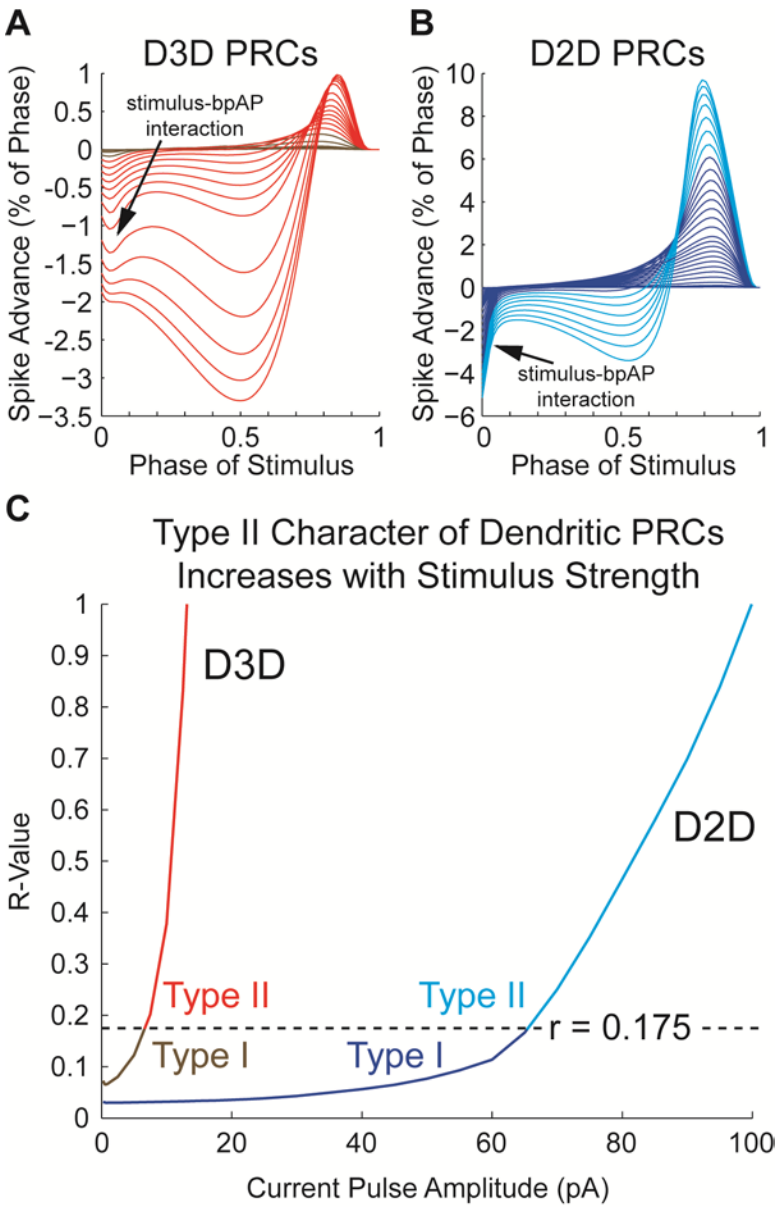

Supplemental Figure 2.4. Type II character of distal dendritic PRCs increases with stronger excitatory current injections. **A.** PRCs for currents injections of 0.25 pA to 50 pA delivered to D3D. Brown traces (stimulus amplitudes <= 5 pA) are type I PRCs. Red traces are type II PRCs by the r-value criterion (r-value > 0.175). **B.** PRCs for currents injections of 0.25 pA to 100 pA delivered to D2D. Blue traces (stimulus amplitudes <= 65 pA) are type I PRCs, and cyan traces are type II PRCs. **C.** R-values for D3D and D2D PRCs (plotted in A&B) as a function of injected current amplitude.

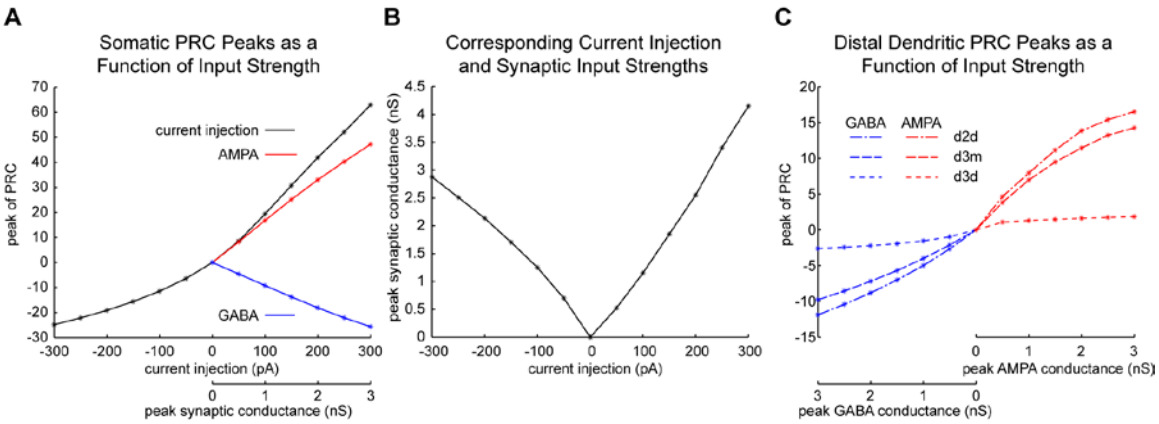

Supplemental Figure 2.5. PRC measures are dependent on the strength of inputs. **A.** The positive and negative peaks of somatic PRCs for positive and negative current pulses scale approximately linearly with input strength. **B.** Current injections and synaptic conductance inputs are related approximately linearly to each other in terms of their effect on the peak of the PRC. **C.** The positive peak of the distal dendritic PRC is related sublinearly to the strength of synaptic inputs.

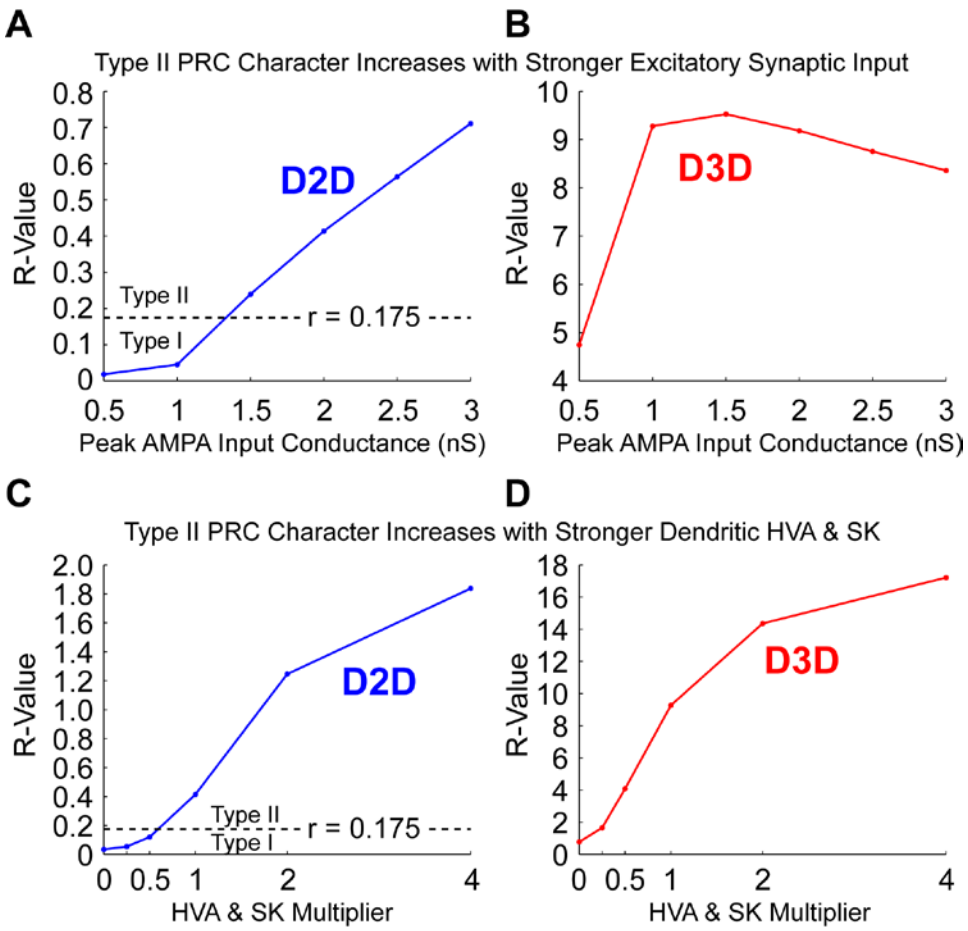

Supplemental Figure 2.6. Type II character of distal dendritic PRCs increases with stronger synaptic excitation and higher densities of CaHVA and SK conductances. **A&B.** R-values for D2D and D3D PRCs, respectively, for excitatory synaptic inputs of 0.5 nS to 3 nS. Note that D2D PRCs transition from type I to type II for stronger inputs, and D3D PRCs are type II for all input strengths tested. The qualitative shape of D3D PRCs is relatively stable and the r-value plateaus for inputs of 1 nS or greater. **C&D.** R-values for D2D and D3D PRCs, respectively, as Ca_{HVA} and SK conductance densities are increased in tandem at the stimulation site. Note, D2D PRCs transition from type I to type II for stronger levels of the Ca_{HVA} and SK conductances, whereas D3D PRCs are type II even when either Ca_{HVA} or SK was entirely removed from the stimulation site.

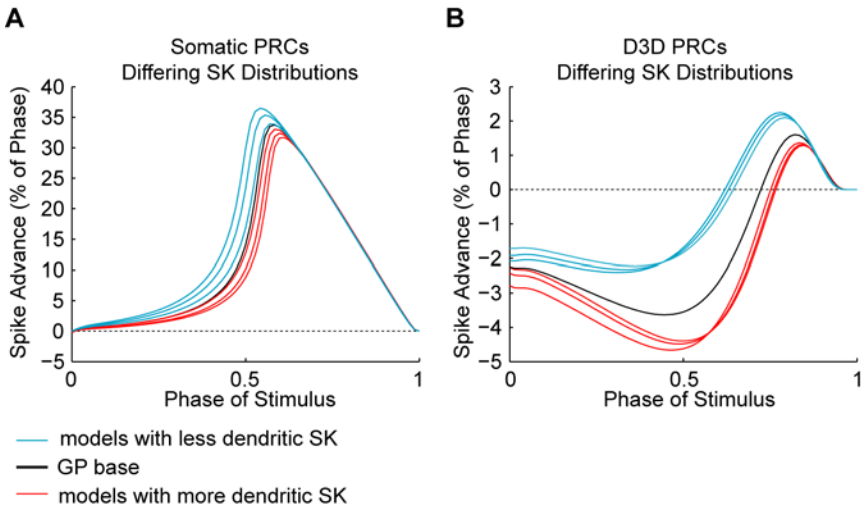

Supplemental Figure 2.7. Dendritic but not somatic PRCs vary strongly with dendritic SK conductance density. **A.** Somatic PRCs for models with different distributions of the SK conductance. (The only deviation of these models from GP_{base} was the SK conductance distribution as described in Supp. Fig. 2.3.) **B.** Dendritic PRCs for models with different SK conductance distributions group according to the dendritic but not somatic density of SK conductance.

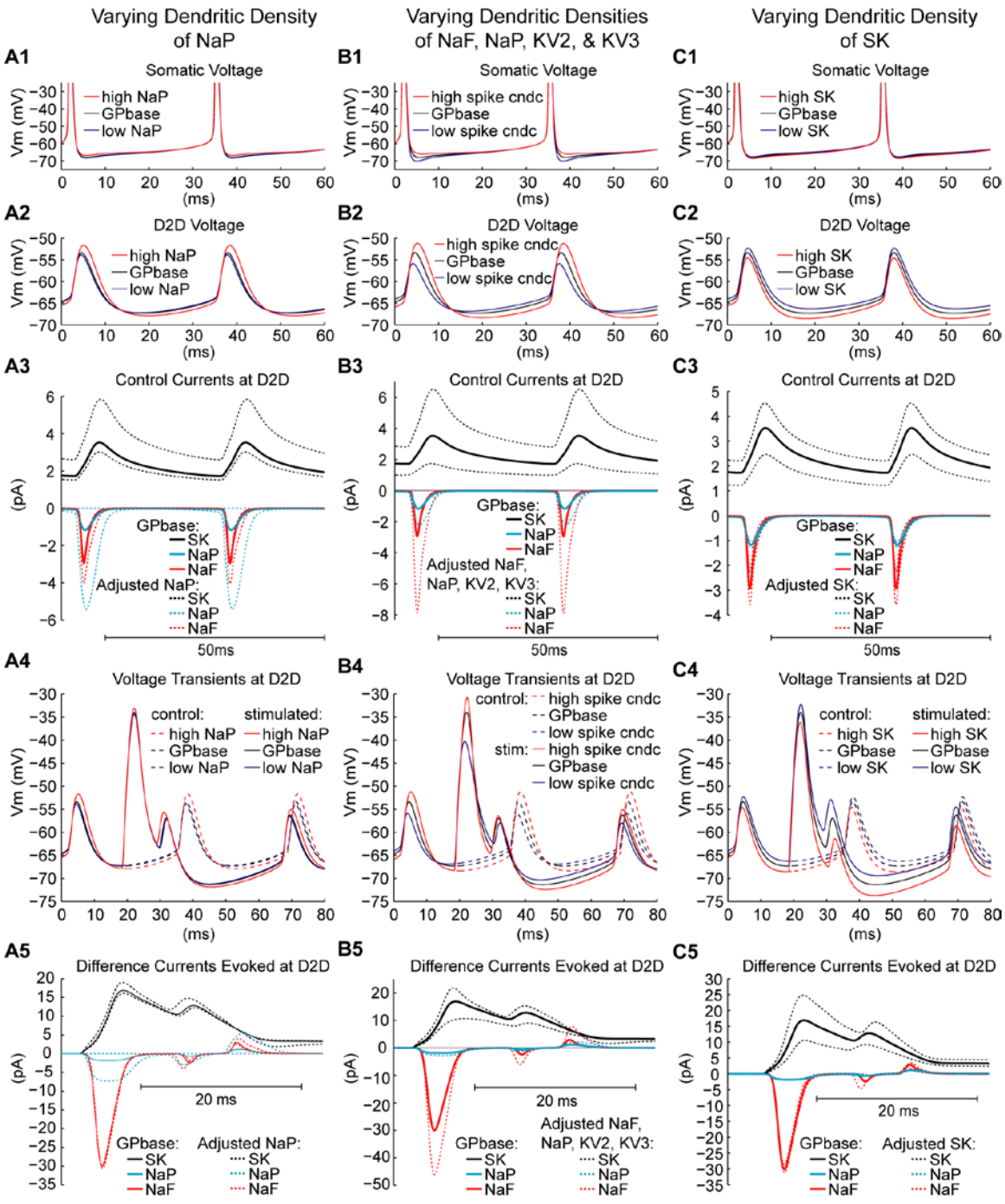

Supplemental Figure 2.8. Manipulation of dendritic conductance densities changes baseline current levels and AMPA input-evoked dendritic current transients. A. Results of changing the dendritic density of the persistent sodium (NaP) conductance to 0

or 400% of the base density. **A1.** The somatic voltage trajectory (spike shape, mAHP, and approach to threshold) during the control spike cycle is essentially unaffected by changing dendritic NaP up or down. **A2.** The voltage trajectory at $D2_D$ during the control spike cycle is slightly amplified by increasing dendritic NaP. **A3.** Greater dendritic NaP increases the activation levels of other membrane currents in the dendrite including NaF and SK (large amplitude dotted traces). Eliminating NaP leads to a small reduction of NaF and SK activation (small amplitude dotted traces). **A4.** Greater dendritic NaP slightly increases the size of depolarization transients in response to dendritic AMPA input as well as the depth of the subsequent hyperpolarization. **A5.** AMPA input to the distal dendrite evokes more NaP current locally in models where the NaP conductance density is greater, which leads to greater local SK activation by amplifying the local depolarization transient. **B.** Results of changing the dendritic densities of the spike conductances (NaF, NaP, K_V2, & K_V3) to 0 or 150% of their base values. **B1.** The control somatic voltage trajectory is unaffected except the fAHP is slightly deeper. **B2.** The voltage oscillation at $D2_D$ during the control spike cycle is amplified more by increasing the 4 spike conductances than by increasing NaP alone. **B3.** Dendritic currents, particularly NaF, during the control spike cycle are larger in models with higher dendritic densities of the spike currents. **B4.** Depolarization transient elicited by AMPA input to $D2_D$ were significantly larger in models with more dendritic spike conductance, and the subsequent hyperpolarization of the local membrane was deeper. **B5.** Explaining the pattern of voltage responses in **B4,** the NaF current transient evoked by AMPA input to $D2_D$ was significantly larger and the SK current was evoked more strongly in models with more dendritic spike conductance. **C.** Results of changing the dendritic density of

the SK conductance to 0 or 200% of the base value. **C1.** The control somatic voltage is unaffected by varying dendritic SK. **C2.** The control voltage trajectory at $D2_D$ is shifted to a more hyperpolarized range in models with more dendritic SK conductance. **C3.** While dendritic SK current is increased, the other dendritic currents are reduced during the control spike cycle in models with more dendritic SK conductance. **C4.** Depolarization transients in response to AMPA inputs to $D2_D$ retain the same amplitude, but the subsequent hyperpolarizations become deeper in models with more dendritic SK conductance. **C5.** Explaining the pattern of voltage responses in **C4**, the SK current evoked by AMPA inputs to $D2_D$ scales in magnitude with the dendritic SK conductance density, while the other dendritic currents evoked by those inputs are essentially unaffected.

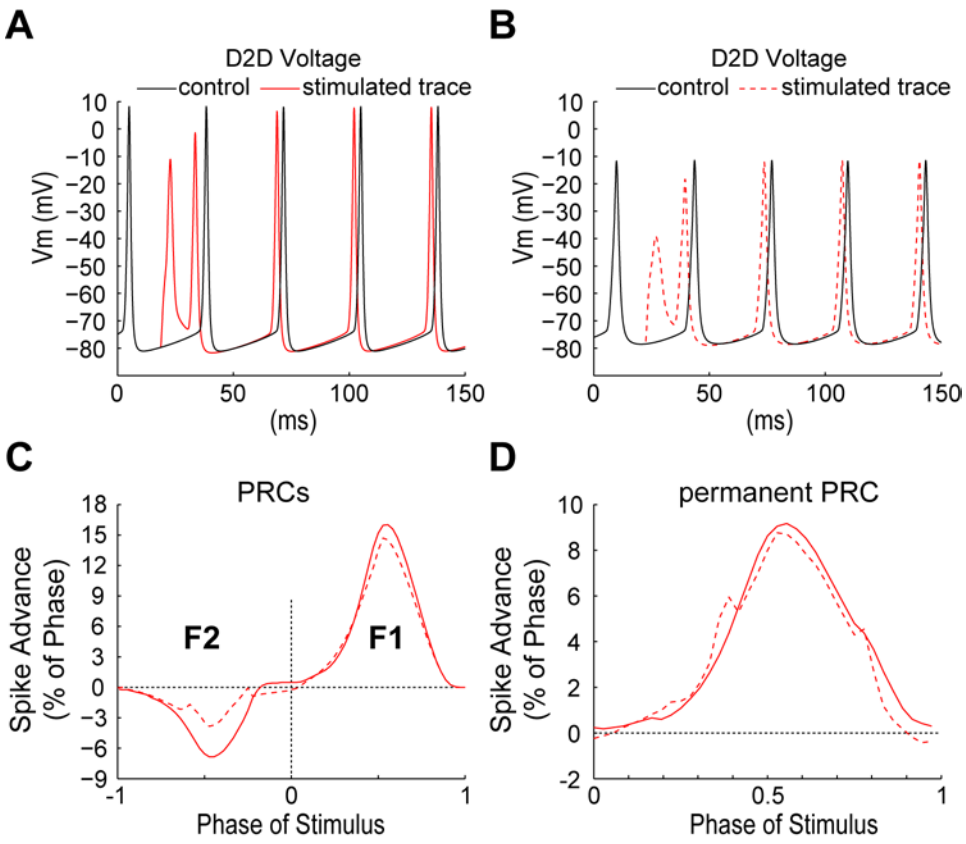

Supplemental Figure 2.9. Models with spiking dendrites have type I distal dendritic PRCs. **A.** Control and stimulated voltage traces from the distal dendrite (D2D) of a model with dendritic spike conductance densities equal to those of the soma. Note the large voltage 'spikes' in the control trace that have propagated back from the soma. **B.** Control and stimulated voltage traces from the distal dendrite (D2D) of a model with dendritic spike conductance densities that are half those of the soma. Note that the control voltage 'spikes' and voltage deflection are still large but reduced compared to the uniform spike conductance model in **A**. C. The F1 and F2 PRCs for these models with sufficient dendritic spike conductance to support dendritic spikes. **D.** Permanent PRCs for these models are nearly identical.

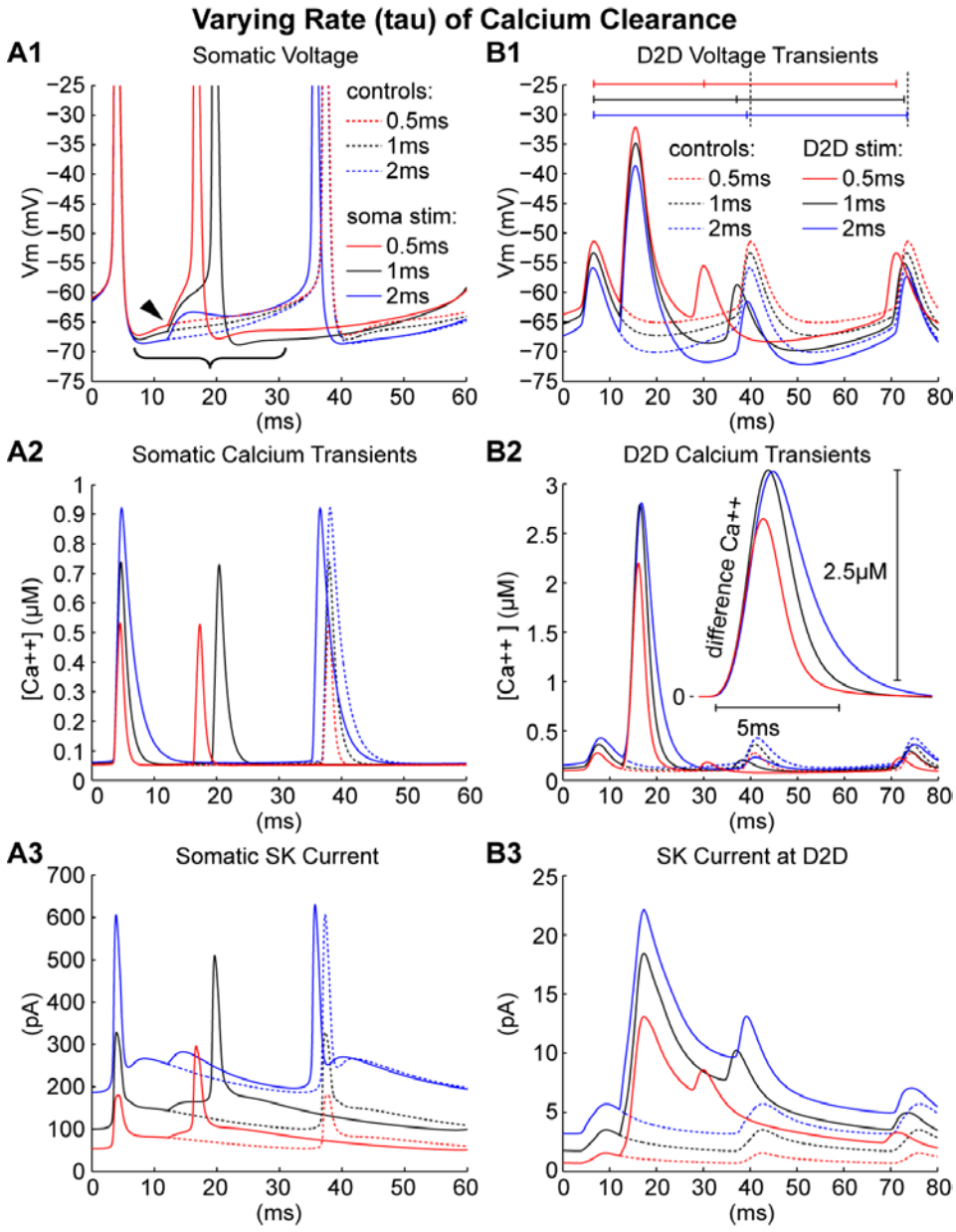

Supplemental Figure 2.10. Faster calcium clearance increases the excitability of the model. **A1.** Models with faster calcium clearance are slightly depolarized during the control spike cycle from the fAHP through the approach to threshold, and somatic inputs are more capable of triggering spikes off cycle in these models. **A2.** Somatic calcium transients elicited by spontaneous or evoked somatic spikes. **A3.** The somatic SK current

maintains a lower level throughout the spike cycle in models with faster calcium clearance, and the evoked SK transient in response to AMPA inputs is diminished. **B1.** Distal dendritic voltage traces for models with varying rates of calcium clearance. **B2.** Distal dendritic calcium transients plateau in models with time constants for calcium clearance of 1 ms or slower. **B3.** Distal dendritic SK current transients in response to AMPA inputs.

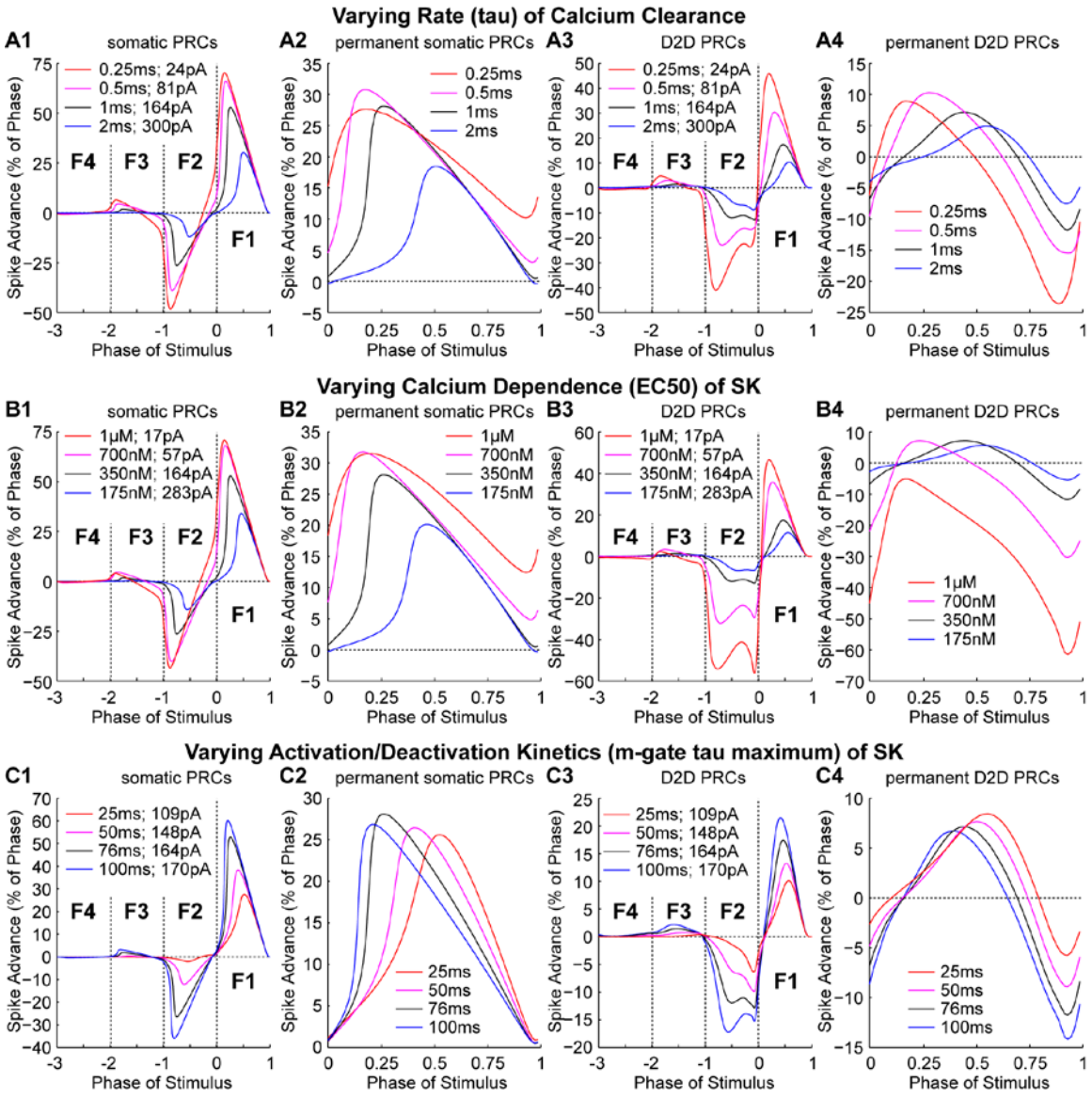

Supplemental Figure 2.11. Varying activation parameters of the SK conductance modulates the shape of the distal dendritic PRC without diminishing its type II character. (Each model was driven to 30 Hz by tonic somatic current injection amplitudes indicated in the legends of columns 1&3.) **A.** Varying the rate of calcium clearance between 25 and 200% of the base 1 ms value. (See also Supp. Fig. 2.7.) **A1&A2.** F1-F4 and permanent somatic PRCs annotated as in Fig. 2.8. **A3&A4** F1-F4

and permanent PRCs for $D2_D$ inputs. Smooth PRC shifts with changing rate of calcium clearance are observed without changing the type II behavior. **B.** Varying the steady-state calcium dependence of the SK conductance yielded a pattern of responses to AMPA inputs summarized by single cycle PRCs (**B1**&**B3**) and permanent PRCs (**B2**&**B4**) that closely resemble those obtained by varying the rate of calcium clearance (**A**). **C.** Varying the calcium dependence of the time constant of SK activation/deactivation also resulted in smooth shifts of PRC shape. However, the peak amplitude of the permanent PRC (**C2**&**C4**) was less affected than by the preceding manipulations (See also Supp. Fig. 2.8).

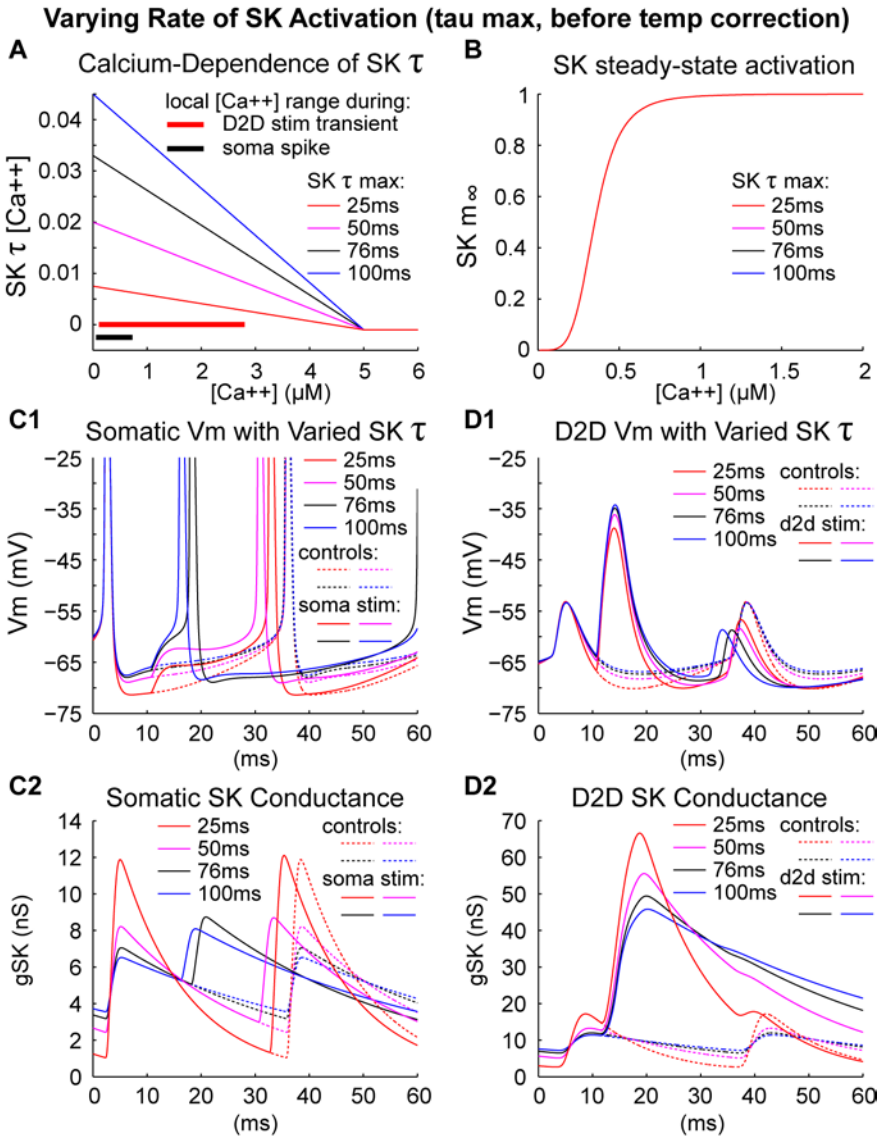

Supplemental Figure 2.12. Faster SK conductance activation reduces the excitability of the model. A. Calcium-dependence of the time constant of SK activation. Note the range of calcium concentrations that occur at the soma during a spontaneous spike and at the distal dendrite in response to an AMPA input. **B.** The steady-state activation curve for SK. **C1.** The somatic voltage is hyperpolarized during the control spike cycle, and it is more difficult to trigger a spike off-cycle. **C2.** In models with faster SK activation, the somatic SK conductance rises faster and to a higher level following a

spike but also falls faster and to a greater depth during the late part of the spike cycle. **D1.** Distal dendritic voltage during the control spike cycle and in response to AMPA input. **D2.** Models with faster SK activation/deactivation demonstrate higher but shorter-lived SK conductance peaks in response to AMPA inputs.

Chapter 3

During *in vivo*-like high conductance states, synaptic background activity and intrinsic mechanisms interact to control spike timing and responses to synaptic input.

Introduction

Neurons *in vivo* are subject to constant barrage by excitatory and inhibitory synaptic inputs distributed throughout the neuronal morphology that put the neuron in a state of high membrane conductance. Such high conductance states are characterized by low input resistance, a fluctuating membrane potential that is depolarized relative to isolated neurons, and an irregular spike pattern that reflects the stochastic synaptic background. Considerable theoretical and experimental attention has been given to the computational implications of high conductances states revealing that under such conditions a neuron's time and space constants are reduced, depolarization-gated membrane conductances maintain higher activation levels, and the neuronal response function becomes a sigmoid (Destexhe and Pare, 1999; Rudolph and Destexhe, 2001; Destexhe et al., 2003; Rudolph and Destexhe, 2003a, b). High conductance states therefore represent a mode of synaptic integration that is fundamentally distinct from that of neurons measured experimentally or simulated in isolation from synaptic background activity. High conductance states are also capable of switching the excitability of a

neuron, i.e. its integrative or resonant properties (Prescott et al., 2008), and affect conductance-based mechanisms of synaptic integration (Rudolph and Destexhe, 2001).

Phase response analysis is a powerful technique derived from dynamical systems theory that describes the responses of biological oscillators to perturbations at different phases of the oscillatory rhythm (Glass and Mackey, 1988). In neuronal systems the phase response curve (PRC) describes how synaptic inputs to a neuron at different times during the spike cycle affect the timing of subsequent spikes, and the shapes of neuronal PRCs have been related extensively to entrainment of spiking to correlated (Galan et al., 2006; Galan et al., 2007a, b; Marella and Ermentrout, 2008; Abouzeid and Ermentrout, 2009) or periodic (Rinzel and Ermentrout, 1998) input and to the emergence of synchronous modes in synaptically-coupled networks of neurons (Hansel et al., 1995; Ermentrout, 1996; Acker et al., 2003). By applying a measure made from individual neurons to prediction of network states, PRC analysis targets the interface between computation at the single neuron and network levels. However, neuronal PRCs are typically measured during the intrinsic oscillatory spiking of a neuron or neuron model in the absence of synaptic background activity. Thus, it remains unclear how PRCs derived during pacemaking relate to network activity during high conductance states *in vivo*.

The globus pallidus (GP) is a critical component of the indirect pathway of basal ganglia circuitry. GP neurons are intrinsic oscillators spiking rhythmically at <10 Hz in slice preparations, but *in vivo* GP neurons are bombarded by thousands of excitatory and inhibitory synaptic inputs per second that drive irregular spiking with a mean frequency of approximately 30 Hz. Using a morphological model we have previously demonstrated that somatic PRCs for GP neurons are type I, indicating that excitatory inputs at all

phases of the spike cycle advance the spontaneous spiking rhythm (Schultheiss et al., 2010). We further showed that distal dendritic PRCs for our GP neuron model are type II, i.e. excitatory inputs at early phases of the spike cycle paradoxically *delay* subsequent spiking. These delays were a consequence of activation of the small conductance calcium-activated potassium current, SK, local to dendritic stimuli (Schultheiss et al., 2010). A major goal of the current study was to determine whether PRCs derived during high-conductance states retain the character of those derived while the neuron oscillates intrinsically as in slice experiments or simulations. Second, we evaluate on a trial-by-trial basis the interactions between phasic inputs to the model and coincident fluctuations in the synaptic background activity. This analysis provides insight into the sources of variability in the responses of the model to excitatory inputs which in turn may be related to the coherence of pallidal network activity. Lastly, we present a method for describing the phase response properties of neurons in high conductance states that distinguishes intrinsic and synaptic effects contributing to the control of spike timing.

Results

The *in vivo* high conductance state poses at least three major challenges to the pattern of phase response properties we have previously described for GP neurons (Schultheiss et al., 2010): 1) Because the classes (type I and type II) of neuronal PRCs are related to neuronal excitability, i.e. the mechanism of spike initiation, high conductance states could switch somatic PRCs for the GP model between type I and II by activating additional membrane conductances during spike initiation; 2) The elevated membrane conductance throughout the neuronal morphology that accompanies a high level of synaptic activation could greatly attenuate the impact of dendritic inputs on spike timing;

and 3) The interaction of PRC stimuli with transients in the synaptic background could yield nonlinear effects on spike timing that are highly variable across trials potentially overwhelming the prominent features in somatic and dendritic PRCs obtained during spontaneous pacemaking. In this section, we first describe the generation of high conductance states in the model by application of stochastic synaptic backgrounds, and then we address the challenges posed by the high conductance state to the pattern of PRCs we previously described for the GP model during intrinsic pacemaking (Schultheiss et al., 2010).

Simulation of High Conductance States

We generated high conductance states in our base GP neuron model (GP_{base}) by applying synaptic backgrounds composed of randomly-timed, spatially-distributed excitatory (AMPA) and inhibitory (GABA) synaptic inputs. We varied critical parameters defining these synaptic backgrounds in order to generate output spiking of the model that covered the range of *in vivo* spike frequencies.

Synaptic Background Parameters Determine Frequency and Regularity of Spiking

For each of three levels of unitary synaptic conductance (0.5 nS, 1 nS, and 2 nS; low-, mid-, and high-gain, respectively) and for mean inhibitory input frequencies ranging from 0 Hz to 5 Hz, we precisely interpolated the frequency of excitatory input necessary to achieve target output spike frequencies of 15 Hz, 30 Hz, and 45 Hz. Figure 3.1A shows the resultant iso-frequency lines, which describe the balances between excitatory and inhibitory input frequencies that yielded the target output spike frequencies for each synaptic gain level. These iso-frequency lines illustrate the

approximately linear relationships between synaptic input frequencies, the net (inward) synaptic current, and the output spike frequency. For example, for the mid-gain synaptic background with 0.5 Hz inhibitory inputs to GP_{base}, excitatory input frequencies of 6.12 Hz, 19.13 Hz, and 38.66 Hz were necessary to drive output spiking to 15 Hz, 30 Hz, and 45 Hz, respectively. We repeated the process of interpolating excitatory input frequencies to achieve the target output spike frequencies for a version of the GP model in which the SK conductance had been removed from the dendrite (GP_{NDSK}) (Figure 3.1B). In the absence of this strong outward dendritic current, lower excitatory input frequencies were able to drive the GP_{NDSK} model to the target spike frequencies than were required for the GP_{base} model. The slopes of the corresponding iso-frequency lines were similar between the two versions of the model, however, indicating that higher input frequencies did not substantially increase baseline levels of SK current in the dendrite of the GP_{base} model.

By manipulating the synaptic gain and input frequency parameters we were able to vary the balance between intrinsic and synaptic drives contributing to output spike frequency, regularity, and spike timing. For each stochastic background, transient imbalances between excitation and inhibition caused the sub-threshold voltage to fluctuate, and higher-gain synaptic backgrounds drove larger sub-threshold voltage fluctuations, more threshold crossings, and thus higher output spike frequencies. Therefore, low- and mid-gain synaptic backgrounds (Figure 1A&B, dashed iso-frequency lines) required higher excitatory input frequencies to achieve the target output spike frequencies than did the high-gain backgrounds (Figure 1A&B, solid iso-frequency lines). Representative current, conductance, and voltage traces during 30 Hz spiking

driven by synaptic backgrounds with different gain and input rate parameters (indicated in A&B) are shown in Figure 3.1C1-3 for GP_{base} and in D for GP_{NDSK}. As illustrated by the ISI histograms and CV plots in Figure 3.2, output spiking driven by higher-gain synaptic backgrounds was more irregular than for the low-gain synaptic background, which more-closely resembled the rhythmic spiking of an intrinsic oscillator.

PRC Analysis During High-Conductance States

During high conductance states, spike timing is influenced by both intrinsic and synaptic drives, and GP neurons *in vivo* are not on a stable oscillatory limit cycle. A major goal of this study was to determine whether PRCs derived during high-conductance states retain the dynamics of those derived while the neuron oscillates due to intrinsic pacemaking (Schultheiss et al., 2010). For PRC analysis, we selected from the iso-frequency lines 9 parameter sets for GP_{base} representing 'low input frequency' synaptic backgrounds (inhibitory input rate = 0.5 Hz) and 9 parameter sets representing 'high input frequency' synaptic backgrounds (inhibitory input rate = 5 Hz), and we selected 9 synaptic background parameter sets for the GP_{NDSK} model. (See filled circles in Figure 3.1A&B.) These 27 parameter sets yielded output spike frequencies that span the range observed in *in vivo* experiments (Mallet et al., 2008). Furthermore, the synaptic background parameter sets sampled thoroughly from a wide parameter space anchored to physiological measurements, thus providing a diversity of plausible *in vivo*-like high conductance states.

For each of the 27 synaptic backgrounds, 100 single-trial PRCs were obtained by delivering a single 2.5 nS AMPA-synaptic input at each of 72 time-points (in separate simulations) within the first spike cycle of each of 100 control spike trains. Because

spiking during the control simulations was driven by the fluctuating synaptic background, the effects of the additional PRC stimuli were quite variable across trials. We averaged the PRCs from 100 trials with each synaptic background to evaluate the dependence of PRC shape on stimulus location, spike frequency, and dendritic SK conductance. For low-gain synaptic backgrounds (Figure 3.3A), the average effect across trials of excitatory somatic stimulation was to advance the first spike subsequent to the stimulus (F1). These advances were diminished in the second spike cycle corresponding to negative values in the second-order PRC (F2) (Figure 3.3A1). Only a slight effect of output spike frequency was evident for somatic inputs delivered during 15 Hz to 45 Hz spiking, similar to the oscillating GP_{base} model driven to the same frequencies by applied current (Supp. Fig. 3.2A). Average PRCs for stimulation of a representative dendritic site, D2D, however, showed a strong dependence on spike frequency: During 15 Hz spiking there was a pronounced negative region early in the F1 PRC and a late-phase negative peak in the F2 PRC. During faster spiking, the negative region of the F1 PRC was reduced and the negative peak in the F2 PRC occurred earlier in phase. We have previously demonstrated that this pattern of spike-frequency dependence of D2D PRCs is a consequence of the time-course of SK current elicited locally by the dendritic stimulus which at higher spike frequencies impinges increasingly on the second spike cycle. The positive peak in the F1 PRC for D2D inputs was also attenuated at higher spike frequencies, but further analysis comparing instantaneous frequencies of the stimulated ISIs for trials with the same synaptic background parameters, revealed this to be a consequence of the increased excitatory conductance used to achieve faster spiking (part of the synaptic background) and not of output spike frequency (Supp. Fig. 3.1).

The defining features of average PRCs for somatic and D2D stimulation were also prominent for the 'high input rate' synaptic backgrounds (Figure 3.3B) and for the mid-gain synaptic backgrounds (Figure 3.3C). With these higher conductance states, however, the membrane voltage fluctuations during the control trials were accentuated leading to greater variability in the effects of PRC stimuli on spike timing and greater standard error surrounding the average PRCs. For the synaptic backgrounds with the highest gain or with both high gain and high input frequency (not shown), average PRCs for D2D inputs were significantly attenuated by the elevated conductance of the dendrite and the important features of average PRCs were not as well defined.

Average PRCs for somatic stimulation of the GP_{NDSK} model (Figure 3.3D1) during mid-gain synaptic backgrounds also reproduced the prominent features of PRCs derived from the intrinsically spiking model (Supp. Fig. 3.2B). At 30 Hz the removal of SK from the dendrite accentuated advancements of the first spike cycle by somatic stimuli and yielded a greater positive peak in the F1 somatic PRC. As we have previously described for the oscillator, the negative peak in the corresponding F2 PRC was also accentuated, a consequence of *somatic* SK which was left intact in the GP_{NDSK} model. For D2D stimulation of the GP_{NDSK} model, the negative regions occurring early in the F1 PRC and late in the F2 PRC for the GP_{base} model were eliminated. Stimulation of D2D in the absence of dendritic SK yielded PRCs that resembled somatic PRCs and exhibited a larger positive peak in the F1 and corresponding negative peak in the F2 PRC.

Taken together, average PRCs derived by the application of single additional synaptic inputs on top of ongoing synaptic backgrounds illustrate the dependence of PRC shape 1) on the site of stimulation within the neuronal morphology, 2) on spike

frequency, and 3) on the presence of SK conductance in the dendrite. Thus, the effects of individual synaptic inputs on spike timing which we have previously described are not limited to the intrinsic oscillatory state but are also likely to shape the responses of these neurons during *in vivo*-like high conductance states.

Interactions of Phasic Synaptic Inputs with Ongoing Synaptic Backgrounds

Although average PRCs derived during high conductance states reproduced the dynamics of GP neuron models during intrinsic spiking and are likely to characterize the average behavior of populations of GP neurons, there was considerable variability in the responses of the models between individual trials with each synaptic background. A second major goal of this study was to characterize on a trial-by-trial basis, the ways in which phasic synaptic inputs used for PRC analysis interacted with transients in the fluctuating synaptic backgrounds. For this analysis we assessed the trajectories by which phasic PRC inputs perturbed spiking in individual trials and how the perturbed spike trains converged back to the control spike train over successive spike cycles.

Figure 3.4A-D illustrates sample control voltage traces (thick black lines) for low-gain (A&B) and high-gain (C&D) synaptic backgrounds. Voltage traces for each of 72 simulations each containing a single phasic stimulus to the soma (A&C) or D2D (B&D) are illustrated in color, where the color represents the phase of the perturbation delivered during the first ISI of the control simulation. In the low-gain example, somatic stimuli at all phases of the first spike cycle advanced the subsequent spike (Figure 3.4A). These advancements of the spike train diminished over the next several spike cycles (corresponding to negative values in the higher order PRCs) until each of the perturbed spike trains had returned to the control spiking pattern driven by the synaptic background

for this trial. Stimuli delivered to D2D either advanced or delayed the next spike depending on the phase of the stimulus (Figure 3.4B), and these shifts of the control spike train also diminished over successive spike cycles. Thus, for fixed patterns of synaptic background inputs (similar to frozen noise), the perturbing effects of additional phasic synaptic inputs were not permanent, and after some number of spike cycles (which varied widely from trial to trial) the synaptic drive exerted by the stochastic background became dominant again in determining the timing of subsequent spikes. When delivered against higher-gain synaptic backgrounds, somatic or D2D stimuli typically perturbed the voltage trajectory of the model from the control spike trains for fewer spike cycles (Figure 3.4C&D) than when the synaptic background was weaker. Thus, as will be described in detail later in this text, the strength of the synaptic background was a major determinant of the longevity of perturbations initiated by individual phasic inputs delivered against ongoing synaptic backgrounds.

Added spikes, skipped spikes, and divergence events. The examples shown in Figure 3.4A-D illustrate relatively smooth convergence of the perturbed voltage trajectories back to the control spike train across successive spike cycles. In many trials, however, the delivery of an additional synaptic input to the soma or dendrite triggered a sequence of events not characterized by the average PRC or smooth convergence. Among these events were instances where perturbed spike trains contained a spike not present in the control spike train or conversely, where perturbed spike trains lacked a spike that was present in the control spike train. Examples of such 'added' or 'skipped' spikes are shown in Figure 3.4E&F, respectively. As illustrated in the former example, it was common for an added spike to be the result of a complex sequence of events initiated

by the PRC stimulus rather than being triggered directly by the stimulus itself: In Figure 3.4E, the advancements of the first spike cycle elicited by phasic stimuli to D2D caused the model to spike on a different set of transient depolarizations in the sub-threshold voltage than it had during the control simulation. Within a few spike cycles (dashed box), the perturbed spike trains had converged to the control spiking pattern, having fired an additional spike in the interim. Conversely, Figure 3.4F illustrates an instance where a spike in the control spike train was skipped by the perturbed spike trains. In this case, very slight initial shifts in spike timing elicited by the D2D stimuli were sufficient to alter the way the model reacted to the synaptic background, and notable delays in spike timing emerged in the third spike cycle. The next control spike was skipped by the perturbed trajectories because they had not yet sufficiently recovered from after-hyperpolarization following the previous spike.

Surprisingly, added or skipped spikes did not always occur in the first few spike cycles following the delivery of phasic PRC stimuli. Figure 3.4G shows a case where an extra spike was added several spike cycles after stimuli and a subsequent control spike 6 spike cycles later was skipped even after the perturbed spike trains had seemed to converge back to the control trajectory. This example highlights that slight perturbations can cause the model to respond very differently to transient components of the fluctuating synaptic background. Further illustrating this principle, Figure 3.4H shows a case where, after having converged, perturbed spike trains diverged gradually across successive spike cycles ultimately resulting in a separate populations of spike events riding on different voltage transients that accompanied fluctuations in the synaptic background. We categorized this type of phenomenon as ‘divergence events’ and included all instances

where perturbed spike trains for a given trial diverged after having drawn within 0.5 ms (mean across the 72 perturbations per trial) of the control spike train.

The incidence of added spikes was considerably higher with somatic stimulation than with D2D stimulation, reflecting the relative strength of somatic perturbations. Added spikes were also more common during 15 Hz spiking (35.7% and 13.7% of trials for somatic and D2D stimuli, respectively, across gain levels) than during 30 Hz (21.7% & 5.3%) or 45 Hz spiking (16% & 1%). The incidence of trials containing skipped spikes initiated by somatic inputs was very low across all synaptic backgrounds (0.6%) but somewhat larger for D2D inputs (9.7%) reflecting extreme cases of the ability of dendritic inputs to delay spiking by local activation of SK current. Consistent with this, in the GP_{NDSK} model, instances of skipped spikes were extremely rare (0.3% of trials). There was no clear difference in the incidence of added spikes or skipped spikes between the mid-gain and high-gain synaptic backgrounds, however, both occurred much less often with the low-gain synaptic background. Divergence events were observed with a relatively low incidence for somatic and D2D stimuli (14.7% and 8% of trials, respectively) and did not exhibit a clear relationship with the gain of synaptic background or with output spike frequency.

To further characterize the variability across trials of the interactions between phasic inputs with synaptic backgrounds, we also examined the incidence of added spikes, skipped spikes, and divergence events over several spike cycles subsequent to stimulation (Figure 3.5A-C) and as a function of the phase of perturbation (Figure 3.5D-F). Surprisingly, the distribution of these event types over the 20 ISIs following stimulation did not strongly favor the first few ISIs, but were relatively smoothly

distributed over many spike cycles perhaps with a peak frequency occurring between 5 and 10 spike cycles subsequent to stimulation. In these instances, shifts in spike timing caused by the phasic perturbations led to differences in excitability associated with the refractory period and fast and medium after-hyperpolarizations (AHPs), and these differences affected the way that the model reacted to the subsequent fluctuations in the synaptic background. These often slight differences between perturbed trajectories led in turn to additional differences in spike timing which mapped differently onto subsequent fluctuations in the synaptic background, and thus propagated indirectly across spike cycles the effect of the original perturbation.

We further evaluated the distribution of added spikes, skipped spikes, and divergence events as a function of the phase of the perturbing inputs. Even though the occurrences of added spikes and divergence events did not take place at the time of stimulation, they did occur most commonly in trials where perturbing stimuli were delivered near the middle of a spike cycle. Instances of skipped spikes, however, were most likely to result in trials where stimuli were delivered to D2D during a brief window early in phase or during the last 20% of phase. This pattern of phase dependence of these events mirrors the phase dependence of inputs effects on spike timing (the PRC), suggesting continuity between the effectiveness of a stimulus in advancing the time of spike and the occurrence of added spike and continuity between the effectiveness of a stimulus to delay spike times and the occurrence of skipped spikes.

For the remaining analysis of interactions between phasic perturbations and stochastic synaptic backgrounds, we excluded trials containing added or skipped spikes and trials in which perturbed spike trains remained unconverged after 20 spike cycles

subsequent to stimulation or diverged after having converged back to the control spike train. Unconverged trials occurred very infrequently (2% and 1% of trials with somatic and D2D stimuli, respectively) except for the low-gain synaptic backgrounds (20% and 6.3%, respectively) which did not drive convergence as strongly. Even after these exclusions, perturbed spike trains did not converge to their respective control spike trains for many spike cycles after the stimulus. Likewise, the mean variance of shifts in spike timing across perturbed simulations persisted across many spike cycles. To characterize the dependence of this variability in spike shifts in perturbed spike trains on input phase we plotted phase response-variance curves (PRVCs). Figure 3.6 illustrates that the variance in spike shifts elicited by somatic stimuli was maximal when stimuli were delivered during the middle of the spike cycle, and near zero when stimuli were delivered coincident with control spikes. Somatic PRVCs contained only a single peak in variance that diminished across spike cycles. PRVCs for D2D inputs, however, were multiphasic, containing an additional peak early in phase for the first spike cycle, reflecting that the effect of dendritic SK conductance is an additional source of variability in spike timing. The F2 PRVC for D2D inputs is also multiphasic, containing additional peaks for both early-phase stimuli and late-phase stimuli and mirroring the phase dependence of the incidence of skipped spikes. Trials containing skipped spikes were excluded prior to generation of PRVCs, however, which suggests strongly that the increased variance in spike shifts elicited by inputs within these regions of phase is also a consequence of dendritic SK conductance that led in some trials to skipped spikes. Confirming this, elimination of the SK conductance from the dendrite (GP_{NDSK}) resulted in PRVCs for

D2D inputs that did not contain multiple peaks and that show a phase dependence resembling that of the variance elicited by somatic inputs to the GP_{base} model.

As described already, perturbations applied in the first spike cycle of control spike trains were propagated across spike cycles leading to prolonged deviations from the control spiking pattern by the complex interactions between spike times, differences in excitability associated with the refractory period and AHPs, and fluctuations in the synaptic background. We defined 'convergence' as being complete when the 72 perturbed spike trains for each PRC trial returned (on average) to within 0.5 ms of the spike times of the control spike train. To assess how the longevity of these perturbations can depend on the synaptic background and on output spike frequency, we plotted for each synaptic background the proportion of trials that remained unconverged against the number of spike cycles since the original perturbation. Interestingly, convergence following somatic perturbations progressed nearly linearly across spike cycles for low gain synaptic backgrounds independent of output spike frequency (Figure 3.7A). This effect was also evident for mid and high gain synaptic backgrounds, but in these cases convergence progressed faster over the first several spike cycles subsequent to stimulation. Thus, for stronger synaptic backgrounds, fewer spike cycles were required on average for perturbed spike patterns to return to the control spike pattern. For example, approximately 40% of trials with low gain synaptic backgrounds and 10% of trials with mid-gain synaptic backgrounds remained unconverged after 10 spike cycles subsequent to perturbation. Therefore, the number of spike events following the perturbation was more strongly related to the proportion of trials that remained unconverged than was the time that had elapsed. This suggests that spikes act as resetting

events by forcing the voltage and activation of intrinsic conductances through the relatively fixed trajectory of a spike. Convergence following stimulation of D2D also exhibited a strong effect of synaptic background strength. In contrast to the pattern of convergence following somatic stimuli, however, perturbations of D2D were shorter-lived when output spiking was faster. We hypothesized that this effect was a consequence of higher SK conductance activation maintained as spikes invaded the dendrite at higher frequencies. Convergence following D2D stimulation of the GP_{NDSK} model showed a dramatically reduced effect of output spike frequency, indicating that elevated SK activation during faster spiking did account for the majority of the spike frequency effect on convergence. In the absence of dendritic SK, convergence following D2D stimulation progressed much the same as following somatic stimulation of the GP_{base} model, further indicating the dendritic SK plays a fundamental role in shaping the nature and time-course of responses of these models to dendritic stimulation. Still, some spike frequency effect on convergence remained indicating that other dendritic conductances were also activated differentially in a frequency dependent manner.

Larger voltage fluctuations accompanying higher-gain synaptic backgrounds caused responses to phasic PRC stimuli to be more variable across trials. Having excluded trials in which added or skipped spikes or divergence events occurred, we obtained a purified sample of trials with which to assess the effect of synaptic background gain on the PRCs for somatic and dendritic stimulation. The F1 somatic PRCs for higher-gain synaptic backgrounds were attenuated relative to the corresponding PRCs for weaker synaptic backgrounds; however, there was no significant difference in the amplitude (minima) of higher order PRCs for somatic inputs between the synaptic

backgrounds of different strengths. These higher order PRCs were composed purely of negative values reflecting the diminution across spike cycles of the spike advances elicited in the stimulated spike cycle. The positive peaks of F1 PRCs for inputs to D2D were also attenuated for the higher gain cases, but each still contained a slight negative region early in phase. D2D PRCs for the low-gain and mid-gain synaptic backgrounds also maintained a significant negative peak late in phase of the F2 PRC reflecting the delaying effect of SK current on the timing of the second spike following stimulation.

In these cases, it is difficult to distinguish the independent effects of the phasic stimuli, evoked currents, and synaptic backgrounds on spike timing. Further confounding these factors, the time course of SK evoked by dendritic inputs spans multiple spike cycles and convergence progresses gradually over several spike cycles. Whereas phasic inputs to an oscillator influence the timing of the next one or a few spikes, after a few spike cycles the entire effect of the stimulus has been exerted and the permanent resetting of the spiking rhythm can be calculated as the sum of F1, F2, and any additional higher-order PRCs to give the permanent PRC. Since synaptic backgrounds eventually restore the control spike pattern, the permanent PRC derived under these conditions will always be zero indicating that stimulus effects on spike timing are eventually washed out. We therefore developed a tool for visualizing the independent effects of phasic stimuli on spike timing and of synaptic backgrounds in attenuating these perturbations across spike cycles restoring the control spike pattern. Cumulative PRCs (cPRCs) describe the total effect of phasic inputs on spike timing assessed at each spike cycle. Thus the F_C1=F1, F_C2=F1+F2, F_C3=F1+F2+F3, and so on. Cumulative PRCs illustrate the evolution of inputs' effects on spike timing from one spike cycle to another. Changes in shape or

y-translations of the cumulative PRC reflect contributions to spike timing made by intrinsic currents while attenuation of the cPRC reflects the effect of the synaptic background to reduce these effects and restore the control spike pattern. Cumulative PRCs derived after excluding added spikes, skipped spikes or divergence events taking place within the first 10 spike cycles subsequent to stimulation are shown in Figure 3.9 for somatic and D2D inputs to GP_{base} and for D2D inputs to GP_{NDSK}. Somatic cPRC for GP_{base} are essentially composed of a single positive peak that attenuates smoothly over 10 spike cycles (Figure 3.9A&B). The F_C1 PRC for D2D inputs is also essentially a single positive peak; however, the F_C2 PRC contains significant negative regions both early and late in phase. This is a consequence of outward SK current evoked locally by D2D stimuli which impacts strongly the second spike cycle. Thus, while inputs delivered to D2D either early or late in the spike cycle had little effect on the timing of the next spike, they significantly delayed the second spike following the stimulus. Spike time advances elicited by inputs delivered during the middle of the spike cycle were dramatically reduced by the impact of SK during the second spike cycle. Taken together these effects of the SK conductance on spike timing are summarized by y-translation of the F_C1 PRC to more negative values in the F_C2, which then attenuated across the next 5 or 6 spike cycles as the synaptic background drove spiking back to the control trajectory. Phasic stimuli delivered to D2D of the GP_{NDSK} model yielded cPRCs with much the same profile as somatic PRCs for GP_{base}. Advances of the first spike cycle were reduced across successive spike cycles as illustrated by the attenuation of the positive peak. No delays were elicited by inputs at any point in phase, and convergence required 10 spike cycles (as with somatic cPRCs for GP_{base}) which was slower than for D2D stimulation of GP_{base}.

These results further illustrate that dendritic SK conductance is a fundamental contributor to spike timing in these models and that in its absence, there does not seem to be a qualitative difference between the effects of somatic and dendritic inputs.

Discussion

High conductance states can represent a fundamentally different mode of synaptic integration of neurons *in vivo* than is exhibited by neurons in isolation from synaptic backgrounds. The primary goals of the current study were to determine whether and how high conductance states change the responses of GP neurons to somatic and dendritic synaptic inputs delivered at different phases of the spike cycle. Our second goal was to characterize the variability observed between trials that results from the highly nonlinear interactions between synaptic background activity and the phasic perturbations. To address these questions we turned to computer simulations using a morphologically reconstructed GP neuron model, because it afforded us exacting control over stimulus delivery to the dendrite and repeatability of spatially-distributed patterns of synaptic activity. These advantages were necessary for parsing the complex interactions of synaptic and intrinsic factors contributing to the precise timing of spikes in the presence of noisy synaptic background activity.

In a previous study of these GP neuron models we demonstrated that during intrinsic spiking, phasic synaptic inputs differentially affect spike timing yielding type I PRCs for somatic inputs and type II PRCs for excitatory stimulation of the distal dendrite. The elevated membrane conductance of synaptic backgrounds poses a considerable challenge to this pattern of phase response properties and might have been expected to wash-out the dependence of PRC shape on the site of stimulus delivery

within the neuronal morphology. We found that for stochastic synaptic backgrounds of moderate amplitude, the pattern of shifts in spike timing evoked by PRC stimuli was generally well preserved, i.e. average somatic PRCs across trials were type I and average D2D PRCs were type II. These average PRCs also exhibited a similar dependence on output spike frequency and on the dendritic SK conductance as we previously observed with the intrinsically spiking model. A second important realization is that the phase dependences of response variance and the incidence of skipped spikes and divergence events, in addition to the phase dependence of input evoked shifts in spike timing, all reflect the influence of intrinsic mechanisms on spike timing.

It is important to note that for our PRC analysis, we used as the perturbing stimulus a single 2.5 nS input. Single STN synapses onto GP may be on the order of 1 nS to 10 nS and may vary widely both in unitary strength and in the synchrony across multiple synapses from a single or few STN neurons. Synchronized excitatory input from STN may also be distributed across multiple dendritic branches maximizing their efficacy in activating intrinsic conductances. Therefore, the effective size of a realistic excitatory input to GP may be greater than a single spatially localized input of the size of our stimulus. The pattern we observed of robustness against synaptic backgrounds with different unitary conductances, suggests that the size of an input relative to the amplitude of ongoing fluctuations is an important determinant of its efficacy in affecting the precise timing of output spiking. It is natural to imagine from a neuron's perspective that an incoming 'signal' is more significant when it stands out above the 'noise' of other ongoing inputs, and that *in vivo* modulation of either the ongoing synaptic 'noise' or of the signal will titrate the relief within which the signal stands apart from the background.

The second major result of this study was the observation that during ongoing synaptic background activity the responses of GP neuron models to phasic excitatory inputs are altered in important ways characteristic of the high conductance state: 1) responses to weak inputs were amplified, and 2) responses to higher amplitude inputs were attenuated relative to the intrinsically oscillating model by the elevated membrane conductance. The mechanism underlying the amplification of weak inputs involves the higher level of SK activation maintained throughout the dendrite during the high conductance state, which leads to a nonlinear increase in the efficacy of weak inputs to yield type II PRCs. This important effect therefore relies on a different mechanism than increased spike probability caused by stochastic resonance, and is an interesting extension of the phenomenon.

The architecture of dendritic trees and the complement of active dendritic conductances are critical features of the computational machinery employed by neurons with diverse functional objectives (Mainen and Sejnowski, 1996; Vetter et al., 2001; Krichmar et al., 2002; Stiefel and Sejnowski, 2007; Chen et al., 2009; Komendantov and Ascoli, 2009). Because most excitatory input to GP neurons is on dendritic sites (Shink and Smith, 1995) it is critical to consider the effects of dendritic inputs in the control of spike timing and network behavior. Very few studies have undertaken PRC analysis with dendritic models (Crook et al., 1998b; Goldberg et al., 2007) or morphologically realistic neurons models (Stiefel et al., 2008; Stiefel et al., 2009; Schultheiss et al., 2010). PRC analysis with noise has also been done in a few key studies, but PRC analysis during synaptic backgrounds composed of realistic barrages of realistic excitatory and inhibitory synaptic inputs is more biologically realistic and to our knowledge has never been

performed. By simulating high conductance states in this way, we are able to assert that variability observed across trials is representative of the variability that might be expected across neurons in pallidal networks. The considerable variability across trials that resulted from interactions of PRC stimuli with fluctuating synaptic backgrounds is reminiscent of the variability across populations of neurons recorded during movement tasks (Churchland and Shenoy, 2007) and may help constrain the relationship between single neuron responses and population coding.

It is difficult to assess the importance of spike time precision of GP neurons for behaviorally relevant neuronal processing, and GP neurons in normal rats and humans are characteristically desynchronized. In models of Parkinson's disease, synchronized oscillations and bursting have been observed in several physiological studies (Plenz and Kitai, 1999; Magill et al., 2000, 2001; Loucif et al., 2005) and network simulations (Terman et al., 2002) suggest that the GP-Subthalamic Nucleus (STN) feedback loop can promote oscillatory pattern generation (Bevan et al., 2002). Furthermore, recent evidence indicates an orchestrating role for GP in the β-frequency synchronization of BG activity in PD (Mallet et al., 2008). It is likely that pathological entrainment of GP neurons to oscillating excitatory input contributes significantly to the pathophysiology of basal ganglia networks in PD, and it is provocative that the time-course of intrinsic effects on spike timing observed in dendritic PRCs, i.e. the time-course of SK activation (approximately 45 ms), matches well with beta. It is plausible that the SK mechanism of spike time delay resonates with beta-frequency oscillatory input from STN contributing to the entrainment and synchronization of pallidal networks in PD.

We have previously used the GP neuron model described here to investigate the influence of conductance densities on spiking properties (Gunay et al., 2008). We observed that most electrophysiological properties of the models were affected by multiple conductances, and each conductance affected multiple electrophysiological measures (Gunay et al., 2008), which is consistent with modeling studies of other types of neurons (Prinz et al., 2003b; Achard and De Schutter, 2006; Taylor et al., 2009). The model was located in a broad basin of models with similar spiking properties when channel densities were varied, as described in our earlier publications (Gunay et al., 2008; Schultheiss et al., 2010). Thus, the model does not represent a unique solution to intrinsic GP spiking properties, and our preliminary findings were robust against considerable model parameter variations (Schultheiss et al., 2010). The synaptic backgrounds used in this study represent generically high conductance states representative of the *in vivo* synaptic environment. We varied critical parameters defining these backgrounds in order to test high conductance states with different characteristics, and to generate output spike frequencies that spanned the range observed *in vivo*. The input frequencies used to achieve the target spike frequencies reflect spike frequencies of the major source of inhibitory input to GP, the striatum (during up and down states), and the major source of excitatory input to GP, the subthalamic nucleus (STN). In-as-much as the GP model and simulated synaptic backgrounds are physiologically realistic, the variance in the model's responses across trials directly reflects a major source of spike time variance across populations of GP neurons *in vivo*.

Type II PRCs are optimal for stochastic synchronization of a population of neurons to shared input (Abouzeid and Ermentrout, 2009). Since the preponderance of

synaptic inputs to GP neurons is on the dendrites, type II dendritic PRCs may contribute to formation and coordination of pallidal ensembles governing normal motor control. Additionally, the cellular mechanisms underlying type II dendritic PRCs for GP neurons could be pathologically modulated in disease states contributing to entrainment of these neurons to β–frequency oscillatory activity that is a critical component of the pathophysiology of Parkinson's disease.

Methods

All simulations were run using the GENESIS simulation platform (www.genesis-sim.org/GENESIS) on Emory University High Performance Compute Clusters (Sun Microsystems). Approximately 1.5 min of processor time was required to simulate one second of data with 20 μs time steps, and custom Matlab (The MathWorks, Natick, MA) routines were used for analysis of voltage, current, conductance, and spike time data.

GP Neuron Model

Morphology and Passive Electrical Properties. The morphology and passive electrical properties of our baseline GP neuron model (GP_{base}) have been previously described in detail (Hanson et al., 2004; Gunay et al., 2008). In brief, we reconstructed the morphology of a GP neuron for which a battery of electrophysiological recordings had been made using Neurolucida (MicroBrightField, Inc.) and created a GENESIS morphology file using CVAPP software (www.compneuro.org). The resultant somato-dendritic morphology of the GP model contained a spherical soma and 511 dendritic compartments, each of which was no more than 0.02 lambdas in electrotonic length. We matched the passive model to experimental voltage responses by setting the specific

membrane capacitance (C_M) to 0.024 F/m^2, the specific membrane resistivity (R_M) to 1.47 Ωm^2, and the specific axial resistivity (R_A) to 1.74 Ωm. To allow axonal spike initiation and realistic axonal current sources and sinks, a standard axon consisting of a highly excitable axon initial segment and nodes of Ranvier separated by myelinated inter-node segments, was adapted from Shen et al. (1999) and attached to the soma.

Active Conductances and Model Tuning. One calcium-activated conductance and eight voltage-gated membrane conductances were added to the passive model based on experimental evidenced of the presence in GP neurons. The voltage-gated conductances were modeled using standard Hodgkin-Huxley equations and included the following channel types: fast-transient and persistent sodium currents, NaF & NaP (Magistretti and Alonso, 1999; Magistretti et al., 1999; Raman and Bean, 2001; Magistretti and Alonso, 2002; Khaliq et al., 2003; Hanson et al., 2004; Mercer et al., 2007); fast and slow delayed-rectifier (K_{dr}) potassium currents, K_V3 & K_V2 (Baranauskas et al., 1999; Baranauskas et al., 2003); A-type potassium current, which we modeled as two channel populations in order to accurately match fast and slow components of the inactivation kinetics, K_V4F & K_V4S (Tkatch et al., 2000); M-type potassium current, KCNQ (Gamper et al., 2003; Prole and Marrion, 2004); hyperpolarization-activated mixed cation current, or h-current, which we also modeled as two channel populations, HCN1 & HCN2 (Wang et al., 2002; Chan et al., 2004); and a high-voltage-activated calcium current (Ca_{HVA}) representing a mixture of L-, N-, and P/Q-type currents. The calcium dependence of the small-conductance calcium-activated potassium current (SK) (Hirschberg et al., 1998b; Hirschberg et al., 1998a, 1999; Keen et al., 1999) was modeled using the Hill equation.

The activation and inactivation parameters for each conductance are listed in Supplemental Table 2.1.

Each conductance was distributed uniformly throughout the dendrite with the exception of Ca_{HVA} whose density was greater in thinner, distal dendritic compartments (Hanson and Smith, 2002). During the tuning process, conductance densities were determined using a semi-automated process comparing model behaviors with physiological recordings, and a thorough exploration of parameter space was performed (Gunay et al., 2008; Schultheiss et al., 2010). The resultant base model for the current investigation, GP_{base}, is identical to Schultheiss et al. 2010. As described in our previous study, GP_{base} falls well within the physiological variability for the following electrophysiological measures: spontaneous spike waveform, spontaneous spike frequency, somatic FI curve, spike frequency adaptation, spike height attenuation during positive currents steps, voltage 'sag' during negative current steps, and latency to the first spike following the offset of negative current steps. The full GENESIS model used in this study is available from ModelDB (http://senselab.med.yale.edu/ModelDB/).

PRC Analysis During High Conductance States

Synaptic Backgrounds. The synaptic backgrounds used to generate high conductance states in the models used in this study were composed of 1022 GABA synapses and 100 AMPA synapses distributed randomly throughout the dendrite. These values reflect the proportion of inhibitory and excitatory inputs to GP, and the kinetics of the synapses were based on physiological data. We determined 27 sets of synaptic background parameters by interpolating excitatory input frequencies necessary to achieve target output spike frequencies of 15 Hz, 30 Hz, and 45 Hz for different combinations of

inhibitory input frequencies (0 Hz to 5 Hz) and unitary synaptic conductance (0.5 nS, 1 nS, and 2 nS). These output spike frequencies span the range of frequencies observed in *in vivo* experiments, and the input frequencies used to achieve them reflect realistic spike frequencies of the major source of inhibitory input to GP, the striatum (during up and down states), and the major source of excitatory input to GP, the subthalamic nucleus (STN). The input frequencies and unitary conductance parameters for each synaptic background are listed in Supplemental Table 2. For each of the 27 synaptic background parameter sets we generated 100 control spike trains differing only in the random timing of the individual synaptic inputs.

PRC Stimulation Protocol. To allow the model to adapt to the ongoing synaptic backgrounds before conducting PRC analysis, we simulated a 10 s period for each background without additional PRC stimuli. To avoid repeating these simulations of adaptation time for each PRC simulation, we saved all state variables in a 'snapshot' file after conducting these simulations once, and used them for subsequent PRC simulations. Next, one hundred single-trial PRCs were generated for each synaptic background by delivering additional excitatory PRC stimuli at different phases of the first inter-spike interval (ISI) of each the 100 control spike trains for each background parameter set. For each trial, in 72 separate simulations a 2.5 nS AMPA input was delivered at each of 72 evenly-distributed time points. The onset of the earliest input was timed to be coincident with the somatic spike delineating the start of first spike cycle. Spike times were recorded using the GENESIS spikehistory element which provided precision of 1e-6 s, and input-evoked shifts in spike timing were calculated relative to the spike terminating the first control spike cycle. PRCs were plotted as spike advances (in units normalized to

the period of the control ISI) as a function of input phase, such that positive values reflected advancements of the spike cycle. Single trial PRCs were highly variable, so to assess the average effect of phasic PRC inputs on spike timing, we generated average PRCs across the 100 trials for each synaptic background. Separate average PRCs were derived for somatic stimuli and for stimulation of a distal dendritic site (D2D) that is representative of a distinct mode of synaptic integration that we have previously characterized.

To characterize the interactions of PRC stimuli with fluctuations in the ongoing synaptic backgrounds, we defined 3 types of events that were commonly observed: added spikes, skipped spikes, and divergence events. Added spikes were instances where spike trains for simulations containing a PRC stimulus contained a spike that was not present in the control simulation without the PRC stimulus, and skipped spikes were instances where the spike train for a control simulation contained a spike that was not present in simulations containing a PRC stimulus. The effect on the spike train of adding a PRC stimulus on top of ongoing synaptic backgrounds often lasted for many spike cycles, but eventually most perturbations diminished and the timing of subsequent spiking returned to that of the control spike train. We defined 'convergence' as the process by which perturbations diminished across successive spike cycles, and deemed the progression of convergence to be complete when the average difference between spike times in the 72 stimulated simulations for each trial was less than 0.5 ms from the control spike times for that trial. In some cases, however, the spiking trajectory in perturbed simulations met our criterion for having converged only to 'diverge' again and deviate from the control spike train. We defined such instances as 'divergence events.' Each of these types of events

was identified using a custom automated algorithm and the phase of stimuli leading to these events as well as the spike cycle in which they occurred were recorded for further analysis. To analyze the variability across trials of the effect of PRC stimuli on spike timing, we invented phase response-variance curves (PRVCs), which plot the phase dependence of the variance of spike shifts for each synaptic background across spike cycles. To characterize the progression of convergence as a function of synaptic background parameters, we plotted the proportion of trials that remained unconverged as a function of the number of spike cycles that had elapsed since stimulus delivery. Trials containing added spike, skipped spikes, or divergence events, as well as trials in which perturbed simulations did not meet our criterion for convergence within 20 spike cycles following stimulation (unconverged trials) were excluded from the population of trials used for these analyses and to generate average PRCs shown in Figure 3.8.

To allow intrinsic effects on spike timing evoked by PRC stimuli to be readily distinguishable from the effect of synaptic backgrounds (driving spikes back onto the control trajectory by the process of convergence) we invented cumulative PRCs which plot for each spike cycle the cumulative effect of perturbations on spike timing assessed at the time of each successive spike in the spike train. Thus, C1 PRC is the same as the average F1 PRC, because only one spike cycle is being considered. The C2 PRC is the sum of the average F1 PRC and the average F2 PRC, the C2 PRC is the sum of average F1, F2, and F3 PRCs, and so on. By plotting cumulative effects on spike timing in this way, changes in the shape of cPRCs or y-translation of cPRCs reflect the contribution of intrinsic mechanisms to spike timing, whereas attenuation of cPRCs reflects the

convergence of perturbed spike trains back to the control spike train across successive spike cycles.

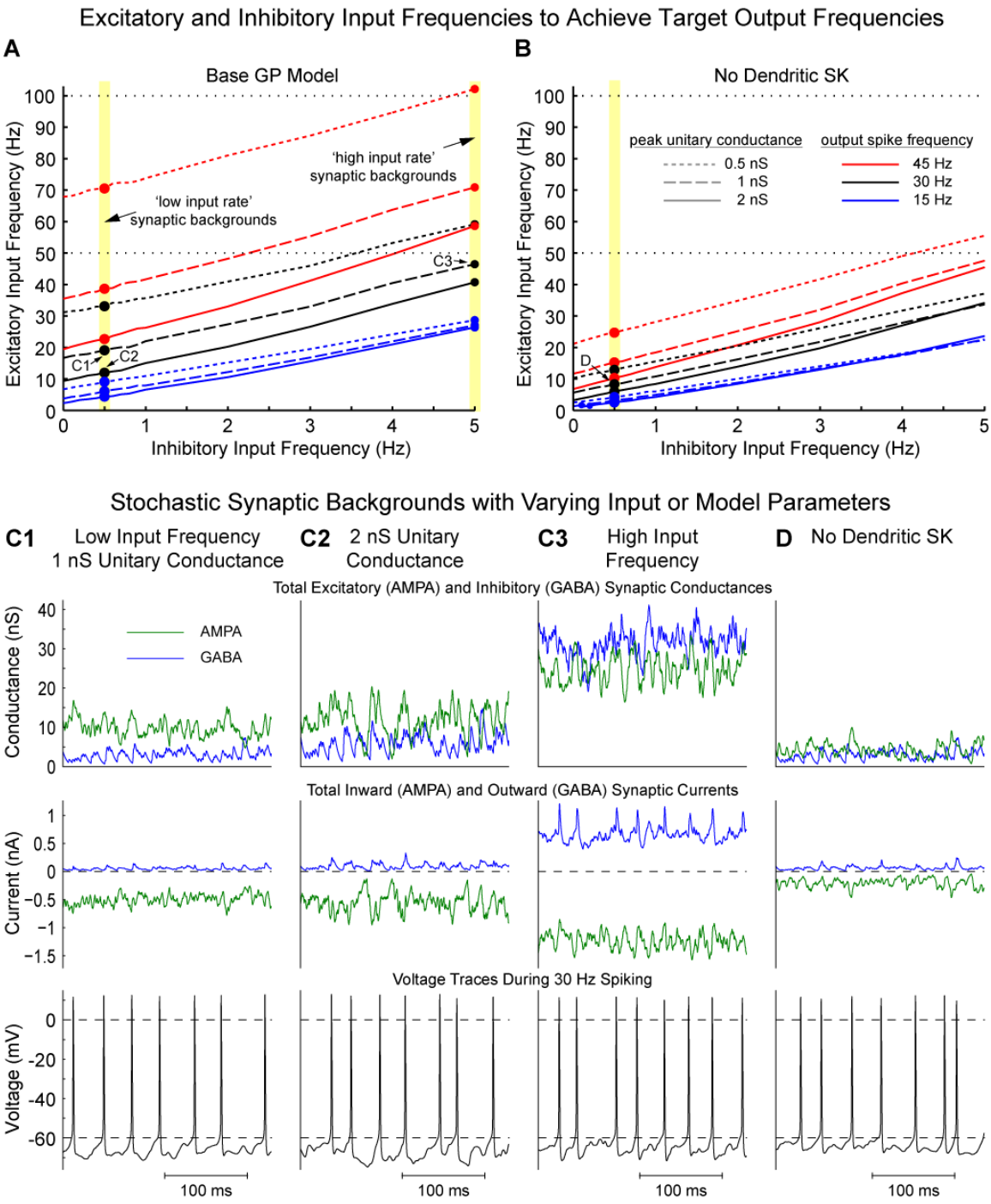

Figure 3.1. Diverse synaptic backgrounds achieve realistic output spiking. A. Iso-frequency lines for GPbase. Each point on each line reflects a pair of excitatory and inhibitory input frequencies that achieves the target output spike frequency (indicated by

color). Dashed and solid lines for each color trace reflect the unitary conductance (gain) of the synaptic events composing that synaptic background. **B.** Iso-frequency lines for the GP_{NDSK} model. **C.** Representative total excitatory and inhibitory current traces, total excitatory and inhibitory conductance traces, and voltage traces for synaptic backgrounds with 1 nS unitary synaptic inputs (C1), 2 nS unitary synaptic inputs (C2), and high frequency inputs (5 Hz inhibitory, 46.47 Hz excitatory) during 30 Hz spiking of the GP_{base} model. **D.** Representative traces for the GP_{NDSK} model during 30 Hz spiking (0.5 Hz excitatory, 8.36 Hz inhibitory, 1 nS unitary conductance).

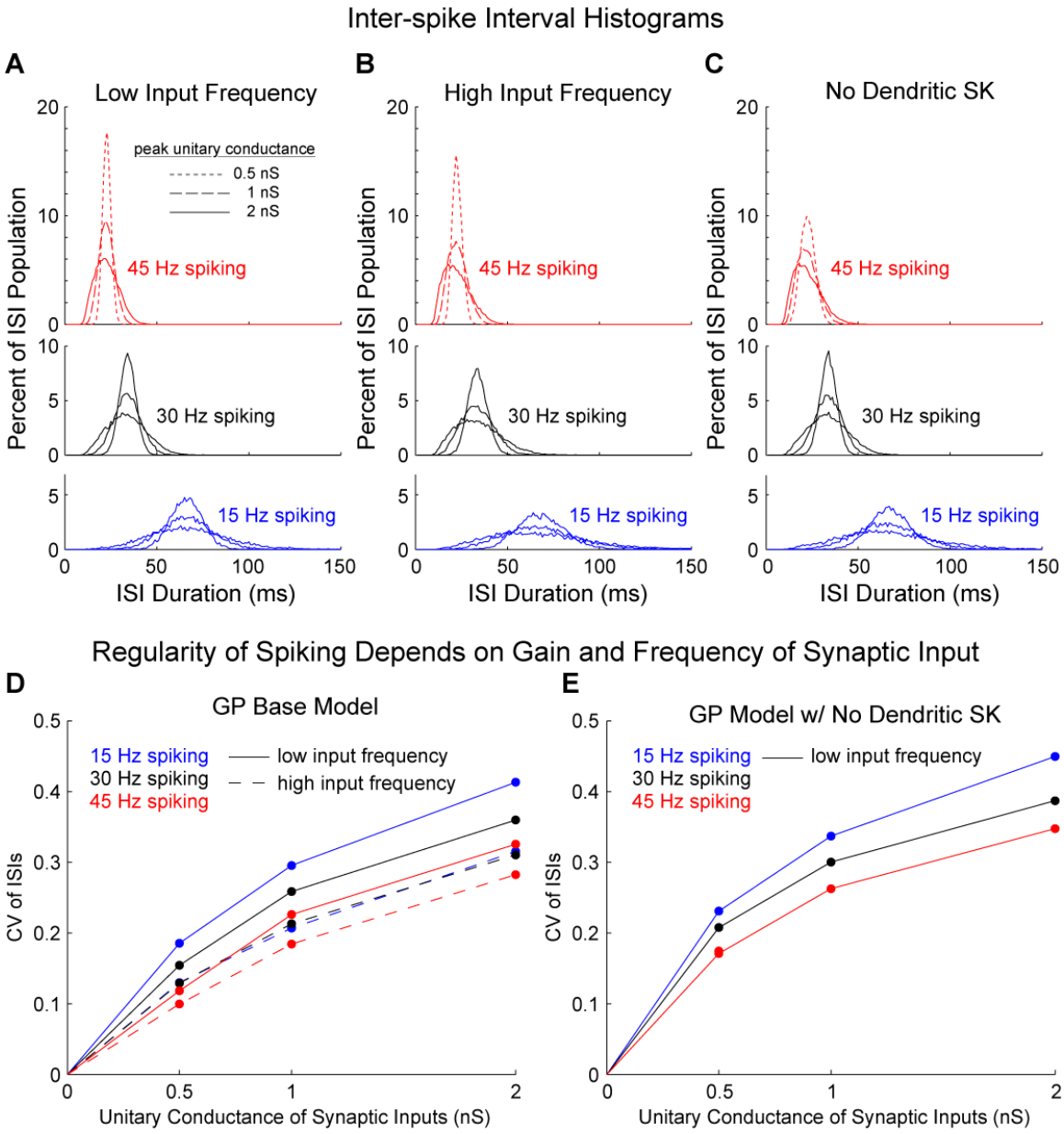

Figure 3.2. Synaptic background parameters determine inter-spike interval distributions. **A.** ISI histograms for the 9 low input rate parameter sets (indicated in Figure 1A). **B.** ISI histograms for the 9 high input rate parameter sets (indicated in Figure 1A). **C.** ISI histograms for the 9 parameter sets for the GP_{NDSK} model (indicated in Figure 1B). **D&E.** CV of ISIs for the GP_{base} model and GP_{NDSK} model.

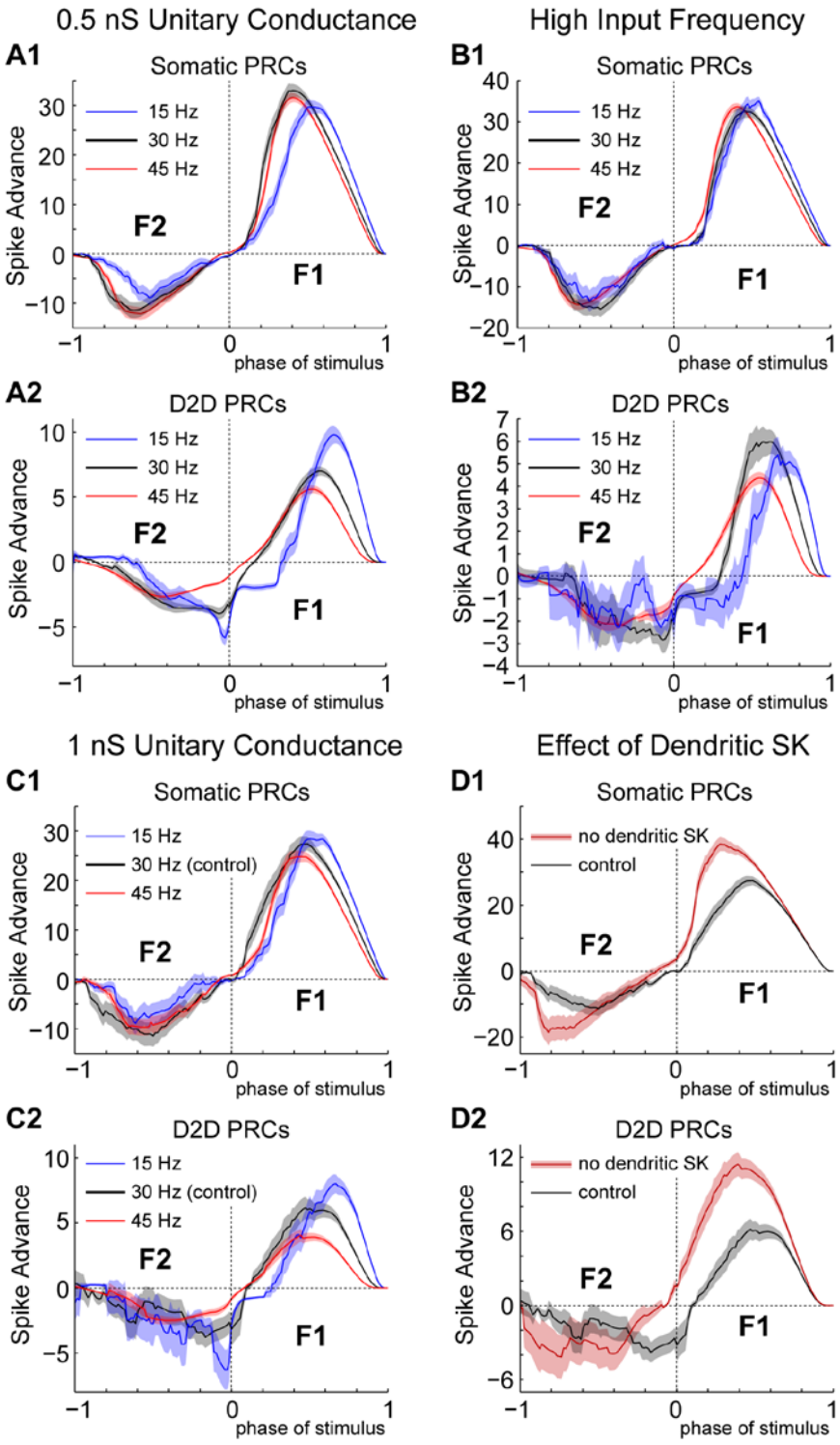

Figure 3.3. Average PRCs during high conductance states maintain the dynamics of PRCs for isolated GP models. A. Somatic and D2D PRCs for the low gain synaptic

background for spike frequencies spanning the in vivo range. Somatic PRCs are type I, whereas D2D PRCs have multiple negative regions that are more pronounced during slower spiking. **B.** Average PRC during high input rate synaptic backgrounds. **C.** Average PRCs for mid-gain synaptic backgrounds. **D.** Average PRCs comparing the GP_{base} GP_{NDSK} models. F1 somatic and D2D PRCs are attenuated when dendritic SK is intact, and the negative region late in phase of the F2 D2D PRC is eliminated when SK is removed from the dendrite.

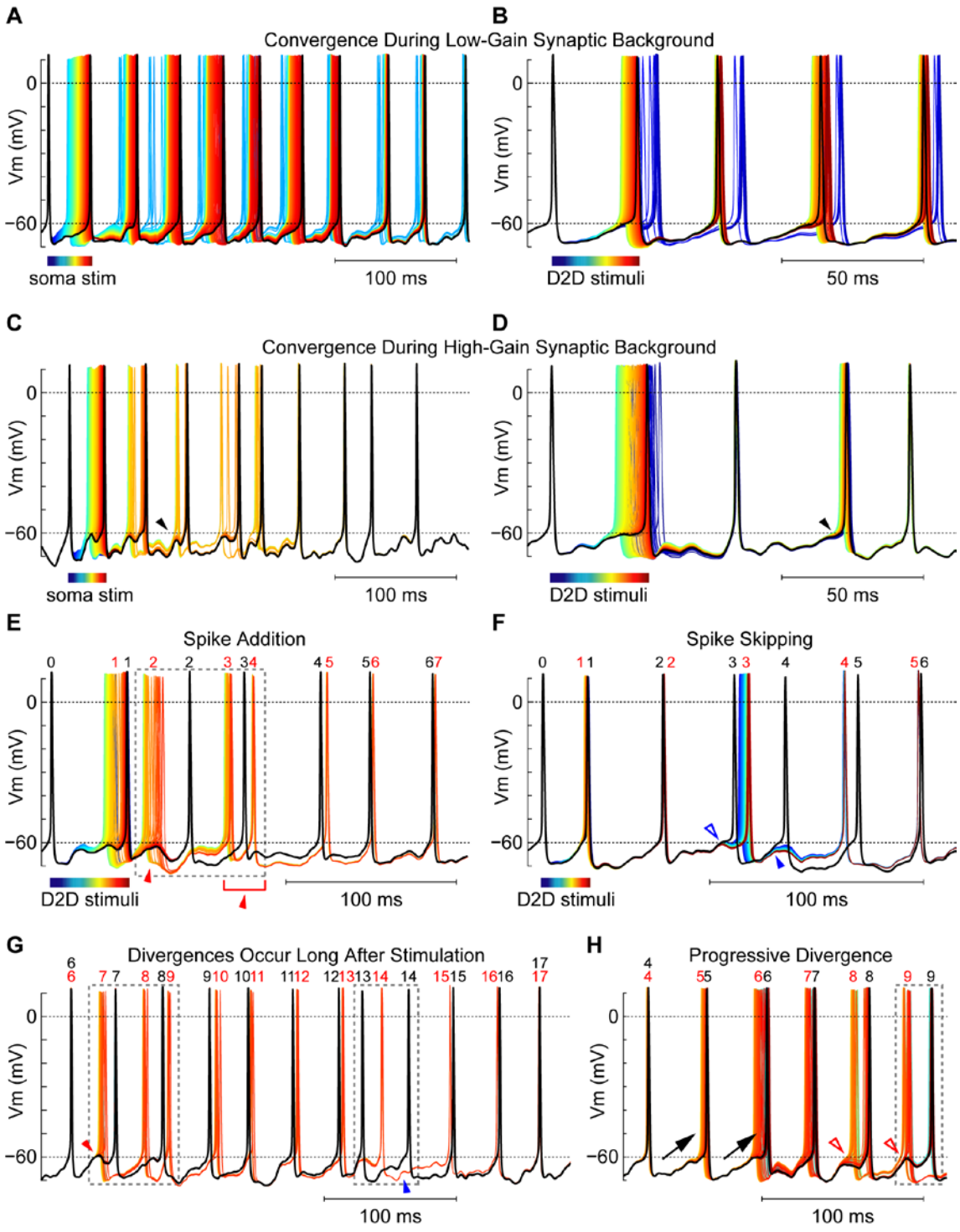

Figure 3.4. Phasic stimuli can lead to long-lasting and unexpected perturbations of spiking patterns. A. Sample voltage trajectories for a control simulation with a low-gain synaptic background (thick black line) and for 72 simulations each containing a phasic

somatic perturbation within the first spike cycle (color traces, color reflects the phase of the input as indicated by the color bar below the stimulated ISI). **B.** Sample voltage trajectories for phasic D2D stimuli delivered during a low-gain synaptic background. **C&D.** Sample voltage trajectories for somatic (C) and D2D stimuli delivered during a high-gain synaptic background. **D.** Perturbations leading to an added spike. Spike numbers indicated above each spike in black for control spikes and red for spikes in simulations containing a stimulus. Note that the added spike is not evoked immediately by the stimuli, but occurs as a result of a complex sequence of events within the boxed region. The red arrowheads indicate points where perturbed trajectories responded differently than the control simulation to fluctuations in the synaptic background. **E.** Perturbations leading to a skipped spike. The open blue arrowhead indicates a deviation of perturbed spiking trajectories from the control spiking pattern that seems to instigate the skipped spike (filled blue arrowhead). **F.** Perturbations leading to an added spike and subsequently, a skipped spike. Note the spike numbers. These added and skipped spike events occurred several spike cycles after stimulation and after the perturbed spiking patterns seemed to have converged back to the control spiking pattern. The red arrowhead indicates the initiation of a sequence of events that resulted in an added spike (first boxed region), and the blue arrowhead indicates a skipped spike that resulted after perturbed trajectories diverged from the control spike pattern (second boxed region). **G.** Gradual divergence of perturbed trajectories over successive spike cycles after the perturbed trajectories seemed to have converged back to the control spiking pattern. Gradual divergence occurred when the voltage passed relatively slowly through the near-threshold range (black arrows). The empty red arrowheads indicate points

where perturbed trajectories spiked on a different set of fluctuations in the synaptic background than did the control simulation.

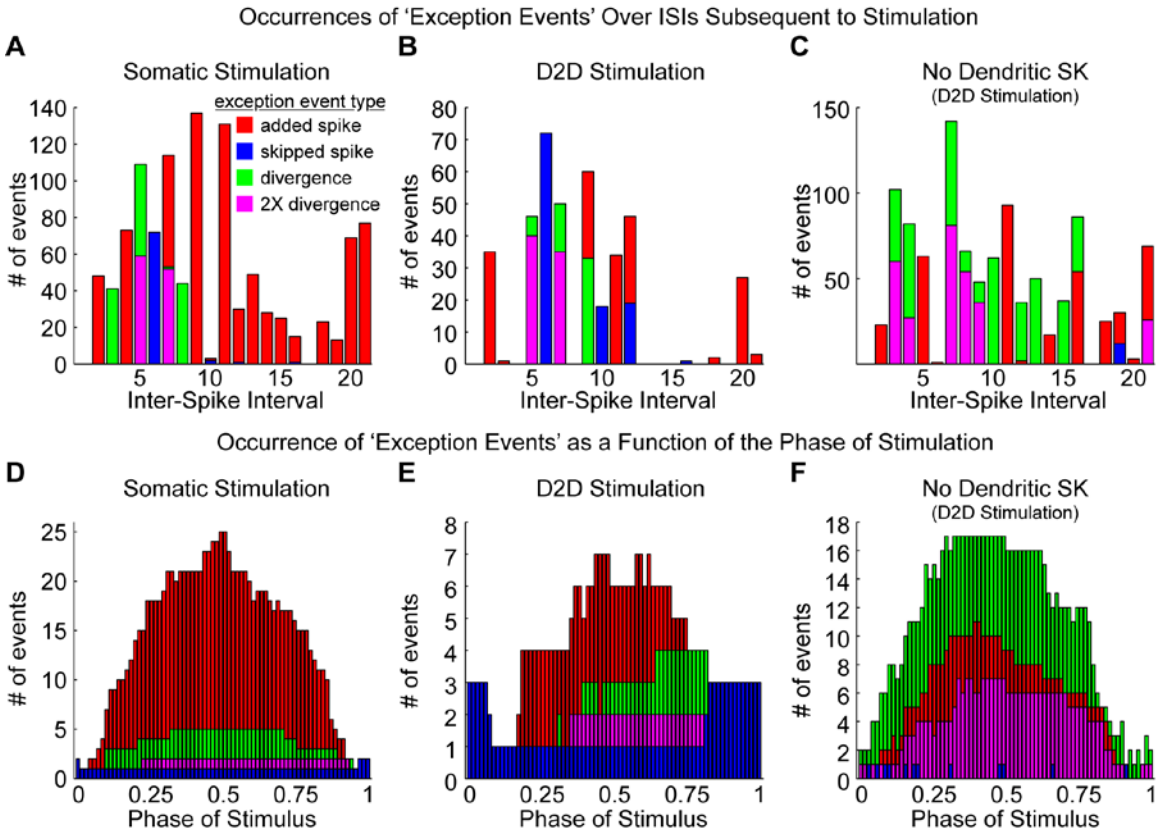

Figure 3.5. Incidence of added spikes, skipped spikes, and divergence events over spike cycles and as a function of input phase. AB&C. Each of these types of events occurred during many spike cycles subsequent to stimulation of the soma of GP_{base} (A), D2D of GP_{base} (B), or D2D of the GP_{NDSK} model (C). **DE&F.** Distributions of these types of events as a function of the phase of the perturbing stimulus. Note that these events typically did not take place during the stimulated spike cycle but still show a strong relationship to input phase. Added spikes and divergence events were most common for stimuli delivered during the middle of phase, independent of the site of stimulation and whether dendritic SK was intact. Skipped spikes were only common for D2D stimulation of the GPbase model and occurred predominantly in simulations where stimuli were delivered near the beginning of the ISI or during the last 20% of the ISI.

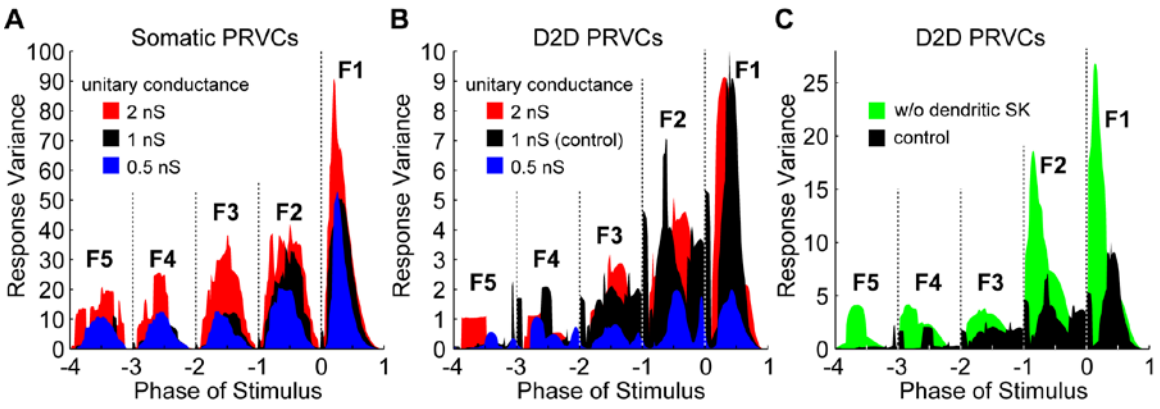

Figure 3.6. Variance of stimulus-evoked shifts in spike timing is phase dependent; Phase Response-Variance Curves (PRVCs). A. PRVCs for somatic stimulation of GPbase show a single peak that diminishes across spike cycles. Variance of shifts in spike timing was near zero when stimuli were delivered coincidentally with a spike in the control spike train (phases of 0 and 1). **B.** PRVCs for D2D stimulation of GPbase are multiphasic reflecting multiple sources of variability. **C.** PRVCs for D2D stimulation of GP_{NDSK} shows a single peak, indicating that dendritic SK conductance accounted for variance peaks early and late in the F2 spike cycle. Note this pattern maps well onto the phase dependent incidence of skipped spikes even though trials with skipped spikes were excluded from this analysis.

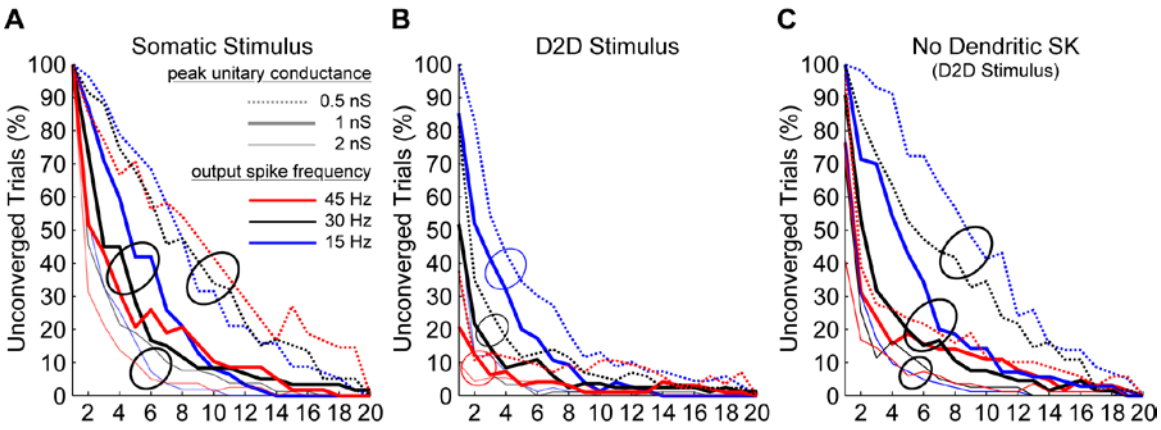

Figure 3.7. Convergence of perturbed spiking back to the control spike pattern takes many spike cycles. A. Proportion of population of trials that remained unconverged over successive spike cycles for somatic stimuli with each synaptic background. Note that the progress of convergence was similar for synaptic backgrounds of the same gain (circled) independent of output spike frequency (indicated by color). **B.** Convergence following D2D stimulation was faster than for somatic stimulation and was also dependent on the gain of the synaptic background. Note that convergence following D2D perturbation also reflected a strong spike frequency dependence (circles). **C.** Convergence following D2D stimulation of the GP_{NDSK} model showed dramatically reduced dependence on spike frequency and resembled convergence following somatic stimulation of GP_{base}.

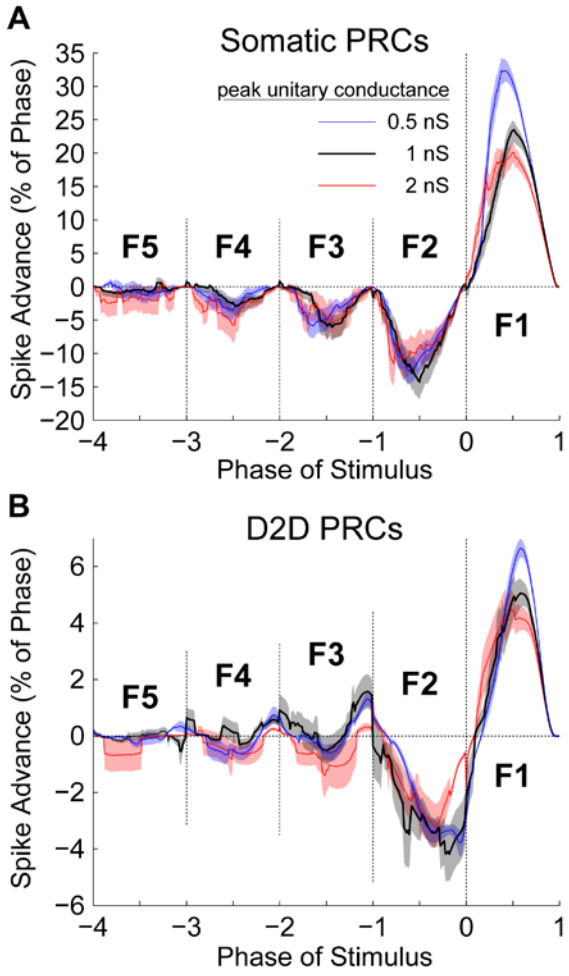

Figure 3.8. Gain of synaptic backgrounds only slightly affects average somatic and D2D PRCs. A. Average PRCs for somatic inputs to GPbase (after removal of trials containing added spikes, skipped spikes, and divergence events). **B.** Average PRCs for D2D inputs to GPbase. The negative region late in phase of the F2 PRC is only noticeably reduced for the high gain case.

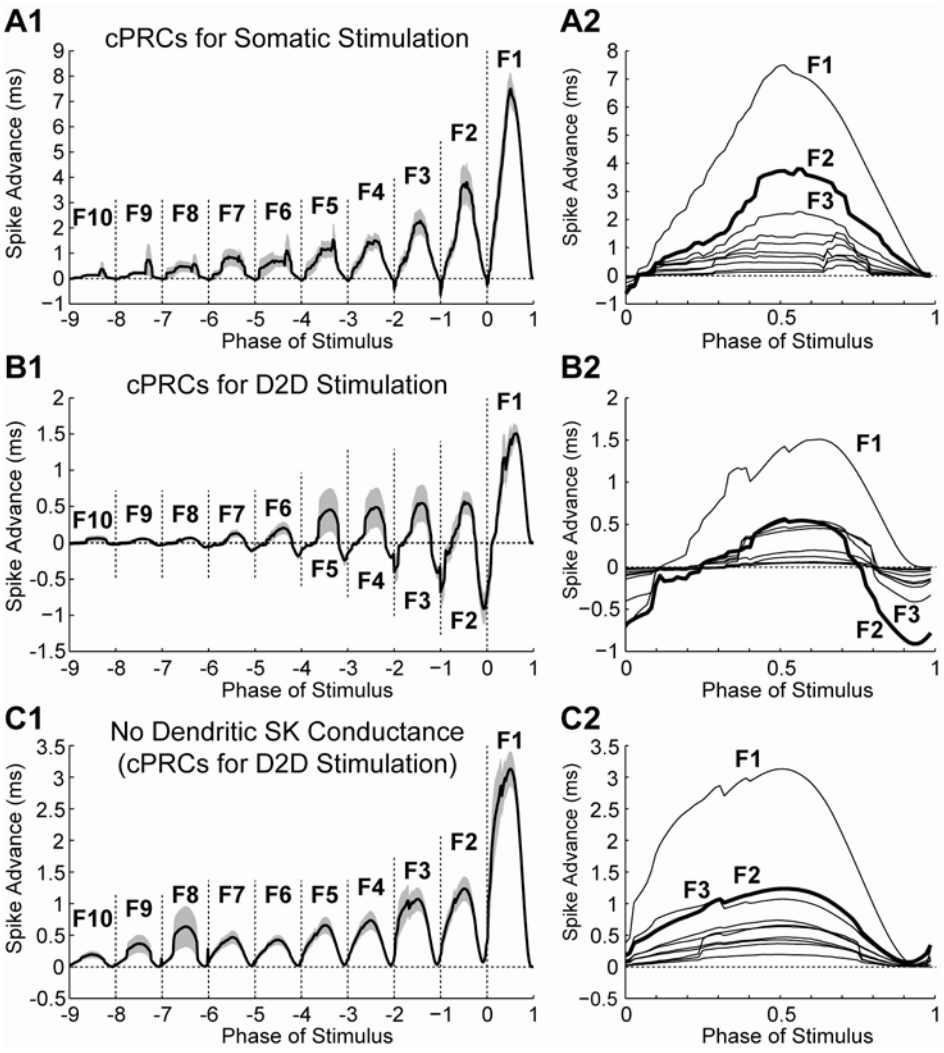

Figure 3.9. Cumulative PRCs make intrinsic and synaptic background contributions to shifts in spike timing distinguishable. A. cPRCs for somatic stimulation of GPbase attenuate gradually over 10 spike cycles (A1) without a notable change in shape or y-translation (A2). **B.** cPRCs for D2D stimulation of GPbase attenuate over 6 or 7 spike cycles (B1), and show a pronounced negative y-translation between the F1 and F2 cPRCs reflecting the contribution of evoked dendritic SK to shifts in spike timing (B2). **C.** cPRCs for D2D stimulation of the GP_{NDSK} model attenuate over 10 spike cycles (F1) without a notable change in shape or y-translation.

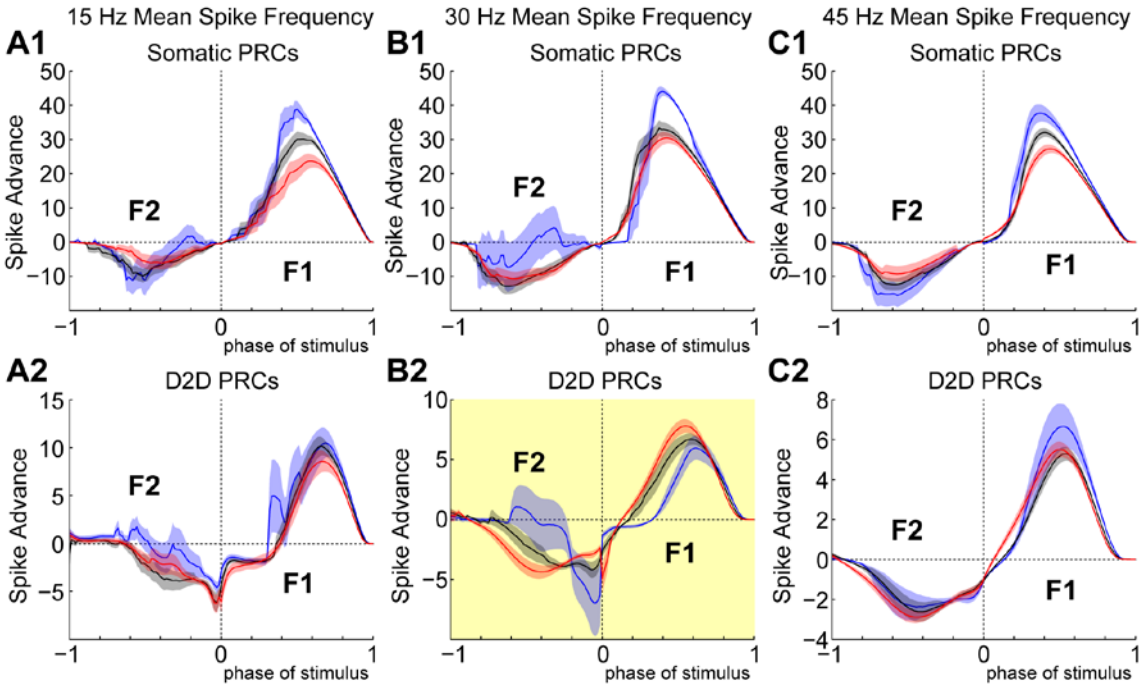

Supplemental Figure 3.1. PRCs for subsets of trials with a gross mean of 30 Hz spiking. **A1&2.** Somatic and D2D PRCs for the subset of trials below 25 Hz (mean ~15 Hz). **B1&2.** Somatic and D2D PRCs for the subset of trials with instantaneous spike frequencies very near 30 Hz. **C1&2.** Somatic and D2D PRCs for the subset of trials above 35 Hz (mean ~45 Hz).

Chapter 4

General Discussion

The studies described here target the interface between neural computation at the single neuron and network levels with the goal of identifying and characterizing cellular mechanisms that contribute to the phase response properties of globus pallidus neurons and the coordinated behavior of pallidal networks. PRCs provide a measure that can be made from individual neurons which allows prediction and interpretation of how individual neurons participate in the emergence of network synchrony and entrainment to correlated input. Therefore, an understanding of how the PRC depends on underlying neuronal dynamics is critical for mechanistic explanations of functional and pathological synchronization and oscillations in the brain. We first applied PRC analysis to our GP neuron model during intrinsic pacemaking and demonstrated that 1) physiological inputs to GP exceed the domain of weak coupling, and 2) PRC shape and type depends on the location of stimulus delivery such that somatic PRCs are type I, whereas local activation of the SK conductance by dendritic stimuli leads to type II dendritic PRCs. We further demonstrated that somatic and dendritic PRCs were dependent on spike frequency driven by tonic somatic current injection or by spatially distributed synaptic background activity. We determined that the shapes of PRCs for somatic and dendritic inputs delivered during pacemaking were generally well preserved during high conductance states representative

of *in vivo* conditions, i.e. average somatic PRCs across trials were type I and average D2D PRCs were type II. Finally, our analyses of the variability in responses of the model during high conductance states provide a framework for extending PRC analyses of idealized systems to more complex *in-vivo* conditions.

Compartmental modeling approach to PRC analysis.

Experimental PRCs. PRCs have been estimated experimentally for some neurons (Prinz et al., 2003a; Oprisan et al., 2004; Galan et al., 2005b; Netoff et al., 2005a; Netoff et al., 2005b; Preyer and Butera, 2005; Stiefel et al., 2008; Sieling et al., 2009), but methodological constraints limit the accurate measurement of small shifts in spike timing relative to the noisy spiking oscillation and the precise delivery of stimuli to different regions of the neuronal morphology. Furthermore, experimental estimation of PRCs typically only provides voltage and gross injected current data, and therefore provides only indirect evidence of the mechanisms underlying a neuron's phase response properties.

Our GP neuron model possesses a full contingent of membrane conductances contributing to synaptic integration and a spatially-extended, branching dendrite reconstructing the morphology of a GP neuron for which a battery of electrophysiological measurements were made in slice. Making possible our primary findings, this modeling approach afforded us: 1) perfect temporal and spatial precision of stimulus delivery, 2) the ability to exactly repeat complex, spatially-distributed patterns of synaptic activity, and 3) access to all voltage, current, and conductance data streams necessary for the analysis of the highly nonlinear dynamics contributing to the phase response properties of the model.

Our GP neuron model has been well characterized in previous studies (Hanson et al., 2004; Gunay et al., 2008) and exhibits realistic electrophysiological behavior. However, the morphological modeling approach introduces the necessity for a balance between the complexity of the model and uncertainty about parameter settings. Whole-cell investigations of the active conductances in the dendrites of GP neurons are not experimentally feasible. Thus, there is considerable uncertainty surrounding the dendritic conductances that contribute to input processing or synaptic integration. Our assessment of the dependence of somatic and dendritic PRCs on model parameters demonstrated the robustness of our results against variations in dendritic conductance densities, SK density and distribution, and the kinetics of calcium dispersion and SK activation. Furthermore, these variations reflect potential sources of heterogeneity within pallidal networks, and suggest how potential targets of modulation could affect network activity by virtue of their effects on PRC shape.

Weak coupling and active membrane conductances.

Theoretical studies have linked PRC shape, i.e. types I and II, to the classes of neuronal excitability by which neurons spontaneously fire action potentials (Hodgkin, 1948; Hansel et al., 1995; Ermentrout, 1996; Rinzel and Ermentrout, 1998; Ermentrout et al., 2001; Oprisan and Canavier, 2002; Brown et al., 2004; Tateno and Robinson, 2007). This approach has been successful in explaining the behavior of networks of simple neuron models with well defined architectures. However, these studies typically rely on a set of simplifying assumptions including most prominently the limitation of coupling between neurons to the very weak regime (Bendels and Leibold, 2007; Varkonyi and Holmes, 2008; Chen and Iwasaki, 2009; Cheng and Ermentrout, 2009). The range of

input strengths that defines the weak coupling domain differs from neuron to neuron and also between regions of the morphology of a given neuron. This variability is largely a consequence of differences in input resistance and different densities of active membrane conductances between neurons and across different morphological regions. Determination of the maximal stimulus strength for which the PRC scales linearly in amplitude is an effective standard for determining the upper limit of the weak coupling regime. However, intrinsic noise and variability in the periodicity of spontaneous spiking make this standard difficult to apply experimentally. Our simulations of intrinsic pacemaking were noiseless, allowing the precise determination of PRC shape for very small stimuli and thus precise comparisons of PRCs for different stimulus strengths. In chapter 2 we demonstrated that the weak coupling domain for our GP neuron model does not include somatic stimuli stronger than ~10 pA, and the weak coupling domain for dendritic inputs is even more restrictive. Thus, excitatory synaptic inputs of physiological strength exceed the weak coupling regime for our GP model, because they yield PRCs whose shape changes with increasing input strength. PRCs for sufficiently weak excitatory and inhibitory inputs should be symmetrical. Furthering our analysis of the limits of weak coupling for the GP model we demonstrated that symmetry was lost for distal inputs stronger than 1 pA and ~5 pA for somatic inputs. These values agree well with our measures of divergence from the shape of the infinitesimal PRC. Furthermore, PRCs were more sensitive to increasing amplitude of excitatory inputs than inhibitory inputs. This observation reflects the activation of intrinsic conductances by excitatory inputs that does not occur for inhibitory inputs, and suggests that dendritic excitation is likely to evoke specialized mechanisms of synaptic integration.

Since the voltage-dependence of activation of membrane conductances is nonlinear, any significant activation of membrane conductances by excitatory inputs will contribute a nonlinearity to the PRC. This effect is most pronounced when the membrane voltage traverses the steep part of a conductance's activation curve. The weak coupling domain for somatic inputs is relatively resistant to these effects, because low somatic input resistance minimizes voltage deflections elicited by somatic inputs and because the sodium and potassium currents that drive spike initiation typically dwarf the other intrinsic currents. As we have demonstrated, regions of dendrite that are electrotonically remote from the soma may possess intrinsic conductances that significantly affect spike timing by acting as current sinks (or sources) mediated by dendritic axial currents.

We are not the first to evaluate the dependence of PRC shape on active conductances (Crook et al., 1998a; Ermentrout et al., 2001; Acker et al., 2003; Gutkin et al., 2005; Goldberg et al., 2007; Stiefel et al., 2009). Previous studies have indicated that slow membrane currents, in particular slow potassium currents, e.g. the spike frequency adaptation (SFA) or m-type potassium current, are particularly potent in shaping neuronal responses to synaptic inputs (Ermentrout et al., 2001; Gutkin et al., 2005). Acker and colleagues demonstrated that excitatory inputs to single compartment models of stellate cells of the medial entorhinal cortex yield nonlinear effects on spike timing by engaging voltage-gated membrane conductances (Acker et al., 2003). Thus, physiological inputs to that neuron type are also likely to exceed the weak coupling regime. The authors evaluated the contributions of a slow potassium current (similar to our SK), I_{KS}, and the hyperpolarization activated cation current, I_h to the synchronization of two mutually excitatory model stellate neurons, finding that both slow conductances increased the

effective strength of excitatory inputs. Studies of this type have typically been limited by the use of single compartment models lacking a full contingent of active conductances which prevents a complete analysis of the interactions between conductances in morphologically distinct regions of the neuron.

Conductance Interactions and Modulation of PRCs

Importantly, we are the first to analyze in detail the phase response properties of a morphologically realistic neuron model with a full contingent of active conductances. We identified the SK conductance as a critical contributor to dendritic PRCs and characterized effects of this conductance during pacemaking and high conductance states, on the longevity of perturbations across spike cycles, and in models with different balances of intrinsic conductances. We found most prominently that SK can reverse the effect of excitatory synaptic input to the dendrite yielding delays of the spiking rhythm. This aspect of our work is consistent with previous studies of slow potassium currents (Gutkin et al., 2005). However, in our morphological model, the effect of SK does not impinge directly on the axo-somatic spiking mechanism. Rather, SK characterizes a spatially separate dynamical subsystem at more distal regions of the dendritic tree that contributes to the timing of spikes through axial current flows. Thus, the SK current evoked by distal stimuli is capable of delaying subsequent spiking through its function as a current sink. Because our model contains a full contingent of spatially-distributed active conductances, our results also further previous work by allowing the investigation of interactions between conductances that would not be predicted on first principles. Most notably, we identified an important relationship between dendritic SK and the fast sodium conductance (NaF) which is known to be present in the dendrites of

GP neurons. For models with stronger dendritic NaF 1) excitatory inputs were amplified contributing to greater advancements of the first spike cycle, and 2) greater SK was activated because of the amplified voltage deflection leading to greater delays of the second spike cycle. The pattern of effects on spike timing of the first two spike cycles following excitatory inputs has the effect of amplifying the permanent PRC. Thus, we demonstrated that modulation of fast inward current sources like NaF, can modulate the amplitude of resultant PRCs. We also found that direct manipulation of the SK current density in the dendrite causes a y-translation in the corresponding PRCs. Taken together, these results illustrate the importance of higher-order interactions between conductances in determining the precise shape of PRCs and highlight the utility of modeling neurons with a level of complexity that approaches neuronal 'realism'. GP neurons *in vivo* receive dopaminergic modulation from the substantia nigra pars compacta and serotonergic modulation from the dorsal raphe nucleus. Parkinson's disease is accompanied by the degeneration of these modulatory inputs (Kita et al., 2007; Hashimoto and Kita, 2008; Rav-Acha et al., 2008). While the specific mechanisms by which these modulators affect GP neuron physiology are a topic of current interest, it is reasonable to suppose that they affect active conductances as in other neuron types and will contribute accordingly to pallidal PRCs.

Potential Effects of Inhibition

The investigations described in this dissertation focused primarily on the effects of excitatory inputs to GP in order to elucidate dendritic mechanisms of synaptic integration that may be evoked by activity of the STN-GP microcircuit within the basal ganglia. GP neurons *in vivo*, however, also receive perisomatic inhibitory input from GP

collaterals that may be time-locked to STN excitation with some delay. Mallet and colleagues have proposed that β-frequency oscillatory inputs to GP neurons may drive two pallidal subpopulations in antiphase as a result of a competitive process subserved by GP collaterals (Mallet et al., 2008). Therefore, perisomatic inhibition from GP collaterals may also contribute importantly to the patterning of network activity. The weak coupling regime for inhibitory inputs to the model was considerably larger than for excitatory inputs (not analyzed in detail in these studies), because hyperpolarizing inputs do not substantially activate voltage-gated membrane currents. Therefore, our finding that dendritic excitation may synchronize GP neurons and entrain them to oscillating STN input may be supplemented in the future by considering competition within GP networks subserved by perisomatic inhibition that does not violate weak coupling assumptions.

A second major source of inhibition distributed throughout the GP neuronal morphology stems from the striatum. Chan and colleagues (2004, 2005) have proposed a role for h-current in resetting and synchronizing GP neurons by eliciting coincident rebound spikes following cessation of shared striatal inhibition. The manipulation of h-current conductance density in our GP model, either local to dendritic sites of stimulation or globally throughout the dendrite, had a negligible effect on the PRC (data not shown), because h-current is minimally activated during baseline spiking and is not activated efficiently by brief hyperpolarizations from single synaptic inputs. Post-inhibitory rebound (via striatum) and excitatory phase response (via STN) mechanisms of pallidal synchronization are compatible and potentially complimentary, but further description of the timing of activity within the indirect and hyperdirect pathways of basal ganglia circuitry would be necessary to integrate the two.

SK Controls Dendritic Processing of Synaptic Inputs to GP

In a variety of neuronal systems the SK conductance has been identified to play critical roles in shaping after-hyperpolarizations and pacemaking (Kohler et al., 1996; Abel et al., 2004; Bond et al., 2005), somatic and dendritic excitability, plasticity, and synaptic integration (Cai et al., 2004; Bond et al., 2005; Faber et al., 2005; Maher and Westbrook, 2005; Ngo-Anh et al., 2005; Gu et al., 2008), and the calcium sensitivity of SK is a known target for modulation (Maingret et al., 2008). A recent investigation in GP neurons revealed that SK plays a role in spike time precision by affecting the availability of other ion channel types during spiking (Deister et al., 2009). Our investigations identified a novel role for the SK conductance in shaping PRCs for excitatory dendritic inputs and illustrate the interrelated contributions of neuronal morphology and membrane conductances to a neuron's phase response properties. Thus, the strong dendritic SK conductance in our GP neuron model was a central focus of each stage of our PRC analyses.

Future Directions

In the studies described in this thesis we applied PRC analysis to a morphological GP neuron model and identified intrinsic mechanisms of potential importance to patterning of activity in pallidal networks. These results illustrate the need to consider synaptic topography within the neuronal morphology as a part of the connectivity structure of modeled networks. We also generalized our results to high conductance states, and show that PRC obtained during pacemaking may be good indicators of neuronal dynamics in vivo, but consideration of the variability in neuronal responses to

phasic inputs is necessary for capturing population activity. We have not, however, explicitly tested our model in response to patterned synaptic inputs.

We are currently in the planning stages for a study to explicitly test the role that dendritic SK plays in the entrainment of our GP neuron model to oscillating excitatory input from STN. Peter Magill has graciously provided spike trains recoded *in vivo* from STN neurons that exhibit β-frequency oscillatory activity synchronized to cortical LFP data. In the proposed study we will activate excitatory synapses distributed throughout the morphology of our GP neuron model based on the spike times in this recorded data and we will evaluate entrainment of the model's output spiking to the beta oscillation. We also plan to drive the excitatory synapses in our model with activation probabilities following a sinusoid with different parameters. So doing we will be able to determine the preferred input frequency for entraining the model. By driving spatially segregated subsets of the excitatory synapses with these stimuli we will also be able to evaluate the dependence of entrainment on the proportion of synapses showing correlated input activity, the distribution of those synapses to different regions of the dendritic morphology, and on the strength of the dendritic SK conductance in the model. We hypothesize that oscillatory input in the beta-frequency range will optimally entrain our model only when the dendritic SK conductance is intact. This result would link the intrinsic properties of GP neurons to the complex patterning of their spiking behavior and prove the principle that type II dendritic PRCs are critical to coordination of synchronized oscillations in pallidal networks.

References

Abel HJ, Lee JCF, Callaway JC, Foehring RC (2004) Relationships between intracellular calcium and afterhyperpolarizations in neocortical pyramidal neurons. Journal of Neurophysiology 91:324-335.

Abouzeid A, Ermentrout B (2009) Type-II phase resetting curve is optimal for stochastic synchrony. Physical Review E 80:8.

Achard P, De Schutter E (2006) Complex parameter landscape for a complex neuron model. Plos Comput Biol 2:794-804.

Achuthan S, Canavier CC (2009) Phase-resetting curves determine synchronization, phase locking, and clustering in networks of neural oscillators. Journal of Neuroscience 29:5218-5233.

Acker CD, Kopell N, White JA (2003) Synchronization of strongly coupled excitatory neurons: Relating network behavior to biophysics. Journal of Computational Neuroscience 15:71-90.

Amitai Y, Friedman A, Connors BW, Gutnick MJ (1993) Regenerative activity in apical dendrites of pyramidal cells in neocortex. Cereb Cortex 3:26-38.

Bar-Gad I, Heimer G, Ritov Y, Bergman H (2003) Functional correlations between neighboring neurons in the primate globus pallidus are weak or nonexistent. Journal of Neuroscience 23:4012-4016.

Baranauskas G, Tkatch T, Surmeier DJ (1999) Delayed rectifier currents in rat globus pallidus neurons are attributable to Kv2.1 and Kv3.1/3.2 K+ channels. Journal of Neuroscience 19:6394-6404.

Baranauskas G, Tkatch T, Nagata K, Yeh JZ, Surmeier DJ (2003) Kv3.4 subunits enhance the repolarizing efficiency of Kv3.1 channels in fast-spiking neurons. Nature Neuroscience 6:258-266.

Bendels MHK, Leibold C (2007) Generation of theta oscillations by weakly coupled neural oscillators in the presence of noise. Journal of Computational Neuroscience 22:173-189.

Bergman H, Wichmann T, Karmon B, Delong MR (1994) The Primate Subthalamic Nucleus .2. Neuronal-Activity in the Mptp Model of Parkinsonism. Journal of Neurophysiology 72:507-520.

Bevan MD, Magill PJ, Terman D, Bolam JP, Wilson CJ (2002) Move to the rhythm: oscillations in the subthalamic nucleus-external globus pallidus network. Trends in Neurosciences 25:525-531.

Bogaard A, Parent J, Zochowski M, Booth V (2009) Interaction of cellular and network mechanisms in spatiotemporal pattern formation in neuronal networks. J Neurosci 29:1677-1687.

Bond CT, Maylie J, Adelman JP (2005) SK channels in excitability, pacemaking and synaptic integration. Current Opinion in Neurobiology 15:305-311.

Bouali-Benazzouz R, Tai CH, Chetrit J, Benazzouz A (2009) Intrapallidal injection of 6-hydroxydopamine induced changes in dopamine innervation and neuronal activity of globus pallidus. Neuroscience 164:588-596.

Bowden SEH, Fletcher S, Loane DJ, Marrion NV (2001) Somatic colocalization of rat SK1 and D class (Ca-v 1.2) L-type calcium channels in rat CA1 hippocampal pyramidal neurons. Journal of Neuroscience 21:NIL_22-NIL_27.

Brown E, Moehlis J, Holmes P (2004) On the phase reduction and response dynamics of neural oscillator populations. Neural Computation 16:673-715.

Brown P, Oliviero A, Mazzone P, Insola A, Tonali P, Di Lazzaro V (2001) Dopamine dependency of oscillations between subthalamic nucleus and pallidum in Parkinson's disease. Journal of Neuroscience 21:1033-1038.

Butera RJ, Preyer AJ (2006) Weak phase-resetting in neural oscillators. 2005 27th Annual International Conference of the IEEE Engineering in Medicine and Biology Society (IEEE Cat No05CH37611C)|2005 27th Annual International Conference of the IEEE Engineering in Medicine and Biology Society (IEEE Cat No05CH37611C):3 pp.|CD-ROM.

Buzsaki G, Draguhn A (2004) Neuronal oscillations in cortical networks. Science 304:1926-1929.

Cai X, Liang CW, Muralidharan S, Kao JPY, Tang CM, Thompson SM (2004) Unique roles of SK and Kv4.2 potassium channels in dendritic integration. Neuron 44:351-364.

Cauller LJ, Connors BW (1994) Synaptic physiology of horizontal afferents to layer I in slices of rat SI neocortex. Journal of Neuroscience 14:751-762.

Chan CS, Shigemoto R, Mercer JN, Surmeier DJ (2004) HCN2 and HCN1 channels govern the regularity of autonomous pacemaking and synaptic resetting in globus pallidus neurons. Journal of Neuroscience 24:9921-9932.

Chen CC, Abrams S, Pinhas A, Brumerg JC (2009) Morphological Heterogeneity of Layer VI Neurons in Mouse Barrel Cortex. Journal of Comparative Neurology 512:726-746.

Chen L, Yung KKL, Chan YS, Yung WH (2008) 5-HT excites globus pallidus neurons by multiple receptor mechanisms. Neuroscience 151:439-451.

Chen ZY, Iwasaki T (2009) Matrix perturbation analysis for weakly coupled oscillators. Syst Control Lett 58:148-154.

Cheng L, Ermentrout G (2009) Synchronization dynamics of two coupled neural oscillators receiving shared and unshared noisy stimuli. Journal of Computational Neuroscience 26:425-443.

Churchland MM, Shenoy KV (2007) Temporal complexity and heterogeneity of single-neuron activity in premotor and motor cortex. Journal of Neurophysiology 97:4235-4257.

Connor JA, Stevens CF (1971) Prediction of repetitive firing behavior from voltage clamp data on an isolated neurone soma. Journal of Physiology-London 213:31-&.

Connor JA, Walter D, McKown R (1977) Neural repetitive firing - modifications of Hodgkin-Huxley axon suggested by experimental results from crustacean axons. Biophysical Journal 18:81-102.

Crook SM, Ermentrout GB, Bower JM (1998a) Spike frequency adaptation affects the synchronization properties of networks of cortical oscillators. Neural Computation 10:837-854.

Crook SM, Ermentrout GB, Bower JM (1998b) Dendritic and synaptic effects in systems of coupled cortical oscillators. Journal of Computational Neuroscience 5:315-329.

De Schutter E, Ekeberg O, Kotaleski JH, Achard P, Lansner A (2005) Biophysically detailed modelling of microcircuits and beyond. Trends in Neurosciences 28:562-569.

Deister CA, Wilson CJ (2008) Variability of fast afterhyperpolarization currents reduces the regularity of spontaneous firing in globus pallidus neurons In.

Deister CA, Chan CS, Surmeier DJ, Wilson CJ (2009) Calcium-activated SK channels influence voltage-gated ion channels to determine the precision of firing in globus pallidus neurons. J Neurosci 29:8452-8461.

DeLong MR, Wichmann T (2007) Circuits and circuit disorders of the basal ganglia. Arch Neurol 64:20-24.

Desai NS, Rutherford LC, Turrigiano GG (1999) Plasticity in the intrinsic excitability of cortical pyramidal neurons. Nature Neuroscience 2:515-520.

Destexhe A, Pare D (1999) Impact of network activity on the integrative properties of neocortical pyramidal neurons in vivo. Journal of Neurophysiology 81:1531-1547.

Destexhe A, Rudolph M, Pare D (2003) The high-conductance state of neocortical neurons in vivo. Nature Reviews Neuroscience 4:739-751.

Di Giovanni G, Di Matteo V, Pierucci M, Benigno A, Esposito E (2006) Serotonin involvement in the basal ganglia pathophysiology: Could the 5-HT2C receptor be a new target for therapeutic strategies? Curr Med Chem 13:3069-3081.

Ermentrout B (1996) Type I membranes, phase resetting curves, and synchrony. Neural Comput 8:979-1001.

Ermentrout B, Pascal M, Gutkin B (2001) The effects of spike frequency adaptation and negative feedback on the synchronization of neural oscillators. Neural Computation 13:1285-1310.

Ermentrout GB, Kopell N (1991) Multiple pulse interactions and averaging in systems of coupled neural oscillators. J Math Biol 29:195-217.

Faber ESL, Delaney AJ, Sah P (2005) SK channels regulate excitatory synaptic transmission and plasticity in the lateral amygdala. Nature Neuroscience 8:635-641.

Falls WM, Park MR, Kitai ST (1983) An intracellular HRP study of the rat globus pallidus. II. Fine structural characteristics and synaptic connections of medially located large GP neurons. The Journal of Comparative Neurology 221:229-245.

Foster WR, Ungar LH, Schwaber JS (1993) Significance of conductances in Hodgkin-Huxley models. Journal of Neurophysiology 70:2502-2518.

Galan RF, Ermentrout GB, Urban NN (2005a) Predicting synchronized neural assemblies from experimentally estimated phase-resetting curves. In: 14th Annual Computational Neuroscience Meeting (CNS 05), pp 1112-1115. Madison, WI: Elsevier Science Bv.

Galan RF, Ermentrout GB, Urban NN (2005b) Efficient estimation of phase-resetting curves in real neurons and its significance for neural-network modeling. Physical Review Letters 94:4.

Galan RF, Ermentrout GB, Urban NN (2007a) Reliability and stochastic synchronization in type I vs. type II neural oscillators. Neurocomputing 70:2102-2106.

Galan RF, Ermentrout GB, Urban NN (2007b) Stochastic dynamics of uncoupled neural oscillators: Fokker-Planck studies with the finite element method. Physical Review E 76.

Galan RF, Fourcaud-Trocme N, Ermentrout GB, Urban NN (2006) Correlation-induced synchronization of oscillations in olfactory bulb neurons. Journal of Neuroscience 26:3646-3655.

Gamper N, Stockand JD, Shapiro MS (2003) Subunit-specific modulation of KCNQ potassium channels by Src tyrosine kinase. Journal of Neuroscience 23:84-95.

Glass L, Mackey MC (1988) From clocks to chaos: The rhythms of life: Princeton Univ Pr.

Goel P, Ermentrout B (2002) Synchrony, stability, and firing patterns in pulse-coupled oscillators. Physica D 163:191-216.

Goldberg JA, Wilson CJ (2005) Control of spontaneous firing patterns by the selective coupling of calcium currents to calcium-activated potassium currents in striatal cholinergic interneurons. Journal of Neuroscience 25:10230-10238.

Goldberg JA, Deister CA, Wilson CJ (2007) Response properties and synchronization of rhythmically firing dendritic neurons. Journal of Neurophysiology 97:208-219.

Gu N, Hu H, Vervaeke K, Storm JF (2008) SK (K(Ca)2) Channels Do Not Control Somatic Excitability in CA1 Pyramidal Neurons But Can Be Activated by Dendritic Excitatory Synapses and Regulate Their Impact. Journal of Neurophysiology 100:2589-2604.

Gunay C, Edgerton JR, Jaeger D (2008) Channel density distributions explain spiking variability in the globus pallidus: A combined physiology and computer simulation database approach. Journal of Neuroscience 28:7476-7491.

Gutkin BS, Ermentrout GB, Reyes AD (2005) Phase-response curves give the responses of neurons to transient inputs. Journal of Neurophysiology 94:1623-1635.

Hallworth NE, Wilson CJ, Bevan MD (2003) Apamin-sensitive small conductance calcium-activated potassium channels, through their selective coupling to voltage-gated calcium channels, are critical determinants of the precision, pace, and pattern of action potential generation in rat subthalamic nucleus neurons in vitro. Journal of Neuroscience 23:7525-7542.

Hansel D, Mato G, Meunier C (1995) Synchrony in excitatory neural networks. Neural Computation 7:307-337.

Hanson JE, Smith Y (2002) Subcellular distribution of high-voltage-activated calcium channel subtypes in rat globus pallidus neurons. Journal of Comparative Neurology 442:89-98.

Hanson JE, Smith Y, Jaeger D (2004) Sodium channels and dendritic spike initiation at excitatory synapses in globus pallidus neurons. Journal of Neuroscience 24:329-340.

Hashimoto K, Kita H (2008) Serotonin activates presynaptic and postsynaptic receptors in rat globus pallidus. Journal of Neurophysiology 99:1723-1732.

Hernandez A, Ibanez-Sandoval O, Sierra A, Valdiosera R, Tapia D, Anaya V, Galarraga E, Bargas J, Aceves J (2006) Control of the subthalamic innervation of the rat

globus pallidus by D-2/3 and D-4 dopamine receptors. Journal of Neurophysiology 96:2877-2888.

Herz AVM, Gollisch T, Machens CK, Jaeger D (2006) Modeling single-neuron dynamics and computations: A balance of detail and abstraction. Science 314:80-85.

Hirschberg B, Maylie J, Adelman JP, Marrion NV (1998a) Gating of recombinant small-conductance Ca-activated K+ channels by calcium. Journal of General Physiology 111:565-581.

Hirschberg B, Maylie J, Adelman JP, Marrion NV (1999) Gating properties of single SK channels in hippocampal CA1 pyramidal neurons. Biophysical Journal 77:1905-1913.

Hirschberg B, Ishii T, Xia XM, Keen J, Johnson T, Maylie J, Marrion NV, Adelman JP (1998b) Determinants of blockade and mechanisms of calcium-gating in small-conductance calcium-activated potassium channels. Naunyn-Schmiedebergs Archives of Pharmacology 358:R23-R23.

Hodgkin AL (1948) The local electric changes associated with repetitive action in a non-medullated axon. Journal of Physiology-London 107:165-181.

Hodgkin AL, Huxley AF (1952a) The dual effect of membrane potential on sodium conductance in the giant axon of Loligo. The Journal of physiology 116:497.

Hodgkin AL, Huxley AF (1952b) A quantitative description of membrane current and its application to conduction in the giant axon of Loligo. J Physiol 117:500-544.

Hodgkin AL, Huxley AF (1952c) The components of membrane conductance in the giant axon of Loligo. The Journal of physiology 116:473.

Hodgkin AL, Huxley AF (1952d) Currents carried by sodium and potassium ions through the membrane of the giant axon of Loligo. The Journal of physiology 116:449.

Hodgkin AL, Huxley AF, Katz B (1952) Measurement of current-voltage relations in the membrane of the giant axon of Loligo. The Journal of physiology 116:424.

Izhikevich EM (2006) Dynamical systems in neuroscience: The geometry of excitability and bursting: The MIT press.

Jellinger KA (1991) Pathology of Parkinsons disease - Changes other than the nigrostriatal pathway. Mol Chem Neuropathol 14:153-197.

Keen JE, Khawaled R, Farrens DL, Neelands T, Rivard A, Bond CT, Janowsky A, Fakler B, Adelman JP, Maylie J (1999) Domains responsible for constitutive and Ca2+-dependent interactions between calmodulin and small conductance Ca2+ activated potassium channels. Journal of Neuroscience 19:8830-8838.

Khaliq ZM, Gouwens NW, Raman IM (2003) The contribution of resurgent sodium current to high-frequency firing in Purkinje neurons: An experimental and modeling study. Journal of Neuroscience 23:4899-4912.

Kita H (1994) Parvalbumin immunopositive neurons in rat globus pallidus - a light and electron microscopic study. Brain Research 657:31-41.

Kita H, Kitai ST (1994a) The morphology of globus pallidus projection neurons in the rat - an intracellular staining study. Brain Research 636:308-319.

Kita H, Kitai ST (1994b) The morphology of globus pallidus projection neurons in the rat: an intracellular staining study. Brain Res 636:308-319.

Kita H, Tachibana Y, Nambu A, Chiken S (2005) Balance of monosynaptic excitatory and disynaptic inhibitory responses of the globus pallidus induced after

stimulation of the subthalamic nucleus in the monkey. Journal of Neuroscience 25:8611-8619.

Kita H, Chiken S, Tachibana Y, Nambu A (2007) Serotonin modulates pallidal neuronal activity in the awake monkey. Journal of Neuroscience 27:75-83.

Kohler M, Hirschberg B, Bond CT, Kinzie JM, Marrion NV, Maylie J, Adelman JP (1996) Small-conductance, calcium-activated potassium channels from mammalian brain. Science 273:1709-1714.

Komendantov AO, Ascoli GA (2009) Dendritic Excitability and Neuronal Morphology as Determinants of Synaptic Efficacy. Journal of Neurophysiology 101:1847-1866.

Krichmar JL, Nasuto SJ, Scorcioni R, Washington SD, Ascoli GA (2002) Effects of dendritic morphology on CA3 pyramidal cell electrophysiology: a simulation study. Brain Research 941:11-28.

LeMasson G, LeMasson S, Moulins M (1995) From conductances to neural network properties: Analysis of simple circuits using the hybrid network method. Prog Biophys Mol Biol 64:201-220.

Lipowsky R, Gillessen T, Alzheimer C (1996) Dendritic Na+ channels amplify EPSPs in hippocampal CA1 pyramidal cells. Journal of Neurophysiology 76:2181-2191.

Loane DJ, Lima PA, Marrion NV (2007) Co-assembly of N-type Ca2+ and BK channels underlies functional coupling in rat brain. Journal of Cell Science 120:985-995.

Loucif KC, Wilson CL, Baig R, Lacey AG, Stanford IA (2005) Functional interconnectivity between the globus pallidus and the subthalamic nucleus in the mouse brain slice. Journal of Physiology-London 567:977-987.

MacLean JN, Zhang Y, Goeritz ML, Casey R, Oliva R, Guckenheimer J, Harris-Warrick RM (2005) Activity-independent coregulation of I-A and I-h in rhythmically active neurons. Journal of Neurophysiology 94:3601-3617.

Magill PJ, Bolam JP, Bevan MD (2000) Relationship of activity in the subthalamic nucleus-globus pallidus network to cortical electroencephalogram. Journal of Neuroscience 20:820-833.

Magill PJ, Bolam JP, Bevan MD (2001) Dopamine regulates the impact of the cerebral cortex on the subthalamic nucleus-globus pallidus network. Neuroscience 106:313-330.

Magistretti J, Alonso A (1999) Biophysical properties and slow voltage-dependent inactivation of a sustained sodium current in entorhinal cortex layer-II principal neurons - A whole-cell and single-channel study. Journal of General Physiology 114:491-509.

Magistretti J, Alonso A (2002) Fine gating properties of channels responsible for persistent sodium current generation in entorhinal cortex neurons. Journal of General Physiology 120:855-873.

Magistretti J, Ragsdale DS, Alonso A (1999) Direct demonstration of persistent Na+ channel activity in dendritic processes of mammalian cortical neurones. Journal of Physiology-London 521:629-636.

Maher BJ, Westbrook GL (2005) SK channel regulation of dendritic excitability and dendrodendritic inhibition in the olfactory bulb. Journal of Neurophysiology 94:3743-3750.

Mainen ZF, Sejnowski TJ (1995) Reliability of spike timing in neocortical neurons. Science 268:1503-1506.

Mainen ZF, Sejnowski TJ (1996) Influence of dendritic structure on firing pattern in model neocortical neurons. Nature 382:363-366.

Maingret F, Coste B, Hao J, Giamarchi A, Allen D, Crest M, Litchfield DW, Adelman JP, Delmas P (2008) Neurotransmitter modulation of small-conductance Ca2+-activated K+ channels by regulation of Ca2+ gating. Neuron 59:439-449.

Mallet N, Pogosyan A, Marton LF, Bolam JP, Brown P, Magill PJ (2008) Parkinsonian Beta Oscillations in the External Globus Pallidus and Their Relationship with Subthalamic Nucleus Activity. Journal of Neuroscience 28:14245-14258.

Marder E, Thirumalai V (2002) Cellular, synaptic and network effects of neuromodulation. Neural Netw 15:479-493.

Marder E, Bucher D (2007) Understanding circuit dynamics using the stomatogastric nervous system of lobsters and crabs. Annu Rev Physiol 69:291-316.

Marella S, Ermentrout GB (2008) Class-II neurons display a higher degree of stochastic synchronization than class-I neurons. Physical Review E 77:12.

Marrion NV, Tavalin SJ (1998) Selective activation of Ca2+-activated K+ channels by co-localized Ca2+ channels in hippocampal neurons. Nature 395:900-905.

Mercer JN, Chan CS, Tkatch T, Held J, Surmeier DJ (2007) Nav1.6 sodium channels are critical to pacemaking and fast spiking in globus pallidus neurons. Journal of Neuroscience 27:13552-13566.

Millhouse OE (1986) Pallidal neurons in the rat. Journal of Comparative Neurology 254:209-227.

Nakao H, Arai K, Kawamura Y (2007) Noise-induced synchronization and clustering in ensembles of uncoupled limit-cycle oscillators. Physical Review Letters 98:4.

Netoff TI, Acker CD, Bettencourt JC, White JA (2005a) Beyond two-cell networks: Experimental measurement of neuronal responses to multiple synaptic inputs. Journal of Computational Neuroscience 18:287-295.

Netoff TI, Clewley R, Arno S, Keck T, White JA (2004) Epilepsy in small-world networks. J Neurosci 24:8075-8083.

Netoff TI, Banks MI, Dorval AD, Acker CD, Haas JS, Kopell N, White JA (2005b) Synchronization in hybrid neuronal networks of the hippocampal formation. Journal of Neurophysiology 93:1197-1208.

Ngo-Anh TJ, Bloodgood BL, Lin M, Sabatini BL, Maylie J, Adelman JP (2005) SK channels and NMDA receptors form a Ca2+-mediated feedback loop in dendritic spines. Nature Neuroscience 8:642-649.

Nini A, Feingold A, Slovin H, Bergman H (1995) Neurons in the globus pallidus do not show correlated activity in the normal monkey, but phase-locked oscillations appear in the MPTP model of parkinsonism. Journal of Neurophysiology 74:1800-1805.

Obeso JA, Rodriguez-Oroz MC, Blesa FJ, Guridi J (2006) The globus pallidus pars externa and Parkinson's disease. Ready for prime time? Experimental Neurology 202:1-7.

Olypher AV, Calabrese RL (2007) Using constraints on neuronal activity to reveal compensatory changes in neuronal parameters. Journal of Neurophysiology 98:3749-3758.

Oprisan SA, Canavier CC (2002) The influence of limit cycle topology on the phase resetting curve. Neural Computation 14:1027-1057.

Oprisan SA, Prinz AA, Canavier CC (2004) Phase resetting and phase locking in hybrid circuits of one model and one biological neuron. Biophysical Journal 87:2283-2298.

Parent A, Sato F, Wu Y, Gauthier J, Levesque M, Parent M (2000) Organization of the basal ganglia: the importance of axonal collateralization. Trends in Neurosciences 23:S20-S27.

Park MR, Falls WM, Kitai ST (1982) An intracellular HRP study of the rat globus pallidus. I. Responses and light microscopic analysis. J Comp Neurol 211:284-294.

Plenz D, Kitai ST (1999) A basal ganglia pacemaker formed by the subthalamic nucleus and external globus pallidus. Nature 400:677-682.

Prescott SA, Ratte S, De Koninck Y, Sejnowski TJ (2006) Nonlinear interaction between shunting and adaptation controls a switch between integration and coincidence detection in pyramidal neuron. Journal of Neuroscience 26:9084-9097.

Prescott SA, Ratte S, De Koninck Y, Sejnowski TJ (2008) Pyramidal neurons switch from integrators in vitro to resonators under in vivo-like conditions. Journal of Neurophysiology 100:3030-3042.

Preyer AJ, Butera RJ (2005) Neuronal oscillators in Aplysia californica that demonstrate weak coupling in vitro. Physical Review Letters|Physical Review Letters 95:138103/138101-138104.

Prinz AA, Thirumalai V, Marder E (2003a) The functional consequences of changes in the strength and duration of synaptic inputs to oscillatory neurons. Journal of Neuroscience 23:943-954.

Prinz AA, Billimoria CP, Marder E (2003b) Alternative to hand-tuning conductance-based models: Construction and analysis of databases of model neurons. Journal of Neurophysiology 90:3998-4015.

Prole DL, Marrion NV (2004) Ionic permeation and conduction properties of neuronal KCNQ2/KCNQ3 potassium channels. Biophysical Journal 86:1454-1469.

Querejeta E, Oviedo-Chavez A, Araujo-Alvarez JM, Quinones-Cardenas AR, Delgado A (2005) In vivo effects of local activation and blockade of 5-HT1B receptors on globus pallidus neuronal spiking. Brain Research 1043:186-194.

Raman IM, Bean BP (2001) Inactivation and recovery of sodium currents in cerebellar Purkinje neurons: Evidence for two mechanisms. Biophysical Journal 80:729-737.

Ramanathan S, Tkatch T, Atherton JF, Wilson CJ, Bevan MD (2008) D-2-like dopamine receptors modulate SKCa channel function in subthalamic nucleus neurons through inhibition of Ca(v)2.2 channels. Journal of Neurophysiology 99:442-459.

Rav-Acha M, Bergman H, Yarom Y (2008) Pre- and postsynaptic serotoninergic excitation of globus pallidus neurons. Journal of Neurophysiology 100:1053-1066.

Raz A, Vaadia E, Bergman H (2000) Firing patterns and correlations of spontaneous discharge of pallidal neurons in the normal and the tremulous 1-methyl-4-phenyl-1,2,3,6-tetrahydropyridine vervet model of parkinsonism. Journal of Neuroscience 20:8559-8571.

Rinzel J, Rall W (1974) Transient-response in a dendritic neuron model for current injected at one branch. Biophysical Journal 14:759-790.

Rinzel JM, Ermentrout GB (1998) Analysis of neural excitability and oscillations. In: Methods in Neuronal Modeling, 2nd Edition (Koch C, Segev I, eds), pp 251-291: MIT Press.

Roskies AL (1999) The binding problem - Introduction. Neuron 24:7-+.

Rudolph M, Destexhe A (2001) Novel dynamics of dendritic integration in the high conductance state of cortical neurons. In: 10th Computational Neuroscience Meeting (CSN 01), pp 141-146. Monterey, California: Elsevier Science Bv.

Rudolph M, Destexhe A (2003a) The discharge variability of neocortical neurons during high-conductance states. Neuroscience 119:855-873.

Rudolph M, Destexhe A (2003b) A fast-conducting, stochastic integrative mode for neocortical neurons in vivo. Journal of Neuroscience 23:2466-2476.

Ruskin DN, Bergstrom DA, Kaneoke Y, Patel BN, Twery MJ, Walters JR (1999) Multisecond oscillations in firing rate in the basal ganglia: Robust modulation by dopamine receptor activation and anesthesia. Journal of Neurophysiology 81:2046-2055.

Sadek AR, Magill PJ, Bolam JP (2007) A single-cell analysis of intrinsic connectivity in the rat globus pallidus. Journal of Neuroscience 27:6352-6362.

Sailer CA, Hu H, Kaufmann WA, Trieb M, Schwarzer C, Storm JF, Knaus HG (2002) Regional differences in distribution and functional expression of small-conductance Ca2+-activated K+ channels in rat brain. Journal of Neuroscience 22:9698-9707.

Sato F, Lavallee P, Levesque M, Parent A (2000) Single-axon tracing study of neurons of the external segment of the globus pallidus in primate. Journal of Comparative Neurology 417:17-31.

Schnitzler A, Gross J (2005) Normal and pathological oscillatory communication in the brain. Nature Reviews Neuroscience 6:285-296.

Schultheiss NW, Edgerton JR, Jaeger D (2010) Phase response curve analysis of a full morphological globus pallidus neuron model reveals distinct perisomatic and dendritic modes of synaptic integration. Journal of Neuroscience 30:2767-2782.

Segev I (1992) Single neuron models - oversimple, complex and reduced. Trends in Neurosciences 15:414-421.

Sharott A, Magill PJ, Harnack D, Kupsch A, Meissner W, Brown P (2005) Dopamine depletion increases the power and coherence of beta-oscillations in the cerebral cortex and subthalamic nucleus of the awake rat. European Journal of Neuroscience 21:1413-1422.

Shen GY, Chen WR, Midtgaard J, Shepherd GM, Hines ML (1999) Computational analysis of action potential initiation in mitral cell soma and dendrites based on dual patch recordings. J Neurophysiol 82:3006-3020.

Shink E, Smith Y (1995) Differential synaptic innervation of neurons in the internal and external segments of the globus pallidus by the GABA- and glutamate-containing terminals in the squirrel monkey. Journal of Comparative Neurology 358:119-141.

Sieling FH, Canavier CC, Prinz AA (2009) Predictions of Phase-Locking in Excitatory Hybrid Networks: Excitation Does Not Promote Phase-Locking in Pattern-

Generating Networks as Reliably as Inhibition. Journal of Neurophysiology 102:69-84.

Sims RE, Woodhall GL, Wilson CL, Stanford IM (2008) Functional characterization of GABAergic pallidopallidal and striatopallidal synapses in the rat globus pallidus in vitro. European Journal of Neuroscience 28:2401-2408.

Smith Y, Bevan MD, Shink E, Bolam JP (1998) Microcircuitry of the direct and indirect pathways of the basal ganglia. Neuroscience 86:353-387.

Spruston N, Jaffe DB, Williams SH, Johnston D (1993) Voltage clamp and space clamp errors associated with the measurement of electrotonically remote synaptic events. Journal of Neurophysiology 70:781-802.

Stiefel K, Gutkin B, Sejnowski T (2009) The effects of cholinergic neuromodulation on neuronal phase-response curves of modeled cortical neurons. Journal of Computational Neuroscience 26:289-301.

Stiefel KM, Sejnowski TJ (2007) Mapping function onto neuronal morphology. Journal of Neurophysiology 98:513-526.

Stiefel KM, Gutkin BS, Sejnowski TJ (2008) Cholinergic neuromodulation changes phase response curve shape and type in cortical pyramidal neurons. PLoS ONE 3:e3947.

Tateno T, Robinson HPC (2007) Phase resetting curves and oscillatory stability in interneurons of rat somatosensory cortex. Biophysical Journal 92:683-695.

Taylor AL, Goaillard JM, Marder E (2009) How multiple conductances determine electrophysiological properties in a multicompartment model. J Neurosci 29:5573-5586.

Terman D, Rubin JE, Yew AC, Wilson CJ (2002) Activity patterns in a model for the subthalamopallidal network of the basal ganglia. Journal of Neuroscience 22:2963-2976.

Tkatch T, Baranauskas G, Surmeier DJ (2000) Kv4.2 mRNA abundance and A-type K+ current amplitude are linearly related in basal ganglia and basal forebrain neurons. Journal of Neuroscience 20:579-588.

Tsubo Y, Takada M, Reyes AD, Fukai T (2007) Layer and frequency dependencies of phase response properties of pyramidal neurons in rat motor cortex. European Journal of Neuroscience 25:3429-3441.

Turrigiano G, Lemasson G, Marder E (1995) Selective regulation of current densities underlies spontaneous changes in the activity of cultured neurons. Journal of Neuroscience 15:3640-3652.

Urbain N, Gervasoni D, Souliere F, Lobo L, Rentero N, Windels F, Astier B, Savasta M, Fort P, Renaud B, Luppi PH, Chouvet G (2000) Unrelated course of subthalamic nucleus and globus pallidus neuronal activities across vigilance states in the rat. European Journal of Neuroscience 12:3361-3374.

Varkonyi PL, Holmes P (2008) On synchronization and traveling waves in chains of relaxation oscillators with an application to lamprey CPG. SIAM J Appl Dyn Syst 7:766-794.

Vetter P, Roth A, Hausser M (2001) Propagation of action potentials in dendrites depends on dendritic morphology. Journal of Neurophysiology 85:926-937.

Wang J, Chen S, Nolan MF, Siegelbaum SA (2002) Activity-dependent regulation of HCN pacemaker channels by cyclic AMP: Signaling through dynamic allosteric coupling. Neuron 36:451-461.

Ward LM (2003) Synchronous neural oscillations and cognitive processes. Trends Cogn Sci 7:553-559.

White JA, Netoff TI (2008) Synchronization in hybrid neuronal networks. In: Computational Neuroscience in Epilepsy (Soltesz I, Staley K, eds), pp 281-287: Elsevier.

Wichmann T, DeLong MR (2006) Basal ganglia discharge abnormalities in Parkinson's disease. Journal of Neural Transmission-Supplement:21-25.

Williams D, Tijssen M, van Bruggen G, Bosch A, Insola A, Di Lazzaro V, Mazzone P, Oliviero A, Quartarone A, Speelman H, Brown P (2002) Dopamine-dependent changes in the functional connectivity between basal ganglia and cerebral cortex in humans. Brain 125:1558-1569.

Wilson CL, Puntis M, Lacey MG (2004) Overwhelmingly asynchronous firing of rat subthalamic nucleus neurones in brain slices provides little evidence for intrinsic interconnectivity. Neuroscience 123:187-200.

Winfree AT (2001) The geometry of biological time: Springer Verlag.

Xia XM, Fakler B, Rivard A, Wayman G, Johnson-Pais T, Keen JE, Ishii T, Hirschberg B, Bond CT, Lutsenko S, Maylie J, Adelman JP (1998) Mechanism of calcium gating in small-conductance calcium-activated potassium channels. Nature 395:503-507.

Yelnik J, Percheron G, Francois C (1984) A Golgi analysis of the primate globus pallidus. II. Quantitative morphology and spatial orientation of dendritic arborizations. J Comp Neurol 227:200-213.